2009

GUST RESPONSES OF BRIDGES TO SPATIALLY VARYING WIND EXCIATIONS AND CALIBRATION OF WIND LOAD FACTORS

Ziran Hu

GUST RESPONSES OF BRIDGES TO SPATIALLY VARYING WIND EXCIATIONS AND CALIBRATION OF WIND LOAD FACTORS

(Spine title: Bridge responses and calibration of wind load factors)

(Thesis format: Integrated-Article)

by

Ziran Hu

Graduate Program in Engineering Science

Department of Civil and Environmental Engineering

Submitted in partial fulfillment of the

requirements for the degree of

Master of Engineering Science

School of Graduate Studies and Postdoctoral Studies

The University of Western Ontario

London, Ontario

Abstract

The study is focused on two aspects relating to the bridge design: the gust factor and wind load factors. The concept and the assessment of the gust factor developed by Alan G. Davenport are essential for bridge design under buffeting forces. However, systematic parametric investigation of the standard deviation of fluctuating wind-induced bridge responses and the gust factor, by considering the spatio-temporal varying along and cross winds and aerodynamic damping has not be given, although a simple to use approximate equation is available. Such an investigation is given in the present study by including/excluding the aeroelastic self-excited forces. The results obtained are used to assess the bias associated with this simple approximate equation, and can be adopted by bridge design codes for predicting the gust factor.

Since the gust factor depends on the dynamic structural characteristics and the characteristics of wind speed, wind load factors are calibrated by incorporating this dependency for both the simple procedure and detailed procedure in the current Canadian Highway Bridge Design Code (CHBDC). Based on the calibration results by considering a target reliability index of 3.5 for a service period of 75 years, a wind load factor of 1.4 for simple procedure, and an equation to evaluate wind load factor for detailed procedure are recommended for the future edition of the CHBDC. Furthermore, the calibration results indicate that an increase of dead load from 1.20 to 1.25 for the ULS combination 4 given in the current CHBDC is desirable to achieve increased reliability consistency in the bridge design.

Key words: bridge, peak factor, gust factor, spatio-temporal correlation, flutter velocity, reliability, wind load factor

Acknowledgements

I would like to express my deepest gratitude to my supervisors Drs. Hanping Hong and J. Peter C. King. This thesis would not have been possible without their continuous guidance and thorough support. It has been a privilege and a pleasure to work with them.

Financial support received from Ministry of Transportation of Ontario and the University of Western Ontario is much appreciated. Constructive comments and suggestions by Drs. B. Tharmabala, C. Lam and A. Au are much appreciated.

My deep appreciation goes to Mr. Weixian He who taught me how the advanced computational tools could be used to carry out the numerical analyses presented in this study. I also thank Drs. X.G. Hua and Q. Ding for providing detailed information for two considered examples shown in Chapter 2.

Finally, a special thanks to my parents for their never-ending love. This thesis is dedicated to them.

Table of Contents

List of Tables

Nomenclature

Symbols used in Chapter 1

A	= ice accretion load
D	= dead load
E	= loads due to earth pressure and hydrostatic pressure including surcharges other than dead load
F	= loads due to stream pressure and ice forces, or debris torrents
H	= collision load arising from highway vehicles or vessels
K	= all strains, deformations, displacements, and their effects, including the effects of their restraint and those of friction or stiffness in bearings. Strains and deformation include those due to temperature change and temperature differential, concrete shrinkage, differential shrinkage and creep; but not elastic strains
L	= live load, including dynamic load allowance when applicable, based on CL-625 Truck or Lane
P	= secondary prestress effects
EQ	= earthquake load
S	= load due to differential settlement and/or movement of the foundation
V	= wind load on traffic
W	= wind load on structure
α_D	= dead load factor
α_E	= load factor for E
α_P	= load factor for P

Symbols used in Chapter 2

A_i	= aerodynamic derivatives for aeroelastic moment
B	= bridge deck width
$\mathbf{C}$	= global structural damping matrix

$\mathbf{C}_{ae}$ = global aeroelastic damping matrix

$\mathbf{C}_{ae}^{e}$ = local aeroelastic damping matrix of the element

$\mathbf{C}_{ae0}^{e}$ = 6×6 matrix defined by (2.10d)

C_1, C_2 = two coefficients ,$C_1 = \rho U^2 B/2$ and $C_1 = \rho U^2 B^2/2$

C_D = static drag coefficient

C_D' = derivative of static drag coefficient with respect to α

C_L = static lift coefficient

C_L' = derivative of static lift coefficient with respect to α

C_M = static moment coefficient

C_M' = derivative of static moment coefficient with respect to α

$C_{uw}(z,\omega)$ = real part of *uw*-cross spectral density function

C_w = exponential decay factor for the coherence of the vertical wind fluctuation *w*

C_x = exponential decay factor for spanwise coherence of the longitudinal wind fluctuations *u*

c' = scaled exponential decay coefficient

$\mathbf{D}(\omega)$ = $m \times m$ diagonal matrix of $\mathrm{L^*DL^T}$ decomposition of $\mathbf{S}_{FF}(\omega)$

$D(t)$ = drag force per unit length

D_s = static drag force per unit length

$d_k(\omega)$ = *k*-th diagonal element of $\mathbf{D}(\omega)$

d_{xi}, d_{yi}, d_{zi} = displacements along *x,y,z* direction at node *i*

$\mathbf{E}_b^e$ = 12×2 aerodynamic coefficient matrix of buffeting force on the bridge deck defined by Eq.(2.14)

EI_y = vertically bending rigidity

EI_z = laterally bending rigidity

$\mathbf{F}(t)$ = global wind loading vector

$\mathbf{F}_{ae}(t)$ = global aeroelastic loading vector

$\mathbf{F}_{ae}^{e}(t)$ = local nodal aeroelastic forces vector of the element

$\mathbf{F}_b$ = global bueffting force in the global coordinate

$\mathbf{F}_b^e$ = nodal buffeting force of the element in the local coordinate

$\mathbf{F}_b^{e,s}$ = nodal buffeting force of the element in the global coordinate

$\mathbf{f}_k(\omega,t)$ = $6(n+1)$ harmonic pseudo force vector defined by Eq.(2.20c)

$F(\bullet)$ = probability distribution function

f = Monin coordinate

f_1 = f_{p1}, f_{h1} or $f_{\alpha 1}$, Monin coordinate evaluated at ω_{p1}, ω_{h1}, $\omega_{\alpha 1}$

$\hat{f}_u$ = defined by Eq.(2.6a)

$\hat{f}_w$ = defined by Eq.(2.6b)

GI_t = torsional rigidity

g_p = peak factor

g_T = gust factor

$\mathbf{H}(i\omega)$ = $6(n+1)\times 6(n+1)$ transfer function matrix

H_i^* = aerodynamic derivatives for aeroelastic lift

h, $\dot{h}$ = vertical displacement and velocity

$\bar{h}$ = mean vertical response

I_m = mass moment of inertia per unit length

I_u = turbulence intensity of longitudinal wind fluctuation

$\mathbf{K}$ = global stiffness matrix

$\mathbf{K}_{ae}$ = global aeroelastic stiffness matrix

$\mathbf{K}_{ae}^e$ = local aeroelastic stiffness matrix of the element

$\mathbf{K}_{ae0}^e$, = 6×6 matrix defined by Eqs.(2.10c)

K = reduced circular frequency, $\omega B/U$

$\mathbf{L}(\omega)$ = $6(n+1)\times m$ low triangular matrix of $\mathbf{L}^*\mathbf{D}\mathbf{L}^T$ decomposition of $\mathbf{S}_{FF}(\omega)$

$\mathbf{L}_k(\omega)$ = k-th column of $\mathbf{L}(\omega)$

L = length of the bridge

$L(t)$ = lift force per unit length

L_s = static lift force per unit length

l = length of the element

$\mathbf{M}$ = global mass matrix

$M(t)$ = pitching moment per unit length

M_s = static pitching moment per unit length

m = rank of $\mathbf{S}_{FF}(\omega)$

m_b = mass density of the bridge per unit length

m_η = mean peak response

n = number of elements used to model the bridge deck

n_{ae} = number of the discrete values to represent the aerodynamic derivatives

$\mathbf{P}$ = $12n\times1$ global vector of nodal buffeting forces in the local coordinate

P_i^* = aerodynamic derivatives for aeroelastic drag

p, $\dot{p}$ = lateral displacement and velocity

$\overline{p}$ = mean horizontal response

$Q_{uw}(z,\omega)$ = imaginary part of uw-cross spectral density function

$\mathbf{q}^e$ = 2×1 wind fluctuations matrix contains along fluctuation and vertical across fluctuation

r, $\overline{r}$ = response of interest and the response due to mean wind speed

$\mathbf{S}_{FF}(\omega)$ = $6(n+1)\times 6(n+1)$ spectral density function matrix of the global forces

$\mathbf{S}^e_{P_iP_j}(\omega)$ = 12×12 cross-spectral density function matrix of the nodal forces on the i-th element and the j-th element

$\mathbf{S}^e_{q_iq_j}(\omega)$ = 12×12 cross-spectral density function matrix of wind fluctuations on the i-th element and the j-th element

$\mathbf{S}_{YY}(\omega)$ = $6(n+1)\times 6(n+1)$ spectral density function matrix of the global displacements

$S_r(\omega)$ = power spectral density function of r

$S_u(z,\omega)$ = PSD for the longitudinal wind fluctuation u

$S_{uu}(s_i,s_j,\omega)$ = cross spectrum of longitudinal fluctuation u at s_i and s_j

$S_{uw}(s_i, s_j, \omega)$, $S_{wu}(s_i, s_j, \omega)$	= cross spectrum of longitudinal u and vertical fluctuation w at s_i and s_j
$S_{uw}(z,\omega)$	= uw-cross spectral density function
$S_w(z,\omega)$	= PSD for the vertical wind fluctuation w
$S_{ww}(s_i, s_j, \omega)$	= cross spectrum of vertical fluctuation w at s_i and s_j
s_i, s_j.	= two points at the bridge deck
$\mathbf{T}$	= global coordinate transformation matrix
$\mathbf{T}^e$	= $6(n+1)\times 12$ local coordinate transformation matrix of element
T	= Time lag
t	= time
$U, U(z)$	= mean wind velocity at z (m)
U_{cr}	= critical wind velocity
u, $u(t)$	= fluctuating wind speed along the mean wind direction
$u^e(t)$	= fluctuating along wind velocity at midpoint of the element
u_*	= shear friction velocity
V	= reduced velocity, $V=2\pi/K$
ν_0^+	= zero up-crossing rate
ν_r	= coefficient of variation of the response r
w, $w(t)$	= upward fluctuating wind speeds orthogonal to the mean wind direction
$w^e(t)$	= fluctuating vertical cross wind velocity at midpoint of the element
x_i, x_j	= along-span coordinates of the two given points s_i, s_j.
$\mathbf{Y}$	= global nodal displacement vector
$\mathbf{Y}^e, \dot{\mathbf{Y}}^e$	= local nodal displacement, velocity vector of the element
z	= bridge deck height
α	= torsional displacement; wind angle of attack
$\dot{\alpha}$	= one differentiation of α with respect to time
$\overline{\alpha}$	= mean torsional response

β_p, β_h, β_α = coefficients associated with the drag, lift, moment coefficients defined in Table 2.1

η = peak response of r

θ_{xi}, θ_{yi}, θ_{yi} = rotations with respect to x ,y ,z axes at node i

ξ = structural damping

ξ_a = aerodynamic damping

ρ = air density

$\sigma(\bullet)$ = standard deviation of $(\bullet)$

$\tilde{\sigma}_p, \tilde{\sigma}_h, \tilde{\sigma}_\alpha$ = normalized standard deviation for the horizontal, vertical, torsional displacement caused by the fluctuating along wind

$\sigma_{pc}, \sigma_{hc}, \sigma_{\alpha c}$ = standard deviation for the horizontal, vertical, torsional displacement caused by the fluctuating vertical across wind

$\tilde{\sigma}_{pc}, \tilde{\sigma}_{hc}, \tilde{\sigma}_{\alpha c}$ = normalized standard deviation for the horizontal, vertical, torsional displacement caused by the fluctuating vertical across wind

ω = circular frequency of structural vibration or wind turbulence

ω_{p1}, ω_{h1}, $\omega_{\alpha 1}$ = first horizontal, vertical and torsional natural vibration frequencies

$(\bullet)^e$ = for the element in the local coordinate

$(\bullet)_{ae}$ = aeroelastic component for $(\bullet)$

$(\bullet)_b$ = buffeting component for $(\bullet)$

$(\bullet)_i$, $(\bullet)_j$, $(\bullet)_k$ = counter subscripts for $(\bullet)$

Symbols used in Chapter 3

$A_2^*(K)$ = aerodynamic derivative for aeroelastic moment evaluated at K

B = bridge deck width

C = analysis coefficient including the exposure area and air density

C_e = exposure coefficient

C_{ED} = exponential decay coefficient for wind fluctuations

C_g = gust effect coefficient

C_h = horizontal wind drag coefficient

C_L = static lift coefficient

C_M = static moment coefficient

D = dead load effect

$D(t)$ = drag force per unit length

D_n = nominal dead load effect

D_s = static drag force per unit length

f_1 = Monin coordinate evaluated at the first vibration mode, f_{p1}, f_{h1} or $f_{\alpha 1}$

g = limit state function

$H_1^*(K)$ = aerodynamic derivative for aeroelastic lift evaluated at K

$h(z)$ = ratio of $U(z)$ to the wind speed at the height of 10 m

I_u = turbulence intensity of longitudinal wind fluctuation

K = reduced circular frequency, $\omega B/U$

$\tilde{K}_j$ = generalized stiffness for j-th modal

L = length of the bridge

$L(t)$ = lift force per unit length

L_s = static lift force per unit length

$M(t)$ = pitching moment per unit length

M_s = static pitching moment per unit length

m_v = mean of V

m_η = mean of peak response

n = number of simulation cycles

n_f = number of times that g is less than zero

$P(g \le 0)$ = probability that $g \le 0$

P_{fT}. = selected tolerable value for the probability of failure for T-year return period

p_T = T-year reference horizontal wind load pressure

q_T = hourly mean T-year reference wind pressure

R = resistance

R_D = factored resistance

t = time

U, $U(z)$ = mean wind velocity at z (m)

V = annual maximum wind speed

v = value of V

ν_0^+ = zero-upcrossing rate

v_T = T-year reference annual maximum wind velocity

v_v = coefficient of variation of V

v_W = coefficient of variation of wind load effect

W = wind load effect

W_n = nominal wind load effect

X_c = ratio of C to its nominal value

X_{ce} = ratio of C_e to its nominal value

X_{cg} = ratio of C_g to its nominal value

X_{ch} = ratio of C_h to its nominal value

z = bridge deck height

α_D = dead load factor

α_W = wind load factor

β_{75} = reliability index for 75-year return period

γ = ratio of nominal wind load to nominal dead load

δ_W = bias factor for wind load effect

η = peak response

λ = integral spanwise turbulence scale

ρ = air density

ϕ_s = resistance factor for the structural steel

ω_1 = ω_{h1} or $\omega_{\alpha 1}$

ω_{h1}, $\omega_{\alpha 1}$ = first vertical, torsional natural vibration frequency

Symbols used in Appendices

$\mathbf{0}$	= 12×1 zero array
$\mathbf{A}_b^e$	= 3×2 aerodynamic coefficient matrix of buffeting forces on the deck
$\mathbf{A}_{b,c}^e$	= 2×1 aerodynamic coefficient matrix of buffeting forces on the cable
$\mathbf{A}_{b,t}^e$	= 3×2 aerodynamic coefficient matrix of buffeting forces on the tower
$\mathbf{B}^e$	= 3×12 shape function matrix of the beam element
$\mathbf{B}_c^e$	= 2×6 shape function matrix of the cable element
C_D	= static drag coefficient
C_D'	= derivative of static drag coefficient with respect to zero angle of attack
C_L	= static lift coefficient
C_L'	= derivative of static lift coefficient with respect to zero angle of attack
C_M	= static moment coefficient
C_M'	= derivative of static moment coefficient with respect to zero angle of attack
$D(x,t)$	= total drag force per unit length
$\tilde{D}_j(t)$	= generalized force for j-th modal
$d(x,t)$	= drag force due to wind fluctuations
$\mathbf{E}_b^e$	== 12×2 aerodynamic coefficient matrix of buffeting forces on the deck defined by Eq.(B3)
$\mathbf{E}_{b,c}^e$	= 6×1 aerodynamic coefficient matrix of buffeting forces on the bridge cable defined by Eq.(B8)
$\mathbf{E}_{b,t}^e$	= 12×2 aerodynamic coefficient matrix of buffeting forces on the tower defined by Eq.(B5)
E	= Young's modulus
$\mathbf{F}_b^e$	= buffeting force vector on the element of the bridge deck

$\mathbf{F}_{b,c}^{e}$ = buffeting force vector on the element of the bridge cable

$\mathbf{F}_{b,t}^{e}$ = buffeting force vector on the element of the bridge tower

f = Monin coordinate

f_{p1} = Monin coordinate evaluated at ω_{p1}

$H_j(\omega)$ = transfer function for j-th mode

$\mathbf{I}$ = 12×12 identity matrix

I_u = turbulence intensity of longitudinal wind fluctuation

I_z = the moment of inertia

$J(A)$ = joint acceptance function

L = length of the bridge

$\tilde{M}_j$ = generalized mass for j-th modal

m = mass of the beam per unit length

n = number of elements used to model the bridge deck

$\mathbf{q}^e$ = 2×1 wind fluctuations matrix contains along fluctuation and vertical across fluctuation

$R(x,x',\omega)$ = normalized co-spectrum of wind fluctuation

$\mathbf{r}^e$ = 2×1 wind fluctuations matrix contains along fluctuation and horizontal across fluctuation

$S_{dd}(z, \omega)$ = PSD function of the fluctuating wind pressure

$S_{pp}(x,\omega)$ = PSD function of $p(x,t)$

$S_{Q_jQ_k}(\omega)$ = PSD function of generalized forces for j-th and k-th modal

$S_u^C(x,x',\omega)$ = co-spectrum of the wind fluctuation u for two points

$\mathbf{T}^e$ = local coordinate transformation matrix of the element

t = time

$\mathbf{u}^e$ = fluctuating along wind velocity at midpoint of the element

$u(x,t)$ = fluctuating wind speed along the mean wind direction

$u^e(t)$ = fluctuating along wind velocity at midpoint of the element

$v^e(t)$ = fluctuating lateral cross wind velocity at midpoint of the

element

v_p = coefficient of variation of the horizontal response at mid span

$w^e(t)$ = fluctuating vertical aross wind velocity at midpoint of the element

x, x' = along-span coordinates

$y_j(t)$ = generalized coordinate for j-th modal

$\bar{y}_j$ = generalized coordinate for j-th modal due to mean wind

η, η' = normalized along-span coordinates

ξ_j = damping ratio for j-th modal

$\sigma(\bullet)$ = standard deviation of $(\bullet)$

σ_B^2 = background component of the variance of the response

$\sigma_p^2(x)$ = variance of $p(x,t)$

$\sigma_{Q_1}^2$ = variance of the generalized forces for the first modal

σ_R^2 = resonant component of the variance of the response

$\phi_j(x)$ = shape function for j-th vibration mode

ψ_i = functions of x used in the expression of $\mathbf{B}^e$

ω = circular frequency wind turbulence

ω_j = frequency of j-th vibration mode

$(\bullet)_c$ = $(\bullet)$ for the bridge cable

$(\bullet)_k$ = counter subscript for $(\bullet)$

$(\bullet)_t$ = $(\bullet)$ for the bridge tower

Chapter 1 Introduction

1.1 Background

Responses due to buffeting and flutter are of concern for bridge design. The former is defined as the wind load caused by the spatio-temporally varying fluctuating wind speed, while the latter invokes the aeroelastic self-excited force caused by the interaction of the wind flow and oscillation of the bridge.

Bridge design codes such as the Canadian Highway Bridge Design Code (CHBDC) (CAN/CSA S6-6 2006), recommend the simplified approach to evaluate bridge responses due to the buffeting force. The simplified approach is based on the gust factor concept developed by Davenport (1962, 1981, 1983). It considers that the wind load (effect) can be approximated by the mean wind load (effect) multiplied by a gust factor that takes into account the impact of the buffeting force on the peak response. The CHBDC recommends that a gust effect coefficient (or factor) of 2.0 for bridges of spans less than 125 m. However, since the gust factor varies and depends on the structural dynamic characteristics and statistics of the fluctuating wind speed, use of the suggested gust factor of 2.0 may not result in reliability-consistent bridge designs for a wide variety of design cases. The Commentary on the CHBDC recommends detailed procedures that are based on Davenport (1981, 1983) and Davenport and King (1982) which give a simple to use expression for evaluating the gust factor for bridges. The expression is derived based on the assumptions that the consideration of the first vibration mode is sufficient, the evaluation of the effect of the spatially varying fluctuating wind can be simplified using a joint acceptance function, and that the variance of the response due to fluctuating wind speed can be approximately expressed as the sum of variances of the background component and the resonant component of the response. Methods and techniques for such evaluation are well established (Davenport 1962, 1981, 1983, Jain et al. 1996, Simiu and Scanlan 1996, Sun et al. 1999, Chen et al. 2000, Caracoglia and Jones 2003). However, a parametric assessment for verifying the accuracy of the mentioned simple expression to evaluate the gust factor for bridge design has not been reported in the literature.

Current bridge designs are based on Limit State Design philosophy (LSD), which is also known as Load and Resistance Factor Design (LRFD). For the Ultimate Limit State

(ULS), the current CHBDC specifies different load combinations shown in Table 1. The code has three different load combinations for the wind load effect in order to ensure the safety of the bridges under possible wind loading scenario (ULS Combinations 3,4 and 7). The calibration of wind load factors is focused on the ULS combination 4 where the dead load and wind load act simultaneously. Furthermore, it is noted that the CHBDC recommends a wind load factor of 1.65 for bridges of spans less than 125 m, and provides an equation, which depends on the coefficient of variation of the annual maximum hourly mean wind velocity, to calculate the wind load factor for wind sensitive structures and wind loads determined from wind tunnel tests. A calibration of the above suggested wind load factors is reported by Bartlett and King (2002). The calibration uses some simplifying assumptions and approaches, including the use of lognormal models, and distribution tail fitting. Further, the dependency of the gust factor on the wind velocity was not taken into account in their calibration analysis, and its impact on the estimated reliability is unknown.

1.2 Objectives and thesis outline

The main objectives of this present study are to assess the gust factor considering the spatio-temporal along and cross fluctuating winds and aeroelastic forces, to verify the accuracy of simple approximate analytical expression to estimate the gust factor, and to present the basis, calibration procedure and results for recommending the wind load factors and gust factor curves for a future edition of the CHBDC.

In Chapter 2, the bridge flutter analysis and evaluation of the critical wind velocity are conducted by using a finite element formulation (Hua et al. 2007); the buffeting analysis which adopts the pseudo-excitation method (Sun et al 1999), considers the spatially correlated wind fluctuations, and includes the aeroelastic self-excited forces is presented. The analysis results are used to validate a simple equation that can be used to estimate the gust factor for bridge responses under wind excitation. The verification of reliability level of bridges designed according to the current CHBDC and calibration of wind load factor to achieve a selected target reliability were carried out in Chapter 3. The reliability analysis, which is based on the simple simulation technique, considers that the

probability distribution of the gust factor is conditioned on the time-averaged wind speed. Finally, a summary of conclusions and recommendations is described in Chapter 4.

References

Bartlett, F.M. and King, J.P.C. (2002), "Wind load factors for the Canadian Highway bridges design code", Developments in Short and Medium Span Bridge Engineering – 2002, I, 683-690

Caracoglia, L. and Jones, N.P. (2003), "Time domain vs. frequency domain characterization of aeroelastic forces for bridge deck sections", Journal of Wind Engineering & Industrial Aerodynamics, Vol.91 (3), 371 -402.

CHBDC (2006), Canadian Standards Association, Canadian Highway Bridge Design Code (CAN/CSA S6-6), Toronto.

Chen, X, Matsumoto, M. and Kareem, A. (2000), "Time Domain Flutter and Buffeting Response Analysis of Bridges", Journal of Engineering Mechanics, Vol.126 (1), 7-16.

Davenport, A.G. (1962), "Buffeting of a suspension bridge by storm winds", Journal of Structural Engineering, ASCE 1962; 88(ST3), 233-68.

Davenport, A. G. (1981), "Reliability of long span bridges under wind loading", Proceedings of ICOSSAR '81, Trondheim, Norway, 679-694.

Davenport, A.G. (1983), "The Relationship of Reliability to Wind Loading.", Journal of Wind Engineering & Industrial Aerodynamics, Vol.13, 3–27.

Davenport, A.G. and King, J.P.C. (1982) "The incorporation of dynamic wind loads into the design specification for long span bridges", ACE Fall Convention and Structures Congress, New Orleans, Louisiana.

Jain, A., Jones, N.P., and Scanlan, R.H. (1996), "Coupled flutter and buffeting analysis of long-span bridges", Journal of Structural Engineering, ASCE, Vol.122 (7), 716-725.

Simiu, E. and Scanlan, R.H. (1996), Wind effects on structures, fundamentals and application to design, New York: John Wiley

Sun, D.K., Xu,Y.L., Ko, J.M, Lin, J.H. (1999), "Fully coupled buffeting analysis of long-span cable-supported bridges: formulation", Journal of Sound and Vibration, Vol. 228(3), 569-588.

Table 1. Load Factors and Load Combinations in the Canadian Highway Bridge Design Code (after CHBDC 2006)

	Permanent Loads				Transitory Loads				Exceptional Loads			
Loads	***D***	***E***	***P***	***L***	***K***	***W***	***V***	***S***	***EQ***	***F***	***A***	***H***
Ultimate Limit States[1]												
ULS Combination 1	α_D	α_E	α_P	1.70	0	0	0	0	0	0	0	0
ULS Combination 2	α_D	α_E	α_P	1.60	1.15	0	0	0	0	0	0	0
ULS Combination 3	α_D	α_E	α_P	1.40	1.00	0.50[2]	0.50	0	0	0	0	0
ULS Combination 4	α_D	α_E	α_P	0	1.25	1.65[2]	0	0	0	0	0	0
ULS Combination 5	α_D	α_E	α_P	0	0	0	0	0	1.00	0	0	0
ULS Combination 6	α_D	α_E	α_P	0	0	0	0	0	0	1.30	0	0
ULS Combination 7	α_D	α_E	α_P	0	0	0.90[2]	0	0	0	0	1.30	0
ULS Combination 8	α_D	α_E	α_P	0	0	0	0	0	0	0	0	1.00
ULS Combination 9	1.35	α_E	α_P	0	0	0	0	0	0	0	0	0

Note:

1 For ultimate limit states, use the maximum or minimum value of α_D, α_E, α_P which denote the load factor for *D*, *E*, and *P*.

2 For wind loads determined from wind tunnel tests, the load factor shall be as specified in Clause 3.10.5.2 of the CHBDC which gives an approximation equation for calculating the wind load factor in ULS combination 4.

Legend:

A ice accretion load

D dead load

E loads due to earth pressure and hydrostatic pressure including surcharges other than dead load

F loads due to stream pressure and ice forces, or debris torrents

H	collision load arising from highway vehicles or vessels
K	all strains, deformations, displacements, and their effects, including the effects of their restraint and those of friction or stiffness in bearings. Strains and deformation include those due to temperature change and temperature differential, concrete shrinkage, differential shrinkage and creep; but not elastic strains.
L	live load, including dynamic load allowance when applicable, based on CL-625 Truck or Lane.
P	secondary prestress effects
EQ	earthquake load
S	load due to differential settlement and/or movement of the foundation
V	wind load on traffic
W	wind load on structure

Chapter 2 Sensitivity of gust responses of bridges to spatially varying wind excitations

2.1 Introduction

Wind loading on bridges is separated into the time-averaged static, buffeting and aeroelastic self-excited force components. The evaluation of the response due to time-averaged static force component is simple. The buffeting force represents the wind load caused by the spatio-temporally varying wind speed; the aeroelastic self-excited force denotes the force caused by the interaction of the wind flow and oscillation of the bridge.

A simplified approach for evaluating bridge responses due to the buffeting force has been recommended in many bridge design codes, including the Canadian Highway Bridge Design Code (CAN/CSA S6-6 2006). The simplified approach is based on the gust factor concept developed by Davenport (1962, 1981, 1983). The gust factor approach considers that the wind load (effect) can be approximated by the mean wind load (effect) multiplied by a gust factor that takes into account the impact of the buffeting force on the peak response. Use of the concept of the gust factor largely simplifies the bridge design. The gust factor depends on the structural dynamic characteristics and the statistical characteristics of the fluctuating wind speed. It also depends on the magnitude of the uncertainty in the mean wind speed. Simple to use expressions for evaluating the gust factor for bridge design were given in Davenport (1981, 1983) and Davenport and King (1982). These simple equations are derived based on the random vibration analysis, and the assumptions that the consideration of the first vibration mode is sufficient, the evaluation of the effect of the spatially varying fluctuating wind can be simplified using a joint acceptance function, and the variance of the response due to fluctuating wind speed can be approximately expressed as the sum of variances of the background component and the resonant component of the response. Methods and techniques for evaluating the gust factor in the frequency domain or time domain are well established (Davenport 1981, Jain et al. 1996, Simiu and Scanlan 1996, Sun et al. 1999, Chen et al. 2000, Caracoglia and Jones 2003). In particular, Sun et al. (1999) provides a finite element formulation and uses the pseudo-excitation method in dealing with fully coupled buffeting analysis, where possible dynamic coupling between vibration modes, dynamic forces on the bridge deck,

towers and cables, and spatio-temporally varying wind speed and structural properties can be considered. However, a parametric assessment for verifying the accuracy of the mentioned simple expression to evaluate the gust factor for bridge design has not been reported in the literature.

The aeroelastic self-excited force can lead to bridge instability (Scanlan and Tomko 1971). A review of the development of bridge flutter analysis and evaluation of the critical wind velocity, including a significant list of references, were given by Ge and Tanaka (2000). The critical wind velocity can also be conveniently estimated using a widely available finite element software, ANSYS, (Hua et al. 2007).

This study reports the assessment of the gust factor considering the spatio-temporal along and cross fluctuating winds, which are characterized by their power spectral density (PSD) function. The analysis adopts the frequency domain approach, uses the finite element formulation, and considers the aeroelastic self-excited forces. The estimated standard deviation and gust factor due to the buffeting force is conveniently expressed as a function of only two parameters: the scaled exponential decay coefficient and the Monin coordinate evaluated at the frequency of the first vibration mode. For the analysis, it is considered that the time-averaged wind speed is below the critical wind velocity, and the flutter instability can be ignored. This implicitly assumes that the quasi-steady theory is applicable (Davenport 1966, Davenport and King 1982, Miyata et al. 1995). The obtained results are compared with those obtained by the simple approximate expression given by Davenport (1981, 1983). Also, results by including/excluding the aeroelastic self-excited forces are evaluated and compared; details of the analysis procedure, numerical results and conclusions are given.

2.2 Wind loads on bridge deck section

Wind actions on a bridge deck are grouped into drag force $D(t)$, lift force $L(t)$ and pitching moment $M(t)$ which are illustrated in Figure 2.1. The actions per unit span of the bridge deck can be conveniently expressed as the sum of the time-averaged static, buffeting and aeroelastic self-excited contributions (Simiu and Scanlan 1996),

$$D(t) = D_s + D_b(t) + D_{ae}(t), \tag{2.1a}$$

$$L(t) = L_s + L_b(t) + L_{ae}(t), \tag{2.1b}$$

and,

$$M(t) = M_s + M_b(t) + M_{ae}(t), \tag{2.1c}$$

where the subscripts *s*, *b* and *ae* represent the static, buffeting and aeroelastic self-excited forces. The calculation of the responses due to static wind load is straightforward, and analyses of bridge responses are often concentrated on those caused by buffeting forces and aeroelastic self-excited forces.

The static wind forces for the unit length of a bridge deck with a width B are given by,

$$D_s = \frac{1}{2}\rho B C_D U^2, \tag{2.2a}$$

$$L_s = \frac{1}{2}\rho B C_L U^2, \tag{2.2b}$$

and,

$$M_s = \frac{1}{2}\rho B^2 C_M U^2, \tag{2.2c}$$

where ρ is the air mass density; U is a simplified notation for the mean wind velocity at the elevation of the bridge deck z (m), $U(z)$; C_D, C_L and C_M are the drag, lift and moment coefficients which are functions of angle of attack α. These coefficients can be determined based on test results obtained from a section model test in a wind tunnel.

By adopting the quasi-steady model advanced by Davenport (1966) where the interaction between the flow and structure can be ignored and the forces are caused by the random fluctuating winds, the buffeting (or the aerodynamic) forces for a unit length are expressed as,

$$D_b(t) = \frac{1}{2}\rho U^2 B\left[C_D \times \frac{2u(t)}{U} + C_D' \times \frac{w(t)}{U}\right], \tag{2.3a}$$

$$L_b(t) = \frac{1}{2}\rho U^2 B\left[C_L \times \frac{2u(t)}{U} + (C_L' + C_D) \times \frac{w(t)}{U}\right], \tag{2.3b}$$

and,

$$M_b(t) = \frac{1}{2}\rho U^2 B^2\left[C_M \times \frac{2u(t)}{U} + C_M' \times \frac{w(t)}{U}\right], \tag{2.3c}$$

where $u(t)$ and $w(t)$ denote the fluctuating wind speeds along the mean wind direction and orthogonal to the mean wind direction; C_D', C_L' and C_M' represent the derivatives of C_D,

C_L and C_M with respect to α. For a given bridge section, these coefficients can be determined experimentally from wind tunnel tests. In writing Eq. (2.3), higher order effects due to the fluctuating wind are ignored.

Several PSD functions have been given in the literature (e.g. Dyrbye and Hansen 1997), including the Davenport's spectrum, Kaimal's spectrum, von Karman spectrum. The Kaimal's PSD function is considered in this study because it makes a very good approximation in the inertial subrange. In such a case, the PSD function for the longitudinal fluctuating wind speed u, $S_u(z,\omega)$, is expressed as (Simiu and Scanlan 1996),

$$S_u(z,\omega)=\frac{200fu_*^2}{\omega(1+50f)^{5/3}}, \tag{2.4a}$$

while the PSD function for w, $S_w(z,\omega)$, is given as,

$$S_w(z,\omega)=\frac{3.36fu_*^2}{\omega(1+10f^{5/3})}, \tag{2.4b}$$

where, ω is the circular frequency of wind fluctuations; f is a non-dimensional quantity known as the Monin coordinate; $f=\omega z/(2\pi U)$; u_* is the shear friction velocity; the standard deviation of the along-wind fluctuation σ_u is considered to be equal to $\sqrt{6}u_*$. By integrating Eq. (2.4b), it can be shown that the standard deviation of the cross wind fluctuation σ_w is equal to $\sqrt{1.7}u_*$.

The uw-cross spectral density function $S_{uw}(z,\omega)$ is given by,

$$S_{uw}(z,\omega)=C_{uw}(z,\omega)+iQ_{uw}(z,\omega) \tag{2.4c}$$

where $i=\sqrt{-1}$; $Q_{uw}(z,\omega)$ is quadrature spectral density, and its quantitative assessment is unavailable; $C_{uw}(z,\omega)$ is co-spectral density, and its empirical formula is given as (Jain et al.1996),

$$C_{uw}(z,\omega)=-\frac{14fu_*^2}{\omega(1+9.6f)^{2.4}} \tag{2.4d}$$

However, since the effect of this co-spectral density on the wind-induced bridge response is considered to be small, it is not presented in this study.

The spanwise cross-spectrum is adopted to measure the degree of correlation of wind fluctuations at two points s_i and s_j. The thickness of bridge deck is acceptably small

compared with z (m), so assume that any point within the bridge deck is at the same elevation above ground or water level. According to the wind tunnel measurements, the cross-spectral density function of longitudinal fluctuation u at two points s_i and s_j, $S_{uu}(s_i, s_j, \omega)$ can be expressed as (Simiu and Scanlan 1996),

$$S_{uu}(s_i, s_j, \omega) = S_u(z, \omega)\exp(-\hat{f}_u) \tag{2.5a}$$

and the cross-spectral density function of vertical fluctuation w at two points s_i and s_j, $S_{ww}(s_i, s_j, \omega)$ can be written as,

$$S_{ww}(s_i, s_j, \omega) = S_w(z, \omega)\exp(-\hat{f}_w) \tag{2.5b}$$

where,

$$\hat{f}_u = \frac{\omega}{2\pi U} C_x \left| x_i - x_j \right|, \tag{2.6a}$$

and,

$$\hat{f}_w = \frac{\omega}{2\pi U} C_w \left| x_i - x_j \right|, \tag{2.6b}$$

where C_x is the exponential decay coefficient for the spanwise coherence of along wind fluctuation; C_w is the exponential decay coefficient for the coherence of vertical wind fluctuation; x_i and x_j represent the coordinates along the span of the two given points. Since information on the uw-cross spectral density function at two points s_i and s_j is not available in the literature, this cross-spectra is not considered.

The aeroelastic self-excited forces are due to the interaction of the wind flow and oscillation of bridge. These forces for a unit length of the bridge deck can be expressed as (Scanlan 1978, Jain et al. 1996),

$$D_{ae}(t) = \frac{1}{2}\rho U^2 B\left[KP_1^* \frac{\dot{p}}{U} + KP_2^* \frac{B\dot{\alpha}}{U} + K^2 P_3^* \alpha + K^2 P_4^* \frac{p}{B} + KP_5^* \frac{\dot{h}}{U} + K^2 P_6^* \frac{h}{B} \right], \tag{2.7a}$$

$$L_{ae}(t) = \frac{1}{2}\rho U^2 B\left[KH_1^* \frac{\dot{h}}{U} + KH_2^* \frac{B\dot{\alpha}}{U} + K^2 H_3^* \alpha + K^2 H_4^* \frac{h}{B} + KH_5^* \frac{\dot{p}}{U} + K^2 H_6^* \frac{p}{B} \right], \tag{2.7b}$$

and,

$$M_{ae}(t) = \frac{1}{2}\rho U^2 B^2\left[KA_1^* \frac{\dot{h}}{U} + KA_2^* \frac{B\dot{\alpha}}{U} + K^2 A_3^* \alpha + K^2 A_4^* \frac{h}{B} + KA_5^* \frac{\dot{p}}{U} + K^2 A_6^* \frac{p}{B} \right], \tag{2.7c}$$

where $K = \omega B/U$ represents the reduced circular frequency; p, h and α are the lateral,

vertical and torsional displacements of the bridge section, respectively. P_i^*, H_i^* and A_i^* for i =1, ..., 6, are flutter (or aerodynamic) derivatives; and each overdot denotes one differentiation with respect to time. These derivatives for bridge sections are functions of the reduced frequency K and are estimated using the experimental results obtained from the specialized wind tunnel tests.

2.3 Procedure for evaluating responses

2.3.1 Flutter analysis

Bridge responds to the wind excitations and could become unstable. To assess the responses, the bridge can be represented by a finite element model and the equation of motion is then expressed as,

$$\mathbf{M}\ddot{\mathbf{Y}} + \mathbf{C}\dot{\mathbf{Y}} + \mathbf{K}\mathbf{Y} = \mathbf{F}(t), \tag{2.8}$$

where $\mathbf{M}$ is the global mass matrix, $\mathbf{C}$ is the global structural damping matrix, $\mathbf{K}$ is the global stiffness matrix, $\mathbf{F}(t)$ represents the wind loading vector, and $\mathbf{Y}$ is the global nodal displacement vector.

If the bridge responses due to the aeroelastic self-excited forces only are of interest, $\mathbf{F}(t)$ in Eq. (2.8) is replaced by the global aeroelastic loading vector $\mathbf{F}_{ae}(t)$. This vector can be assembled using a standard finite element method if the load vector for each element of the bridge is known. For example, if the bridge deck of a simply supported bridge is represented by the beam element of length l shown in Figure 2.2, the distributed areoelastic force can be lumped on the nodes and the nodal forces $\mathbf{F}_{ae}^e(t)$ expressed as (Hua et al. 2007),

$$\mathbf{F}_{ae}^e(t) = \mathbf{K}_{ae}^e \mathbf{Y}^e + \mathbf{C}_{ae}^e \dot{\mathbf{Y}}^e \tag{2.9}$$

in which ,

$$\mathbf{K}_{ae}^e = \frac{l}{2}\begin{bmatrix} \mathbf{K}_{ae0}^e & 0 \\ 0 & \mathbf{K}_{ae0}^e \end{bmatrix}, \tag{2.10a}$$

$$\mathbf{C}_{ae}^e = \frac{l}{2}\begin{bmatrix} \mathbf{C}_{ae0}^e & 0 \\ 0 & \mathbf{C}_{ae0}^e \end{bmatrix}, \tag{2.10b}$$

$$\mathbf{K}_{ae0}^{e}=\begin{bmatrix}0 & 0 & 0 & 0 & 0 & 0\\ 0 & C_1K^2P_4^*\frac{1}{B} & C_1K^2P_6^*\frac{1}{B} & C_1K^2P_3^* & 0 & 0\\ 0 & C_1K^2H_6^*\frac{1}{B} & C_1K^2H_4^*\frac{1}{B} & C_1K^2H_3^* & 0 & 0\\ 0 & C_2K^2A_6^*\frac{1}{B} & C_2K^2A_4^*\frac{1}{B} & C_1K^2A_3^* & 0 & 0\\ 0 & 0 & 0 & 0 & 0 & 0\\ 0 & 0 & 0 & 0 & 0 & 0\end{bmatrix}, \tag{2.10c}$$

$$\mathbf{C}_{ae0}^{e}=\begin{bmatrix}0 & 0 & 0 & 0 & 0 & 0\\ 0 & C_1K^2P_1^*\frac{1}{U} & C_1K^2P_5^*\frac{1}{U} & C_1KP_2^*\frac{B}{U} & 0 & 0\\ 0 & C_1KH_5^*\frac{1}{U} & C_1KH_1^*\frac{1}{U} & C_1KH_2^*\frac{B}{U} & 0 & 0\\ 0 & C_2KA_5^*\frac{1}{U} & C_2KA_1^*\frac{1}{U} & C_2KA_2^*\frac{B}{U} & 0 & 0\\ 0 & 0 & 0 & 0 & 0 & 0\\ 0 & 0 & 0 & 0 & 0 & 0\end{bmatrix} \tag{2.10d}$$

in which, $C_1=\rho U^2B/2$, and $C_2=\rho U^2B^2/2$, $\mathbf{K}_{ae}^{e}$ and $\mathbf{C}_{ae}^{e}$ are known as the element aeroelastic stiffness matrix and aeroelastic damping matrix, and $\mathbf{Y}^e=[d_{xi},d_{yi},d_{zi},\theta_{xi},\theta_{yi},\theta_{zi},d_{xj},d_{yj},d_{zj},\theta_{xj},\theta_{yj},\theta_{zj}]^T$ is the 12×1 local nodal displacement vector of the element shown in Figure 2.3. For simplicity, it is assumed that the flutter derivatives for each element of the bridge deck are the same. By assembling $\mathbf{F}_{ae}(t)$ based on the aeroelastic stiffness and damping coefficients of the elements, $\mathbf{F}_{ae}(t)$ can be expressed in terms of the global aeroelastic stiffness matrix $\mathbf{K}_{ae}$ and the global aeroelastic damping matrix $\mathbf{C}_{ae}$,

$$\mathbf{F}_{ae}(t)=\mathbf{K}_{ae}\mathbf{Y}+\mathbf{C}_{ae}\dot{\mathbf{Y}}, \tag{2.11}$$

and Eq. (2.8) can be expressed as,

$$\mathbf{M}\ddot{\mathbf{Y}}+(\mathbf{C}-\mathbf{C}_{ae})\dot{\mathbf{Y}}+(\mathbf{K}-\mathbf{K}_{ae})\mathbf{Y}=0, \tag{2.12}$$

which indicates that the aeroelastic force are incorporated in the stiffness and damping matrix. This is advantageous since it can be modeled using a commercial finite element software such as ANSYS (i.e., Matrix 27, which can have user-specified coefficients of stiffness or damping matrices) to carry out the flutter analysis (i.e., eigenvalue analysis) and to find the critical wind velocity U_{cr} that is associated with the instability. This is illustrated in Figure 2.4 for a simply supported bridge.

To illustrate this approach and the sensitivity of U_{cr} to the numerical modeling, consider a simply supported beam-like bridge with a thin-airfoil cross section and length of 300 m (Hua et al. 2007). It is considered that use of the flutter derivatives of thin-airfoil cross section is adequate. The cross sectional properties of the bridge deck are: width of the bridge deck B =40m; vertical bending rigidity EI_y =2.1×10^6 MPam^4; lateral bending rigidity EI_z =1.8 × 10^7 MPam^4; torsional rigidity GI_t =4.1×10^5 MPam^4; mass density m_b =20,000 kg/m; mass moment of inertia I_m =4.5×10^6 kg·m^2/m. The air density ρ = 1.248 kg/m^3 is considered. By modeling this bridge using ANSYS Parametric Design Language (APDL) (Hua et al. 2007) and considering Theodorsen's theoretical solution of the eight aerodynamic derivatives (i.e., H_i^* and A_i^* for i = 1, 2, 3 and 4) for the thin-airfoil cross section (Scanlan 1993) (see Appendix A), the obtained eigenvalues are shown in Figure 2.5a. These results are obtained by considering that the bridge can be modeled using 30 beam elements, and that use of 26 values of each aerodynamic derivative evaluated at the reduced velocity V (=2π/K) equal to 0, 1, ..., 25 is adequate. The figure shows that the critical wind velocity corresponding to the incipient of positive real part of an eigenvalue equals 137.9 m/s with the corresponding frequency equal to 0.3844 Hz. The unsmoothed solution associated with the complex mode 1 is likely due to numerical inaccuracy. These values differ slightly from those given by Hua et al. (2007) which are 135.1 m/s, and 0.3940 Hz. The reason for the differences is that the aerodynamic derivative H_4^* used by Hua et al. (2007) differs from the one employed in the present study. Furthermore, the results presented by Hua et al. (2007) (reproduced and shown in Figure 2.5b) lead to a constant real part of the eigenvalue of the first mode for the wind velocity U greater than 80m/s, while the results presented in the present study do not follow such a peculiar behavior although it does not affect the estimated critical wind velocity. After detailed inspection of the analyses results, it was concluded that the behavior associated with Hua et al's results was caused by the fact that for their analysis the aerodynamic derivative values for V only up to 10 were considered.

Also, an analysis was carried out to investigate the sensitivity of the critical wind velocity to the number of (finite) elements, n, used to model the bridge deck, and to the number of the discrete values n_{ae} used to represent the aerodynamic derivatives (for V ranging from 0 to 25). For n ranging from 30 to 90, and n_{ae} ranging from 26 to 251, the

differences between the obtained critical wind velocities to that shown in Figure 2.5a is always less than 2%.

It must be emphasized that the example results shown in Figure 2.5 is for a thin-airfoil section rather than a typical bridge section, and it is used to illustrate the use of described approach for flutter analysis. For a typical bridge section, the critical wind speed is much smaller than that shown in the figure.

2.3.2 Buffeting analysis

For the buffeting analysis, consider again that the bridge deck can be modeled using 2 node beam element (i.e., 3-D 2-node line element with rotational degrees of freedom shown in ANSYS) as shown in Figure 2.3. For the element, it is considered that the distributed buffeting force acting along the length can be approximated by the equivalent nodal forces as shown in Figure 2.2, resulting in,

$$\mathbf{F}_b^e = \mathbf{E}_b^e \mathbf{q}^e \tag{2.13}$$

where $\mathbf{F}_b^e$ denotes the nodal forces, $\mathbf{q}^e = \left[u^e(t), w^e(t)\right]^{\mathrm{T}}$ denotes the fluctuating along and cross wind velocities at midpoint of the element, and $\mathbf{E}_b^e$ is given by (Sun et al. 1999),

$$\mathbf{E}_b^e = \begin{bmatrix} 0 & C_1 C_D \frac{l}{U} & C_1 C_L \frac{l}{U} & C_2 C_M \frac{l}{U} & -\frac{C_1 C_L}{6}\frac{l^2}{U} & \frac{C_1 C_D}{6}\frac{l}{U} \\ 0 & \frac{C_1 C_D'}{2}\frac{l}{U} & \frac{C_1 (C_L' + C_D)}{2}\frac{l}{U} & \frac{C_2 C_M'}{2}\frac{l}{U} & -\frac{C_1 (C_L' + C_D)}{12}\frac{l^2}{U} & \frac{C_1 C_D'}{12}\frac{l^2}{U} \\ 0 & C_1 C_D \frac{l}{U} & C_1 C_L \frac{l}{U} & C_2 C_M \frac{l}{U} & \frac{C_1 C_L}{6}\frac{l^2}{U} & -\frac{C_1 C_D}{6}\frac{l}{U} \\ 0 & \frac{C_1 C_D'}{2}\frac{l}{U} & \frac{C_1 (C_L' + C_D)}{2}\frac{l}{U} & \frac{C_2 C_M'}{2}\frac{l}{U} & \frac{C_1 (C_L' + C_D)}{12}\frac{l^2}{U} & -\frac{C_1 C_D'}{12}\frac{l^2}{U} \end{bmatrix}^{\mathrm{T}} \tag{2.14}$$

In deriving the above equation, it is assumed that these coefficients remain unchanged within the element length, and that the fluctuating wind velocities within an element can be represented by their values at the midpoint of the element. Details of the mathematical derivation are included in Appendix B for easy reference.

The nodal forces $\mathbf{F}_b^e$ in the local coordinate for the element are converted into the global coordinate system through the $6(n+1)\times 12$ coordinate transformation matrix $\mathbf{T}^e$ (n denotes the number of elements), and the forces in global coordinate represented by $\mathbf{F}_b^{e,s}$

are given by,

$$\mathbf{F}_b^{e,s} = \mathbf{T}^e \mathbf{F}_b^e \tag{2.15}$$

For the case of simply supported beam considered in this study, the derivation of $\mathbf{T}^e$ is also included in Appendix B. By assembling the buffeting force vector $\mathbf{F}_b^{e,s}$ for all the elements, the global buffeting force vector for the bridge deck $\mathbf{F}_b$ is,

$$\mathbf{F}_b = \sum_{k=1}^{n} \left(\mathbf{T}^e \mathbf{F}_b^e\right)_k = \sum_{k=1}^{n} \left(\mathbf{T}^e \mathbf{E}_b^e \mathbf{q}^e\right)_k = \mathbf{TP} \tag{2.16}$$

where $\mathbf{T} = [(\mathbf{T}^e)_1, (\mathbf{T}^e)_2, \ldots, (\mathbf{T}^e)_k, \ldots, (\mathbf{T}^e)_n]$, $\mathbf{P}^{\mathrm{T}} = \left[(\mathbf{E}_b^e \mathbf{q}^e)_1, (\mathbf{E}_b^e \mathbf{q}^e)_2, \ldots, (\mathbf{E}_b^e \mathbf{q}^e)_k, \ldots, (\mathbf{E}_b^e \mathbf{q}^e)_n\right]^{\mathrm{T}}$, and the subscript k denotes the k-th element.

Since $u^e(t)$ and $w^e(t)$ are stochastic processes that are characterized by their corresponding PSD functions, $\mathbf{F}_b$ represents vector of stochastic processes for given $\mathbf{T}^e$ and $\mathbf{E}_b^e$. In such a case, it can be shown that the spectral density function matrix of $\mathbf{F}_b$, $\mathbf{S}_{FF}(\omega)$, can be expressed as,

$$\mathbf{S}_{FF}(\omega) = \mathbf{T} \begin{bmatrix} \mathbf{S}_{P_1P_1}^e(\omega) & \mathbf{S}_{P_1P_2}^e(\omega) & \cdots & \mathbf{S}_{P_1P_n}^e(\omega) \\ \mathbf{S}_{P_2P_1}^e(\omega) & \mathbf{S}_{P_2P_2}^e(\omega) & \cdots & \mathbf{S}_{P_2P_n}^e(\omega) \\ \vdots & \vdots & \ddots & \vdots \\ \mathbf{S}_{P_nP_1}^e(\omega) & \mathbf{S}_{P_nP_1}^e(\omega) & \cdots & \mathbf{S}_{P_nP_n}^e(\omega) \end{bmatrix} \mathbf{T}^{\mathrm{T}} \tag{2.17a}$$

where the submatrix $\mathbf{S}_{P_iP_j}^e(\omega)$ representing the 12×12 cross-spectral density function matrix of the nodal forces on the i-th element and the j-th element, is given by

$$\mathbf{S}_{P_iP_j}^e(\omega) = \left(\mathbf{E}_b^e\right)_i \mathbf{S}_{q_iq_j}^e(\omega) \left[\left(\mathbf{E}_b^e\right)_j\right]^{\mathrm{T}} \tag{2.17b}$$

in which,

$$\mathbf{S}_{q_iq_j}^e(\omega) = \begin{bmatrix} S_{uu}(s_i, s_j, \omega) & S_{uw}(s_i, s_j, \omega) \\ S_{wu}(s_i, s_j, \omega) & S_{ww}(s_i, s_j, \omega) \end{bmatrix} \tag{2.17c}$$

s_i and s_j are the midpoints of the i-th and j-th element, respectively. The quantities $S_{uu}(s_i, s_j, \omega)$, and $S_{ww}(s_i, s_j, \omega)$ were already given in Eq. (2.5), and $S_{uw}(s_i, s_j, \omega)$ and $S_{wu}(s_i, s_j, \omega)$ are assumed to be zero.

There are several approaches that one could adopt for solving Eq. (2.8) when $\mathbf{F}$ equals $\mathbf{F}_b$, which is characterized by the cross-spectral density matrix shown in Eq. (2.17a). The

approaches can be classified as time domain approach and frequency domain approach. The time domain approach uses simulated time histories of wind velocities, and determines the response time history; the frequency domain approach uses Fourier transformation and the concept of PSD function, and evaluates the probabilistic characterization of the responses, such as the mean and standard deviation. For frequency domain analysis, there are several ways to determine the buffeting responses of the bridge deck, such as the square-root-of-the-sum-of-squares (SRSS) method, the complete quadratic combination (CQC) method and the pseudo-excitation method. In this study, for easy implementation we adopted the pseudo-excitation method (Sun et al. 1999). For the selected frequencies, this method basically decomposes the spectral density matrix of the buffeting force, carries out structural analysis under harmonic excitations, and evaluates the values of the PSD function of the response.

More specifically, the spectral density matrix of the buffeting force $\mathbf{S}_{FF}(\omega)$, which is a real symmetric matrix with the dimension $6(n+1)\times 6(n+1)$, can be decomposed as,

$$\mathbf{S}_{FF}(\omega) = \mathbf{L}^{*}(\omega)\mathbf{D}(\omega)\mathbf{L}^{T}(\omega) \tag{2.18a}$$

in which $\mathbf{L}(\omega)$ is a low triangular matrix with dimension of $6(n+1)\times m$, m is the rank of $\mathbf{S}_{FF}(\omega)$, $\mathbf{D}(\omega)$ i s a $m\times m$ diagonal matrix, and the superscript $\star$ denotes the complex conjugate.

Let $\mathbf{L}_k(\omega)$ denote the k-th column of $\mathbf{L}(\omega)$ and $d_k(\omega)$ denote the k-th diagonal element of $\mathbf{D}(\omega)$. $\mathbf{S}_{FF}(\omega)$ shown in Eq. (2.18a) can then be re-written as,

$$\mathbf{S}_{FF}(\omega) = \sum_{k=1}^{m} d_k(\omega)\mathbf{L}_k^{*}(\omega)\mathbf{L}_k^{T}(\omega) \tag{2.18b}$$

Then the spectral density function of $\mathbf{Y}$, $\mathbf{S}_{YY}(\omega)$, is given by (Sun at el. 1996),

$$\mathbf{S}_{YY}(\omega) = \sum_{k=1}^{m} \mathbf{d}_k(\omega)\mathbf{Y}_k^{*}(\omega)\mathbf{Y}_k^{T}(\omega) \tag{2.19}$$

where,

$$\mathbf{Y}_k(\omega) = \mathbf{H}(i\omega)\mathbf{f}_k(\omega), \tag{2.20a}$$

$\mathbf{H}(i\omega)$ is the transfer function for the bridge system represented by Eq. (2.8) and can be written as,

$$\mathbf{H}(i\omega) = \left[-\omega^2\mathbf{M} + i\omega(\mathbf{C} - \mathbf{C}_{ae}) + (\mathbf{K} - \mathbf{K}_{ae})\right]^{-1} \quad (2.20b)$$

and,

$$\mathbf{f}_k(\omega,t) = \mathbf{L}_k(\omega)\exp(i\omega t) \quad (k=1,2.....m) \quad (2.20c)$$

After establishing the bridge model in ANSYS, the $6(n+1)$ vector $\mathbf{f}_k(\omega,t)$ can be applied to the corresponding degrees of freedom of the bridge system to evaluate its responses due to the buffeting force, and $\mathbf{S}_{YY}(\omega)$ according to Eq. (2.19).

To illustrate the pseudo-excitation method for evaluating $\mathbf{S}_{YY}(\omega)$, consider the same simple bridge shown in Figure 2.4. The structural damping ratio for each natural vibration mode was assumed to be 0.005. The static coefficients of the bridge deck section at the zero angle of attack are $C_D = 0.0697$, $C_L = 0.128$, $C_M = -0.0074$, $C_D' = 0$, $C_L' = -5.56$ and $C_M' = 1.27$; the elevation of the bridge deck was considered to be 60 m above the ground (i.e., $z = 60$ m); the shear friction velocity u_* was assumed to be 1.84 m/s; and the exponential decay coefficients C_x and C_w were taken equal to 16 and 8, respectively (Ding et al. 2002). The cross spectra between u and w is neglected in this study. $\mathbf{E}_b^e$ is assumed to be the same for all the elements. The structural analysis was carried out using the pseudo-excitation method for the frequency ranging from 0.0003 Hz to 1.6 Hz with an increment of 0.0003 Hz, and the obtained PSD functions of the responses at midspan of the bridge under both along and cross wind fluctuations (which are obtained by using the Frontal Solver option in the ANSYS) are shown in Figure 2.6 for a mean wind speed of 40m/s.

2.3.3 Probabilistic characterization of the peak responses

Once the PSD function of the response of interest r, such as the bridge midspan horizontal, vertical or torsional displacement, is known (e.g., see Figure 2.6), the remaining task is to assess the statistics of peak response or mean peak response of r from its PSD function and its response due to mean wind speed. Let η denote the peak response of r over a period T (s). According to Davenport (1964), the probability distribution of peak response η can be approximated by the Gumbel probability distribution expressed as,

$$F(\eta) = \exp\left(-\exp\left(-\frac{\sqrt{2\ln(v_0^+ T)}}{\sigma_r}\left(\eta - \bar{r} - \sigma_r\sqrt{2\ln(v_0^+ T)}\right)\right)\right) \tag{2.21a}$$

where $\bar{r}$ is the response due to mean wind speed, the zero up-crossing rate v_0^+ is given by,

$$v_0^+ = \frac{1}{2\pi}\frac{\sigma_{\dot{r}}}{\sigma_r} \tag{2.21b}$$

and σ_r and $\sigma_{\dot{r}}$ are the standard deviations of r and its temporal derivative, respectively that can be calculated using,

$$\sigma_r^2 = \int_0^\infty S_r(\omega)d\omega \tag{2.22a}$$

and,

$$\sigma_{\dot{r}}^2 = \int_0^\infty \omega^2 S_r(\omega)d\omega \tag{2.22b}$$

in which $S_r(\omega)$ denotes the PSD function of r.

The mean peak response (i.e., the mean of η), m_η, based on the Gumbel probability distribution shown in Eq. (2.21) is,

$$m_\eta = \bar{r} + g_p\sigma_r \tag{2.23}$$

where $g_p = \sqrt{2\ln(v_0^+ T)} + 0.577/\sqrt{2\ln(v_0^+ T)}$ is known as the peak factor, and

$$g_T = 1 + v_r g_P \tag{2.24}$$

is known as the gust factor, in which v_r equals $\sigma_r/\bar{r}$, representing the coefficient of variation of the response.

For example, by using the PSD function of the midspan displacement shown in Figure 2.6 and the above equations the obtained standard deviation for the horizontal displacement at the midspan, p, equals 3.6×10^{-3} (m). The corresponding peak factor and gust factor are 3.94 and 1.87.

2.4 Numerical results

2.4.1 Responses to buffeting force

2.4.1.1 Responses to along wind excitations

Based on the formulation given in the previous section, a sensitivity analysis was conducted to investigate the impact of each of the parameters on the obtained standard

deviation of the displacement due to fluctuating wind loading.

For the analysis, it can be shown (see Appendix C) that if the bridge is modeled as a simply supported beam with uniform cross sectional properties and equal damping ratio for each natural vibration mode ξ, the normalized standard deviation, $\tilde{\sigma}_p$, for the horizontal displacement caused by the fluctuating along wind defined by,

$$\tilde{\sigma}_p = \sigma_p / (\bar{p} I_u \pi) \tag{2.25}$$

depends only on $c' = C_x L / z$ and $f_{p1} = z\omega_{p1} / (2\pi U)$, where I_u denotes the turbulence intensity of the longitudinal fluctuation, $\bar{p} = \frac{4 D_s L^4}{\pi^5 E I_z}$ represents the horizontal response to the mean wind pressure by considering only the first vibration mode, EI_z is the laterally bending rigidity of the bridge deck and ω_{p1} is the first horizontal natural vibration frequency. This largely simplifies the parametric study since we only need to vary the scaled exponential decay coefficient c' and the f_{p1} (i.e., Monin coordinate evaluated at the fundamental frequency).

The calculated values of $\tilde{\sigma}_p$ based on the formulation shown in Section 3.2 are shown in Figure 2.7a for a few selected c' and a range of f_{p1} values. The figure indicates that as c' increases (i.e., the correlation decreases) the normalized standard deviation decreases, which is expected.

A simple equation for $\tilde{\sigma}_p$ that is derived based on an often used approximation given in Davenport (1981) and Davenport and King (1982) can be expressed as (see Appendix C),

$$\tilde{\sigma}_p \approx \tilde{\sigma}(0.045, f_{p1}), \tag{2.26a}$$

where,

$$\tilde{\sigma}(b, f) = \sqrt{\frac{1}{\pi^2/4 + L/\lambda} + \frac{1}{\pi^2/4 + c' f} \frac{\pi}{4(\xi + \xi_a)} b f^{-2/3}}, \tag{2.26b}$$

ξ_a represents the aerodynamic damping ratio and λ is a constant known as the integral spanwise turbulence scale, which is equal to about 60 m. It is instructive to compare this solution with those depicted in Figure 2.7a. Such a comparison is shown in Figure 2.7b

for a bridge with a span length of 100 m. The results shown in the figure indicates that the use of the approximation shown in Eq. (2.26) introduces a maximum relative error of about 16%. Further comparison indicates that the error is an increasing function of the span length. For L equal to 150, 200 and 250 m and for c' less than about 10, the maximum error is about 23%, 28% and 32%, respectively. This implies that for such cases the higher mode or cross modal contribution becomes more significant. Also, inspection of the results depicted in Figure 2.7b indicates that the accuracy of Eq. (2.26) depends on the values of c' and f_{p1}.

The derived approximation shown in Eq. (2.26) is based on Davenport's PSD function. If the PSD function shown in Eq. (2.4a) is used, for consistency, in deriving the approximate equation, the value of b equal to 0.045 is to be replaced by 0.049, and a slight improved match between the approximation and the results shown in Figure 2.7a can be observed.

Similarly, we can derive the expressions for the normalized standard deviations for the vertical and the torsional displacements. For comparison purpose, these expressions are summarized in Table 2.1. The approximations for the normalized standard deviations for responses p, h and α are identical, while it can be shown that theoretically $\tilde{\sigma}_p$ is identical to $\tilde{\sigma}_h$ but $\tilde{\sigma}_\alpha$ differs from $\tilde{\sigma}_p$. Values of $\tilde{\sigma}_\alpha$ obtained by numerical analysis (i.e., by using the finite element method and random vibration theory) is depicted in Figure 2.8a; comparison of the numerical solution to those calculated using the approximate expression with L equal to 100 m is shown in Figure 2.8b. The results shown in the figure indicate that the adequacy of the approximation for $\tilde{\sigma}_\alpha$ is similar to that for $\tilde{\sigma}_p$.

Since comparison of the results shown in Figures 2.7 and 2.8 suggests that the difference between $\tilde{\sigma}_\alpha$ and $\tilde{\sigma}_p$ is negligible, one can use $\tilde{\sigma}_p$ to represent $\tilde{\sigma}_\alpha$ as well. This is advantageous because the gust factor for horizontal, vertical or torsional displacement under fluctuating along wind, g_T, can be represented by,

$$g_T = 1 + g_P \times I_u \pi \tilde{\sigma}_p . \tag{2.27}$$

The calculated peak factor g_p and the gust factor g_T for typical values of I_u equal to 0.11 and 0.15 are shown in Figure 2.9, where the abscissa f_1 represents f_{p1}, f_{h1} or $f_{\alpha 1}$; while the

ordinate represents the gust factor for the horizontal, vertical or torsional displacement under fluctuating along wind loading. Figure 2.9 indicates that the estimated g_T based on Eq. (2.26) differs from that obtained based on the normalized standard deviation shown in Figures 2.7a and 2.8a. The difference depends on both c' and f_1.

2.4.1.2 Responses to cross wind excitations

As shown in Eqs. (2.3) and (2.4), the buffeting force due to cross wind differs from those due to along wind; the PSD function for the cross wind is not the same as that for the along wind. Therefore, the results shown in Figure 2.7 and 2.8 are not applicable to those associated with the cross wind. Let σ_{pc}, σ_{hc} and σ_{ac} denote the standard deviations of the horizontal, vertical and torsional responses at midspan due to cross wind fluctuation. Similar to Section 2.4.1.1, their corresponding normalized values, denoted by $\tilde{\sigma}_{pc}$, $\tilde{\sigma}_{hc}$ and $\tilde{\sigma}_{ac}$, respectively, which are defined in Table 2.1, are calculated numerically and shown in Figures 2.10 and 2.11 for several values of $c'=C_w L/z$. In these figures, these estimated values are compared with their corresponding approximations given in Table 2.1. Inspection of the results shown in these figures to those shown in Figures 2.7 and 2.8 indicates that the conclusions drawn from the results for the along wind excitations are equally applicable to those for the cross wind excitations.

Again, the derived approximation shown in Eq. (2.26) is based on a PSD function that is different from the adopted one shown in Eq. (2.4b). For consistency, if Eq. (2.4b) is used to derive the approximation, the value of b equal to 0.24 is to be replaced by 0.20, and a slight improved match can be observed.

For the cross wind excitations, the gust factor for the horizontal, vertical or torsional displacement g_T,

$$g_T = 1 + g_P \times \beta_p I_u \pi \tilde{\sigma}_{pc}, \tag{2.28}$$

can be calculated by using $\tilde{\sigma}_{pc}$ values shown in Figure 2.10 and g_p values shown in Figure 2.12a for given values of β_p and I_u. Since β_p depends on the considered bridge, values of $g_P \times I_u \pi \tilde{\sigma}_{pc}$ for typical values of I_u equal to 0.11 and 0.15 rather than g_T are plotted in Figures 2.12b and 2.12c to indicate the magnitude of the buffeting force induced response.

2.4.2 Impact of aeroelastic phenomena on estimated responses

The results presented in the previous section do not include the effect of aeroelastic self-excited contributions discussed in Section 2.3.1. To investigate the impact of this effect on the estimated bridge responses, it is considered that the flutter derivatives given by Theodorsen's solution for the thin airfoil are applicable, and that only H_i^* and A_i^*, for $i = 1, 2, 3$ and 4, are of interest since usually the effect of aeroelastic self-excited force on the lateral response is small. Table 2.2 shows a set of cases used to assess the impact of the flutter derivatives on the estimated normalized standard deviations. For the analysis, the buffeting forces due to along wind and cross wind excitations are considered. The obtained normalized standard deviations by including/excluding the self-excited contributions are shown in Table 2.2 as well. Comparison of these standard deviations suggests that the consideration of aeroelastic self-excited forces (for time-averaged wind speed much less than the critical wind speed) decreases the normalized standard deviations. In other words, the estimated responses are conservative by ignoring the aeroelastic self-excited forces, provided that the wind velocity is lower than the critical wind velocity. Furthermore, using the structural properties and the flutter derivatives, values of the aerodynamic damping ξ_a for some of the cases are calculated and used to estimate the approximate normalized standard deviations according to the equations shown in Table 2.2. The calculated values are compared to those obtained based on the finite element method and random vibration theory in Table 2.2. The comparison indicates that:

a) The latter is greater than the former for the cases without or with the consideration of aeroelastic self-excited forces for the fluctuating along wind excitations; this trend is reversed for the fluctuating cross wind excitations; and
b) In all cases, the inaccuracy is more pronounced by considering aeroelastic self-excited forces.

The observed differences in the estimated gust factors shown in Figures 2.9 and 2.12 and in Table 2.2 could have implications in bridge design or bridge design code calibration if they are not properly taken into account. Furthermore, we note that an improved equation to predict the gust factor could be achieved by modifying L/λ shown in Eq. (2.26b). However, this is not pursued in this study.

2.5 Conclusions

A parametric study of the gust responses of bridges to spatio-temporally varying wind excitations was carried out. For the analysis, the bridge was modeled using the finite element method and the wind excitations were represented by their power spectral density functions. It was shown that the standard deviation of a response of interest, such as the bridge midspan horizontal, vertical or torsional displacement, is directly proportional to a normalized standard deviation, which depends on two parameters: a scaled exponential decay coefficient for the spanwise coherence of fluctuating winds and Monin coordinate evaluated at the frequency of the first vibration mode. This largely simplifies the parametric investigation and also allows us to provide a set of gust factors considering spatio-temporally varying fluctuating winds such as those shown in Figures 2.9 and 2.12. It is recommended that the estimated gust factors to be implemented in bridge design codes.

Numerical results suggest that an often used practical approximation underestimates the gust factor. The underestimation depends on the spanwise coherence of the fluctuating wind, and is more significant for an increased bridge span length. Furthermore, the approximation becomes increasingly biased if the effect of aeroelastic self-excited contributions is considered.

References

Caracoglia, L. and Jones, N.P. (2003), "Time domain vs. frequency domain characterization of aeroelastic forces for bridge deck sections", Journal of Wind Engineering & Industrial Aerodynamics, Vol.91(3), 371-402.

Chen, X, Matsumoto, M. and Kareem, A. (2000), "Time Domain Flutter and Buffeting Response Analysis of Bridges", Journal of Engineering Mechanics, Vol.126(1), 7-16.

Davenport, A.G. (1966), "The action of wind on suspension bridge", Proc. Int'l Conf. Suspension bridge, Lisbon, 79-100.

Davenport, A. G. (1981), "Reliability of long span bridges under wind loading", Proceedings of ICOSSAR '81, Trondheim, Norway, 679-694.

Davenport, A.G. (1962), "Buffeting of a suspension bridge by storm winds", Journal of Structural Engineering, ASCE 1962; 88(ST3), 233-68.

Davenport, A.G., (1964), "Note on the distribution of the largest value of a random function with application to gust loading", Proceedings-Institution of Civil Engineers, Vol. 24, 187-196.

Davenport, A.G. (1983), "The Relationship of Reliability to Wind Loading", Journal of Wind Engineering & Industrial Aerodynamics, Vol.13, 3-27.

Davenport, A.G. and King, J.P.C. (1982), "The incorporation of dynamic wind loads into the design specification for long span bridges", ACE Fall Convention and Structures Congress, New Orleans, Louisiana.

Davenport, A.G.(1966), "The action of wind on suspension bridges", Keynote Paper, Intnl. Symp. Suspension bridges, Lisbon, Portugal

Ding, Q., Chen A. and Xiang, H. (2002), "Coupled buffeting response analysis of long-span bridges by the CQC approach", Structural Engineering and Mechanics, Vol. 14(5), 505-520.

Dyrbye, C. and Hansen, S.O. Wind Loads on Structures. Wiley: New York, 1997.

Ge, Y.J. and Tanaka, H. (2000), "Aerodynamic flutter analysis of cable-supported bridges by multi-mode and fullmode approaches", Journal of Wind Engineering & Industrial Aerodynamics, Vol. 86, 125–153.

Hua, X.G., Chen, Z.Q., Ni, Y.Q., and Ko, J.M. (2007), "Flutter analysis of long-span bridges using ANSYS", Wind and Structures, Vol. 10(1), 61-82.

Jain, A., Jones, N.P., and Scanlan, R.H. (1996), "Coupled flutter and buffeting analysis of long-span bridges", Journal of Structural Engineering, ASCE, Vol.122(7), 716-725.

Kaimal, J.C., Wyngaard, J.C., Izumi, Y., Cote, O.R. (1972), "Spectral characteristics of surface-layer turbulence", Journal of the Royal Meteorological Society., Vol. 98(417), 563-589.

Miyata, T., Yamada, H., Boonyapinyo, V. and Santos, J.C. (1995),"Analytical investigation on the response of a very long suspension bridge under gusty wind", Proceedings of Ninth ICWE, New Delhi, Vol. 2 , 1006-1017.

Scanlan, R.H.(1993), "Problematic in formulation of wind-force model for bridge decks", Journal of Structural Engineering, ASCE, Vol. 119(7), 1433-1446.

Scanlan, R.H. and Jones, N.P. (1990), "Aeroelastic analysis of cable-stayed bridges", Journal of Structural Engineering, ASCE, Vol.116(2), 229-297

Scanlan, R.H. and Tomko, J.J. (1971), "Airfoil and bridge deck flutter derivatives", Journal of the Engineering Mechanics Division, ASCE, Vol. 97(EM6), 1717-1737.

Simiu, E. and Scanlan, R.H. (1996), Wind effects on structures, fundamentals and application to design, New York: John Wiley

Sun, D.K., Xu,Y.L., Ko, J.M, Lin, J.H. (1999), "Fully coupled buffeting analysis of long-span cable-supported bridges: formulation", Journal of Sound and Vibration, Vol. 228(3), 569-588.

Table 2.1 Derived equations for estimating the standard deviations of along wind induced responses

Responses	Horizontal	Vertical	Torsion
Mean[1]	$\bar{p} = 4D_s L^4/(\pi^5 EI_z)$	$\bar{h} = 4L_s L^4/(\pi^5 EI_y)$	$\bar{\alpha} = 4M_s L^2/(\pi^3 GI_t)$
Standard deviation for along wind	$\sigma_p = \tilde{\sigma}_p(\bar{p} I_u \pi)$	$\sigma_h = \tilde{\sigma}_h(\bar{h} I_u \pi)$	$\sigma_\alpha = \tilde{\sigma}_\alpha(\bar{\alpha} I_u \pi)$
Approximate normalized standard deviation for along wind excitations[2,3]	$\tilde{\sigma}_p \approx \tilde{\sigma}(0.045, f_{p1})$, $f_{p1} = z\omega_{p1}/(2\pi U)$	$\tilde{\sigma}_h \approx \tilde{\sigma}(0.045, f_{h1})$ $f_{h1} = z\omega_{h1}/(2\pi U)$	$\tilde{\sigma}_\alpha \approx \tilde{\sigma}(0.045, f_{\alpha 1})$, $f_{\alpha 1} = z\omega_{\alpha 1}/(2\pi U)$
Numerically evaluate normalized standard deviation for along wind excitations	See Figure 2.7a	See Figure 2.7a	See Figure 2.8a
Standard deviation for cross wind excitations[4]	$\sigma_{pc} = \tilde{\sigma}_{pc}(\beta_p \bar{p} I_u \pi)$, $\beta_p = \left\lvert \frac{\sigma_w}{\sigma_u} \frac{C_D'}{2C_D} \right\rvert$	$\sigma_{hc} = \tilde{\sigma}_{hc}(\beta_h \bar{h} I_u \pi)$, $\beta_h = \left\lvert \frac{\sigma_w}{\sigma_u} \frac{(C_L' + C_D)}{2C_L} \right\rvert$	$\sigma_{\alpha c} = \tilde{\sigma}_{\alpha c}(\beta_\alpha \bar{\alpha} I_u \pi)$, $\beta_\alpha = \left\lvert \frac{\sigma_w}{\sigma_u} \frac{C_M'}{2C_M} \right\rvert$
Approximate normalized standard deviation for cross wind excitations[5]	$\tilde{\sigma}_{pc} \approx \tilde{\sigma}(0.24, f_{p1})$	$\tilde{\sigma}_{hc} \approx \tilde{\sigma}(0.24, f_{h1})$	$\tilde{\sigma}_{\alpha c} \approx \tilde{\sigma}(0.24, f_{\alpha 1})$
Numerically evaluate normalized standard deviation for cross wind excitations	See Figure 2.10a	See Figure 2.10a	See Figure 2.11a
Aerodynamic damping[6] ξ_a		$-\rho B^2 H_1^*\left(\frac{\omega_{h1} B}{U}\right)/(4m)$	$-\rho B^4 A_2^*\left(\frac{\omega_{\alpha 1} B}{U}\right)/(4I_m)$

Note 1) Response to the mean wind pressure by considering only the first vibration mode; 2) ω_{p1}, ω_{h1} and $\omega_{\alpha 1}$ are the first vibration frequency for horizontal, vertical and torsional responses, respectively; 3) Approximations are for the value of the non-dimensional Monin coordinate evaluated at first vibration mode greater than about 0.5; for along wind fluctuation $c' = C_x L/z$; 4) For the adopted spectrum the ratio of σ_w to σ_u equals 0.532 (i.e., $\sigma_w/\sigma_u = \sqrt{1.7/6}$); 5) for cross wind fluctuation $c' = C_w L/z$ and 6) the equations for aerodynamic damping are taken from Davenport and King (1982), $H_1^*\left(\frac{\omega_{h1} B}{U}\right)$ represents value of H_1^* evaluated at $\omega_{h1} B/U$, and $A_2^*\left(\frac{\omega_{\alpha 1} B}{U}\right)$ represents value of A_2^* evaluated at $\omega_{\alpha 1} B/U$.

Table 2.2a Sensitivity of normalized responses due to fluctuating along wind to structural and wind characteristics.

Modified Variables		f_{p1}	$\tilde{\sigma}_p$	f_{h1}	$\tilde{\sigma}_h$	Approx. solution[2] for $\tilde{\sigma}_h$	$f_{\alpha 1}$	$\tilde{\sigma}_\alpha$	Approx. solution[2] for $\tilde{\sigma}_\alpha$
	Base Case[1]	0.785	0.628	0.268	0.998, 0.505	0.919, 0.418	0.755	0.630, 0.537	0.519, 0.415
m_b (10^4 kg/m)	$m_b = 1.6$	0.878	0.611	0.300	0.938, 0.496	0.854, 0.407	0.755	0.630, 0.539	0.519, 0.415
	$m_b = 2.4$	0.717	0.645	0.245	1.052, 0.515	0.976, 0.430	0.755	0.630, 0.534	0.519 0.415
I_m (10^4 kgm^2/m)	$I_m = 360$	0.785	0.628	0.268	0.998, 0.505	0.919, 0.418	0.844	0.611, 0.522	0.497, 0.405
	$I_m = 540$	0.785	0.628	0.268	0.998, 0.505	0.919 0.418	0.689	0.648, 0.550	0.540, 0.425
B (m)	$B = 32$	0.785	0.628	0.268	0.998, 0.513	0.919, 0.427	0.755	0.630, 0.560	0.519, 0.437
	$B = 48$	0.785	0.628	0.268	0.998, 0.500	0.919, 0.412	0.755	0.630, 0.520	0.519, 0.400
U (m/s)	$U = 32$	0.982	0.595	0.335	0.884, 0.577	0.796, 0.413	0.943	0.595, 0.591	0.478, 0.408
	$U = 48$	0.655	0.663	0.224	1.109, 0.578	1.038, 0.422	0.629	0.668, 0.656	0.563, 0.422
I_y (m^4)	$I_y = 8$	0.785	0.628	0.240	1.064, 0.506	0.989, 0.421	0.755	0.630, 0.539	0.519, 0.415
	$I_y = 12$	0.785	0.628	0.294	0.949, 0.505	0.866, 0.416	0.755	0.630, 0.534	0.519, 0.415
I_t (m^4)	$I_t = 4.06$	0.785	0.628	0.268	0.998, 0.505	0.919, 0.418	0.675	0.652, 0.544	0.545, 0.419
	$I_t = 6.09$	0.785	0.628	0.268	0.998, 0.505	0.919, 0.418	0.827	0.614, 0.530	0.501, 0.412
L (m)	$L = 240$	1.227	0.571	0.419	0.792, 0.505	0.696, 0.408	0.943	0.595, 0.518	0.478, 0.408
	$L = 360$	0.545	0.708	0.186	1.237, 0.506	1.175, 0.426	0.629	0.668, 0.564	0.563, 0.422

Note 1) For the base case, (m_b, I_m, B, U, I_y, I_t ,L)=(2.0, 400, 40, 40, 10, 5.08, 300), and C_x equals 16; For $\tilde{\sigma}_h$ and $\tilde{\sigma}_\alpha$, the first and second entries represent the results without and with aerodynamic derivatives, respectively; and 2) these values are calculated according to equations shown in Table 2.1.

Table 2.2b Sensitivity of normalized responses due to fluctuating cross wind to structural and wind characteristics.

Modified Variables		f_{p1}	$\tilde{\sigma}_p$	f_{h1}	$\tilde{\sigma}_{hc}$	Approx. solution[2] for $\tilde{\sigma}_{hc}$	$f_{\alpha 1}$	$\tilde{\sigma}_{\alpha c}$	Approx. solution[2] for $\tilde{\sigma}_{\alpha c}$
	Base Case[1]	0.785		0.268	1.881, 0.527	2.646, 0.728	0.755	1.118, 0.693	1.236, 0.728
m_b (10^4 kg/m)	$m_b = 1.6$	0.878		0.300	1.804, 0.500	2.439, 0.664	0.755	1.116, 0.695	1.236, 0.728
	$m_b = 2.4$	0.717		0.245	1.940, 0.548	2.826, 0.787	0.755	1.116, 0.688	1.236, 0.728
I_m (10^4 kgm^2/m)	$I_m = 360$	0.785		0.268	1.881, 0.525	2.646, 0.728	0.844	1.048, 0.636	1.140, 0.667
	$I_m = 540$	0.785		0.268	1.881, 0.526	2.646, 0.728	0.689	1.178, 0.742	1.321, 0.784
B (m)	$B = 32$	0.785		0.268	1.881, 0.559	2.646, 0.776	0.755	1.118, 0.800	1.236, 0.850
	$B = 48$	0.785		0.268	1.881, 0.504	2.646, 0.690	0.755	1.118, 0.605	1.236, 0.634
U (m/s)	$U = 32$	0.982		0.335	1.721, 0.548	2.248, 0.704	0.943	0.983, 0.652	1.053, 0.683
	$U = 48$	0.655		0.224	1.994, 0.500	3.017, 0.745	0.629	1.242, 0.724	1.412, 0.762
I_y (m^4)	$I_y = 8$	0.785		0.240	1.953, 0.509	2.868, 0.738	0.755	1.118, 0.690	1.236, 0.728
	$I_y = 12$	0.785		0.294	1.818, 0.538	2.476, 0.718	0.755	1.118, 0.692	1.236, 0.728
I_t (m^4)	$I_t = 4.06$	0.785		0.268	1.881, 0.528	2.646, 0.728	0.675	1.191, 0.713	1.340, 0.749
	$I_t = 6.09$	0.785		0.268	1.881, 0.524	2.646, 0.728	0.827	1.059, 0.674	1.157, 0.710
L (m)	$L = 240$	1.227		0.419	1.549, 0.562	1.906, 0.677	0.943	0.983, 0.654	1.053, 0.683
	$L = 360$	0.545		0.186	2.084, 0.466	3.433, 0.760	0.629	1.242, 0.723	1.412, 0.762

Note 1) For the base case, (m_b, I_m, B, U, I_y, I_t , L)=(2.0, 400, 40, 40, 10, 5.08, 300) and C_w equals 8; For $\tilde{\sigma}_{hc}$ and $\tilde{\sigma}_{\alpha c}$, the first and second entries represent the results without and with aerodynamic derivatives, respectively; and 2) these values are calculated according to equations shown in Table 2.1.

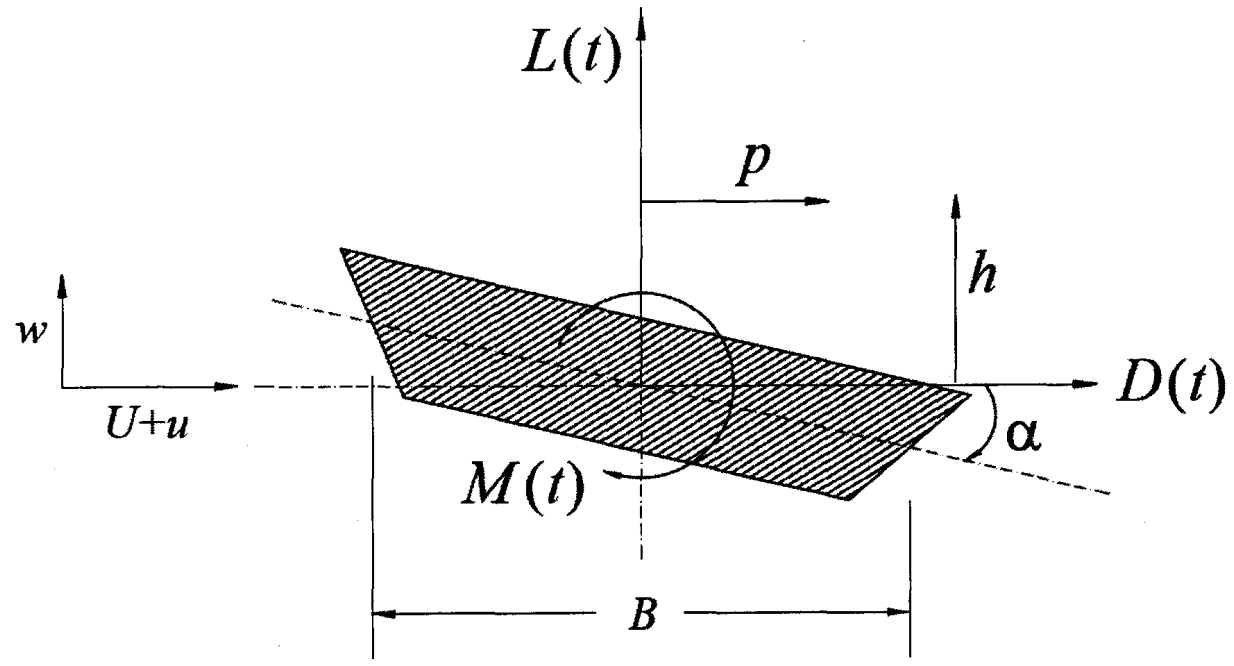

Figure 2.1 The wind actions on the deck section.

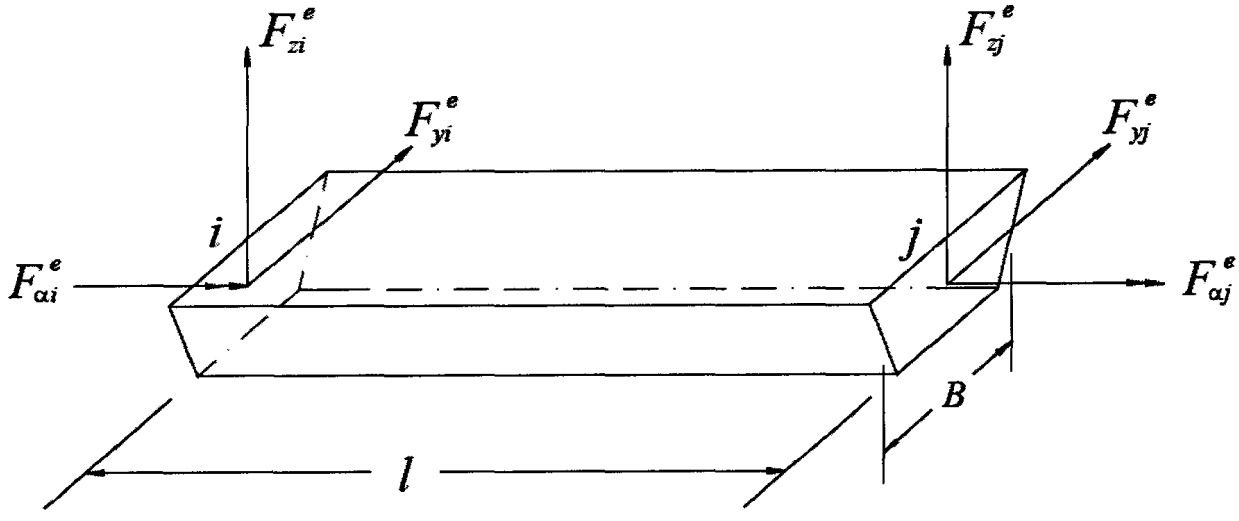

Figure 2.2 The lumped forces on the beam element.

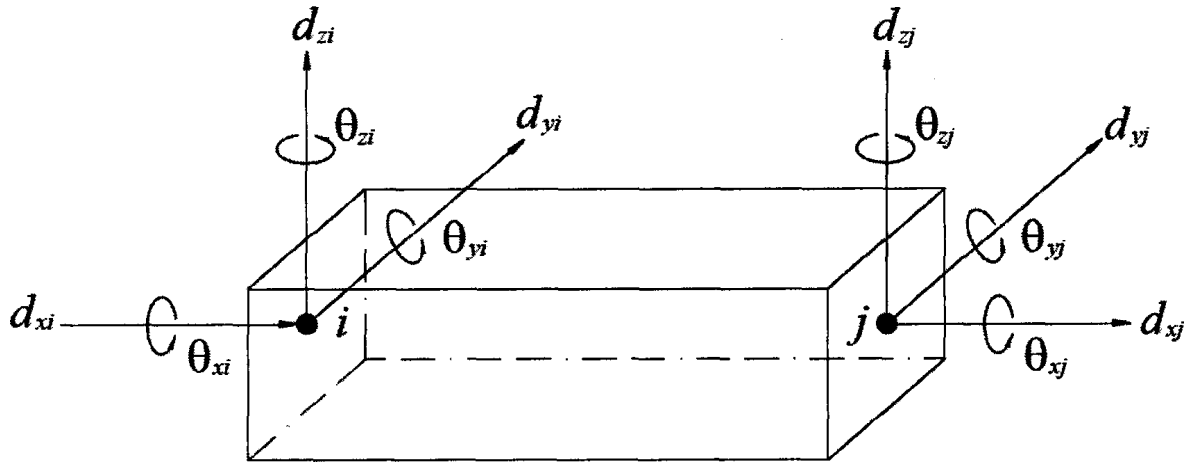

Figure 2.3 Illustration and adopted displacement notations for the two-node beam element.

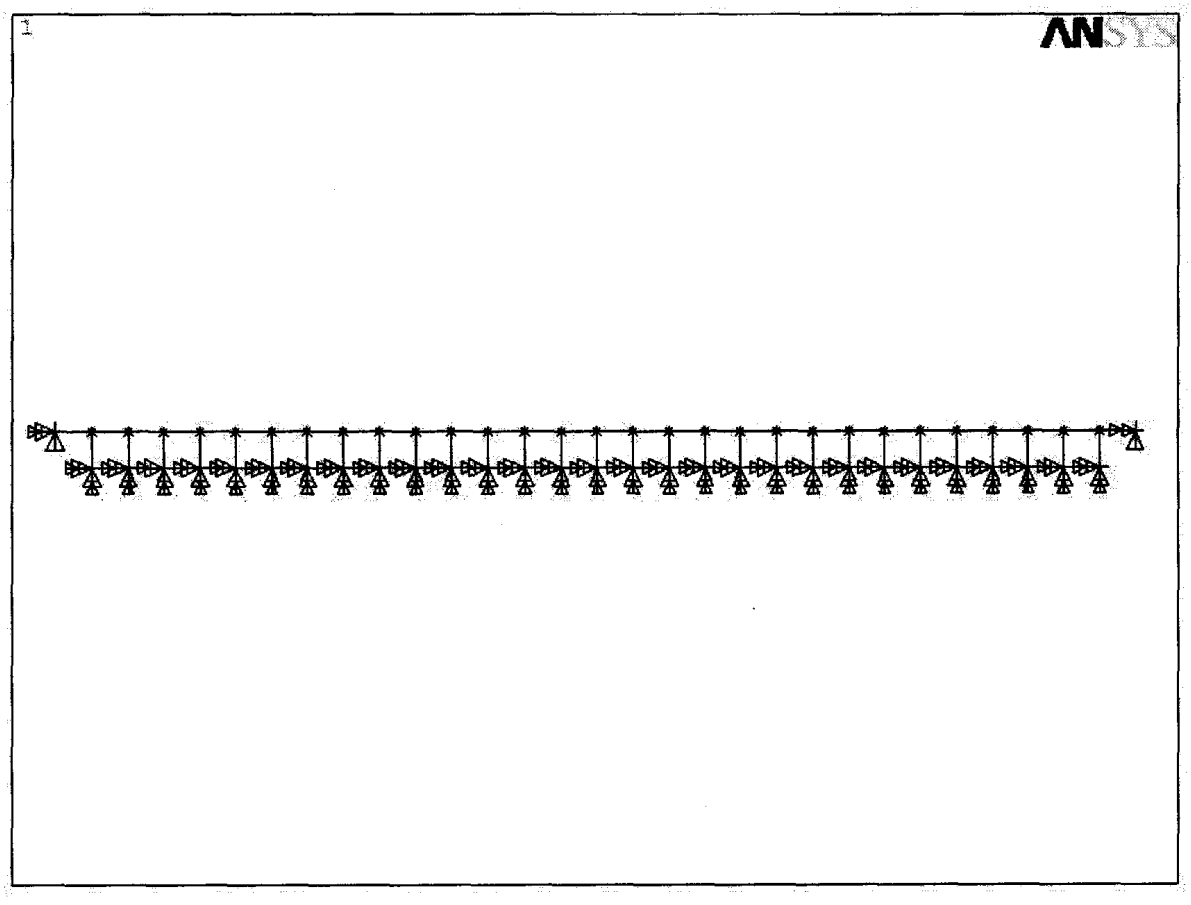

Figure 2.4 The finite element model of the bridge deck.

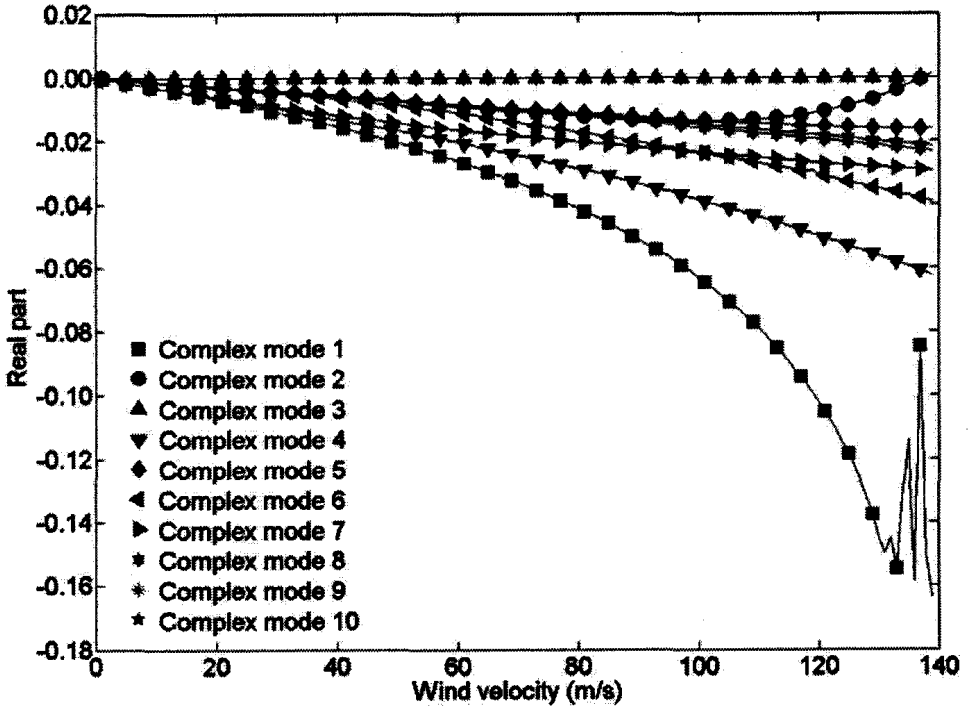

(a) Aerodynamic derivatives are specified for V up to 25

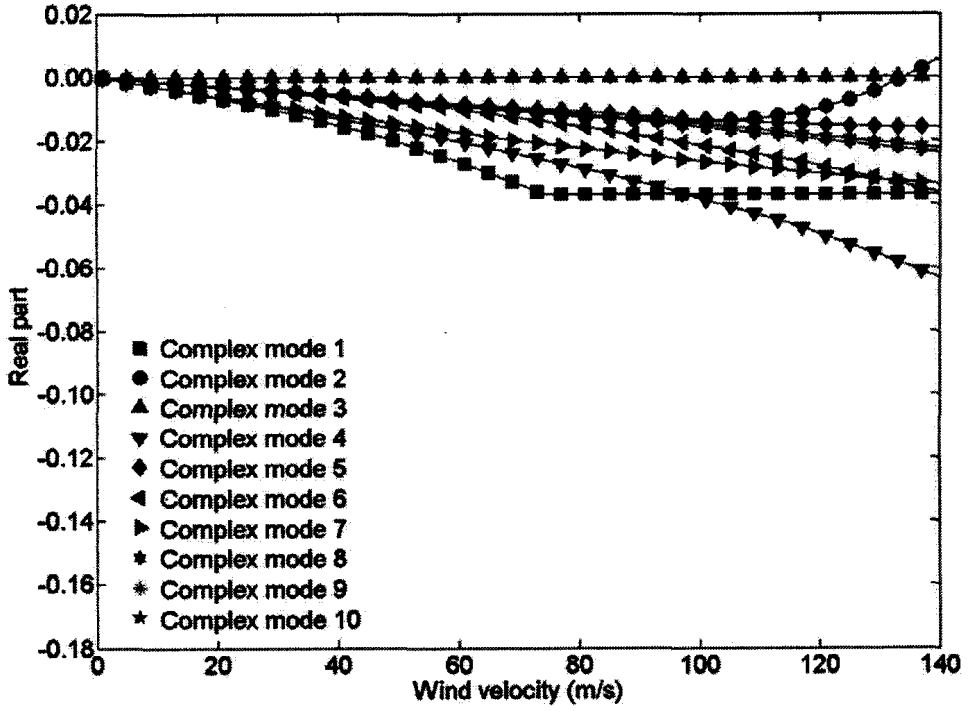

(b) Aerodynamic derivatives are specified for V up to 10 (Hua et al. 2007, Hua personal communication 2008)

Figure 2.5 The variation of complex eigenvalue versus wind velocity.

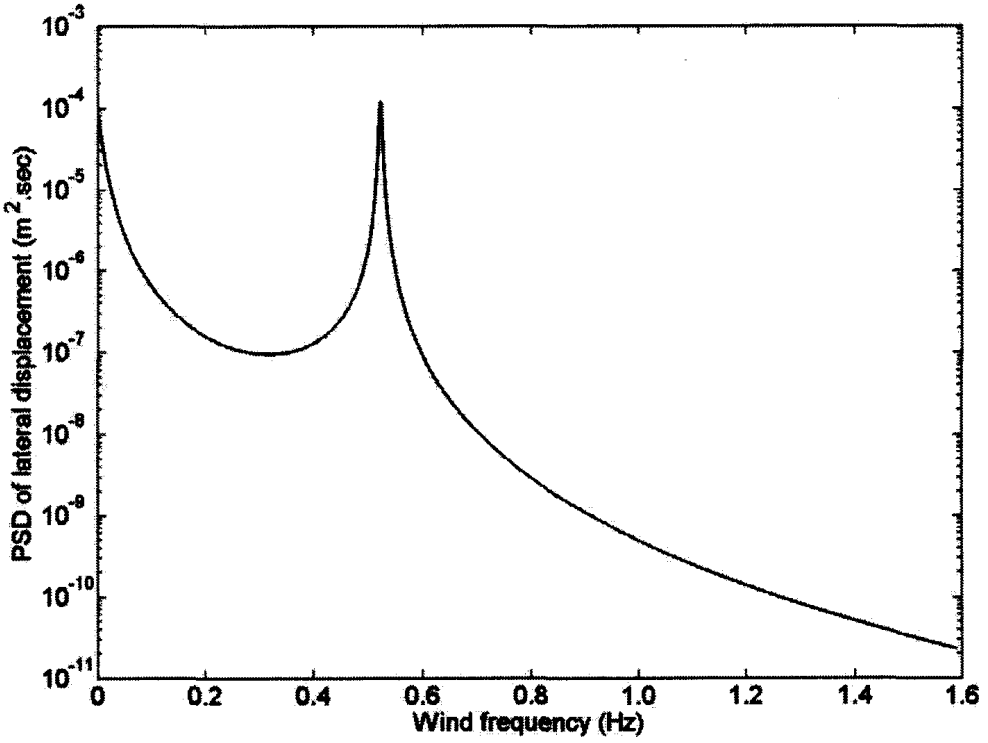

(a) PSD of lateral response of the deck at the midspan

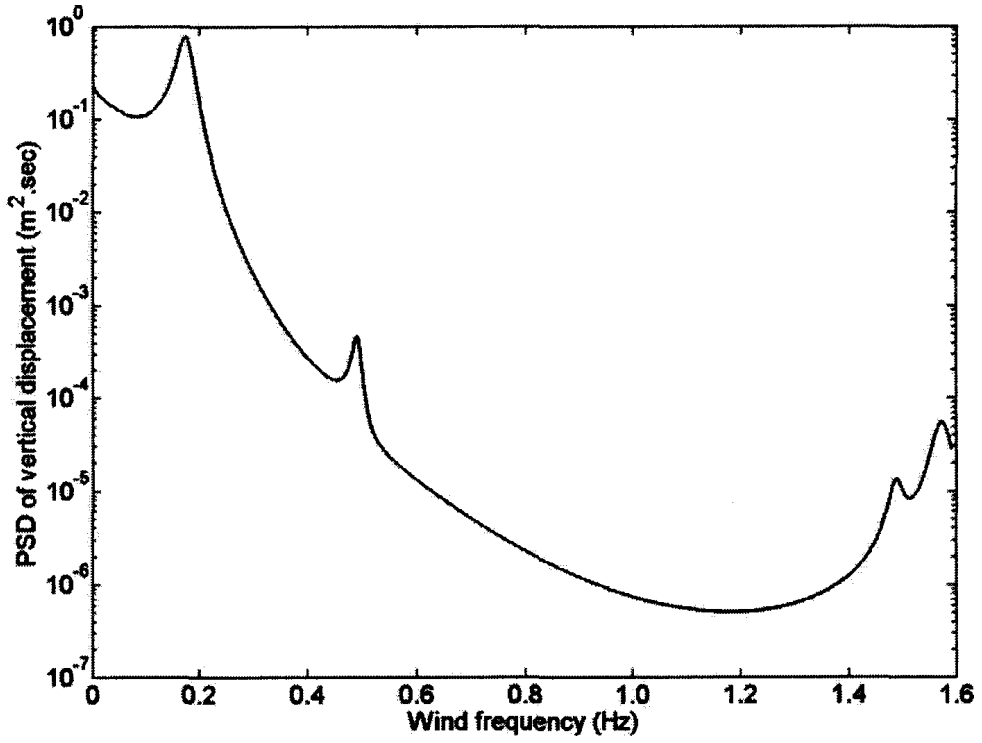

(b) PSD of vertical response of the deck at the midspan

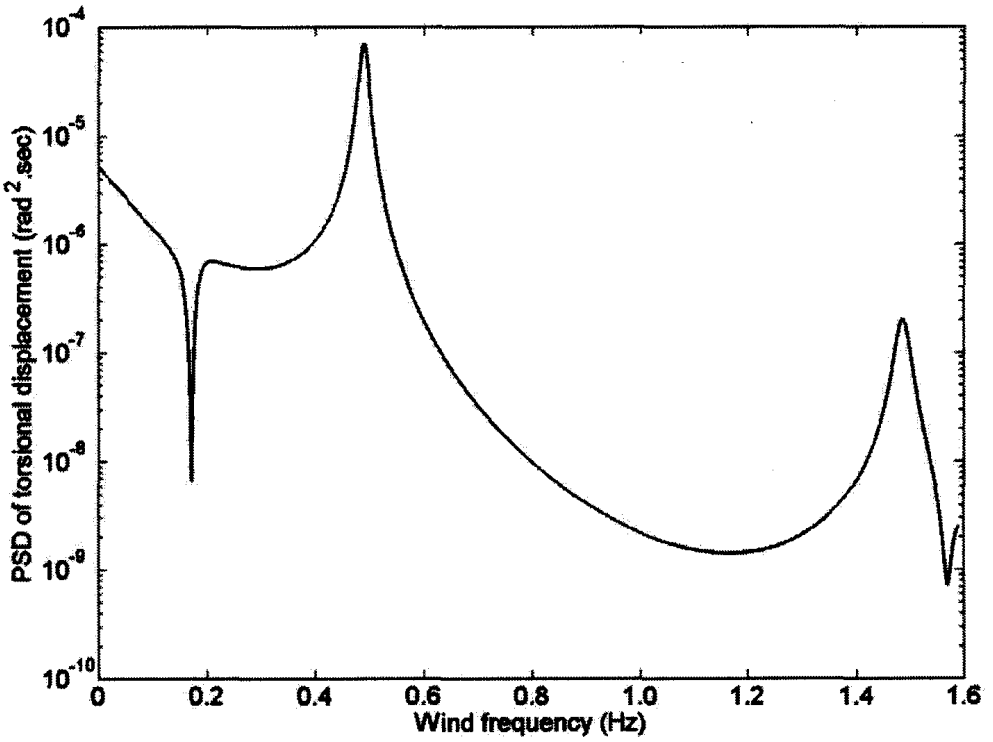

(c) PSD of torsional response of the deck at the midspan

Figure 2.6 Spectral density function of the displacements of deck at the bridge midspan.

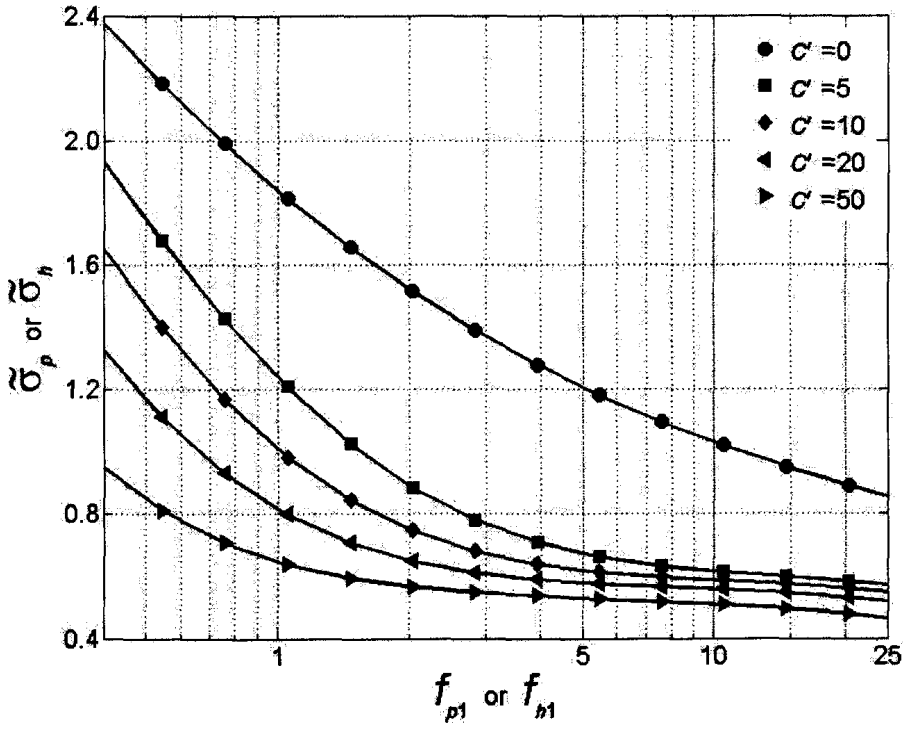

(a) Numerical solutions for $\tilde{\sigma}_p$ and $\tilde{\sigma}_h$

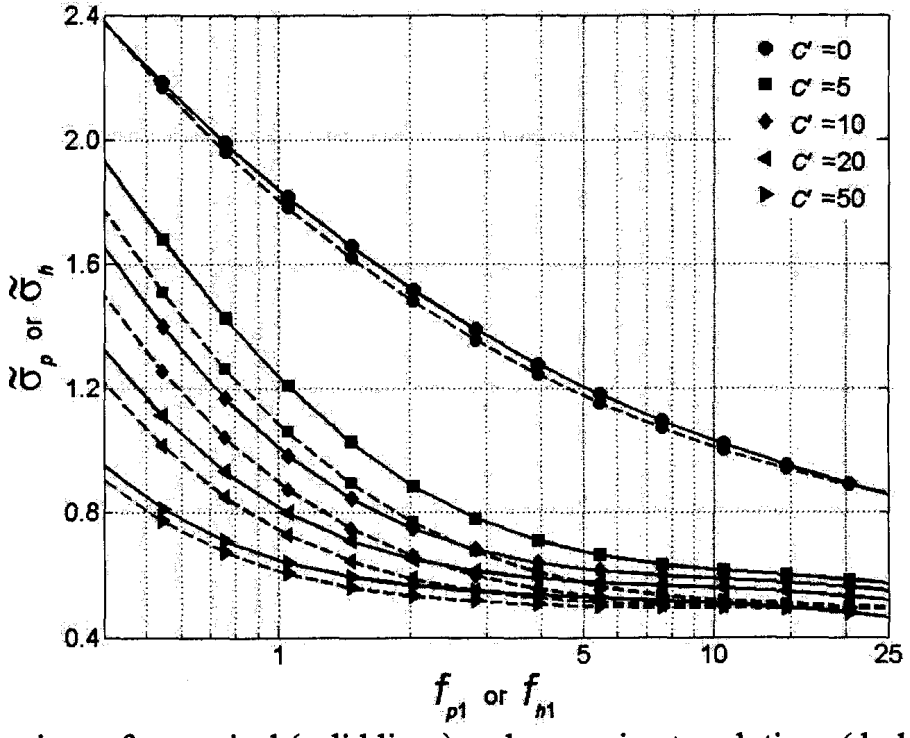

(b) Comparison of numerical (solid lines) and approximate solutions (dashed lines) for $\tilde{\sigma}_p$ and $\tilde{\sigma}_h$

Figure 2.7 Normalized standard deviation of horizontal and vertical displacements under along wind fluctuation with and without spatial correlation (for $\xi = 0.5\%$ and $\xi_a = 0$).

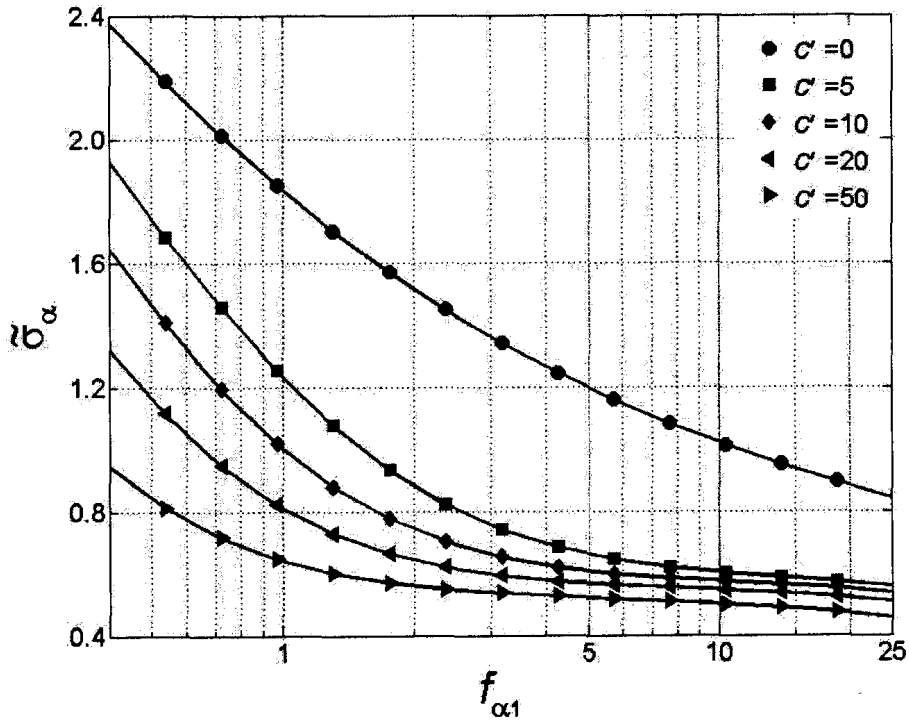

(a) Numerical solution for $\tilde{\sigma}_\alpha$

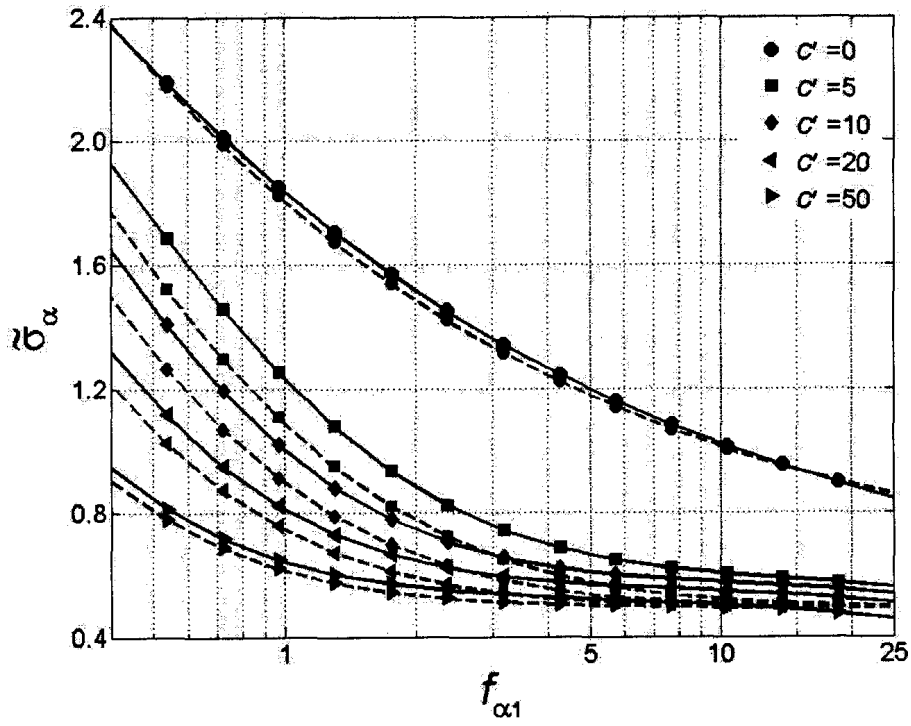

(b) Comparison of numerical (solid lines) and approximate solutions (dashed lines) for $\tilde{\sigma}_\alpha$

Figure 2.8 Normalized standard deviation for the torsional response under along wind fluctuation with and without spatial correlation (for $\xi = 0.5\%$ and $\xi_a = 0$).

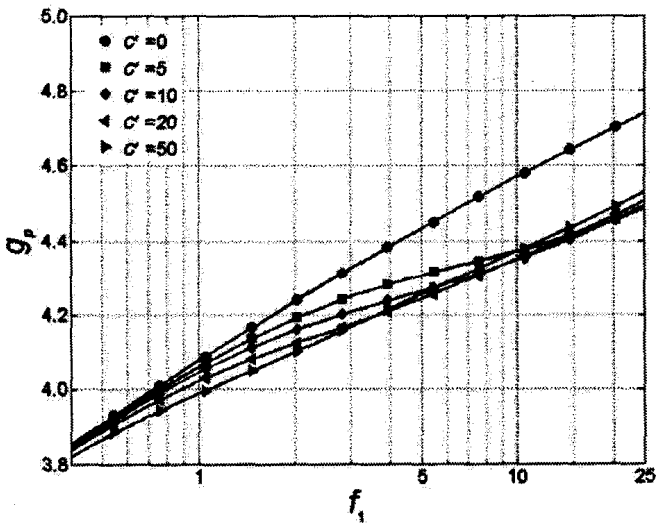

(a) Peak factor

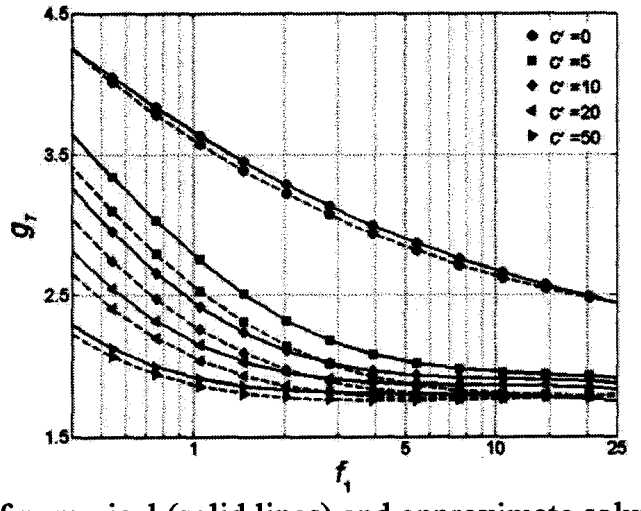

(b) Comparison of numerical (solid lines) and approximate solutions (dashed lines) for gust factor for $I_u = 0.11$

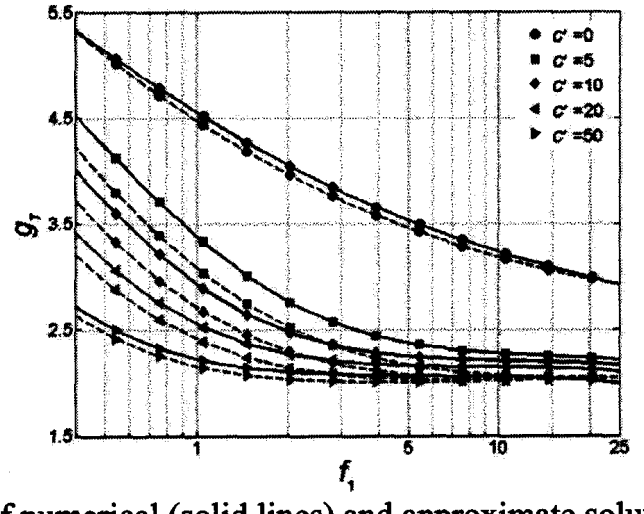

(c) Comparison of numerical (solid lines) and approximate solutions (dashed lines) for gust factor for $I_u = 0.15$

Figure 2.9 Gust factor for fluctuating along wind excitations ($f_1 = f_{p1}$ or f_{h1}).

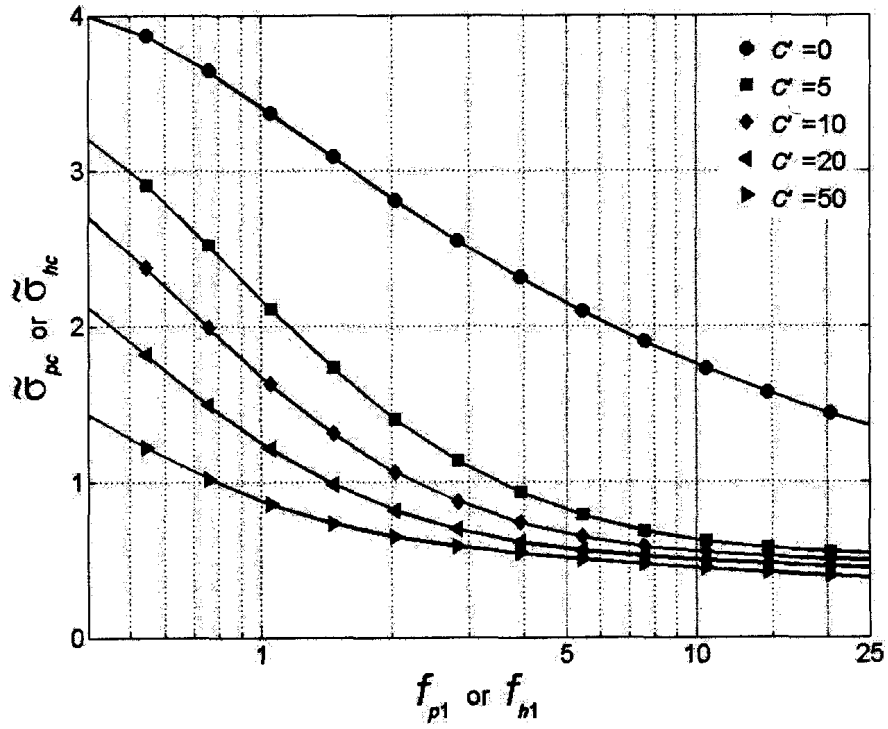

(a) Numerical solutions for $\tilde{\sigma}_{pc}$ and $\tilde{\sigma}_{hc}$

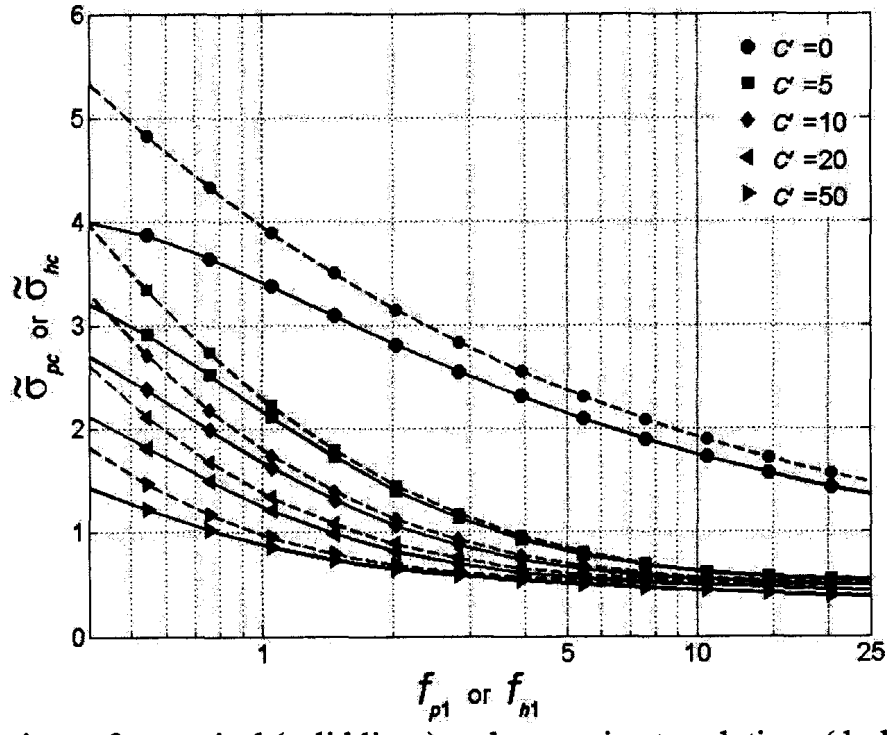

(b) Comparison of numerical (solid lines) and approximate solutions (dashed lines) for $\tilde{\sigma}_{pc}$ or $\tilde{\sigma}_{hc}$

Figure 2.10 Normalized standard deviation of horizontal and vertical displacements under cross wind fluctuation with and without spatial correlation (for $\xi = 0.5\%$ and $\xi_a = 0$).

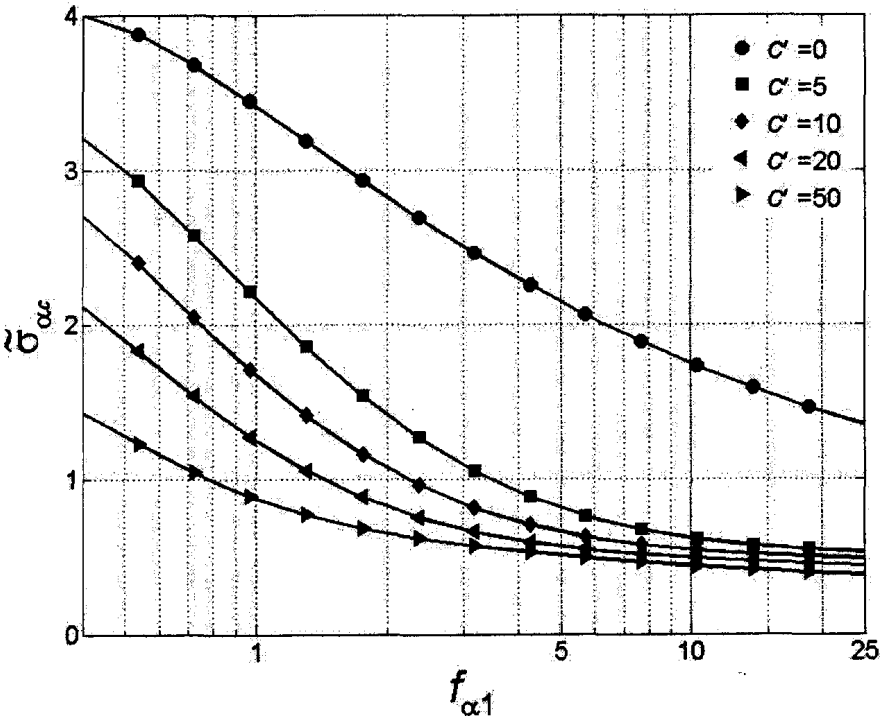

(a) Numerical solution for $\tilde{\sigma}_{\alpha c}$

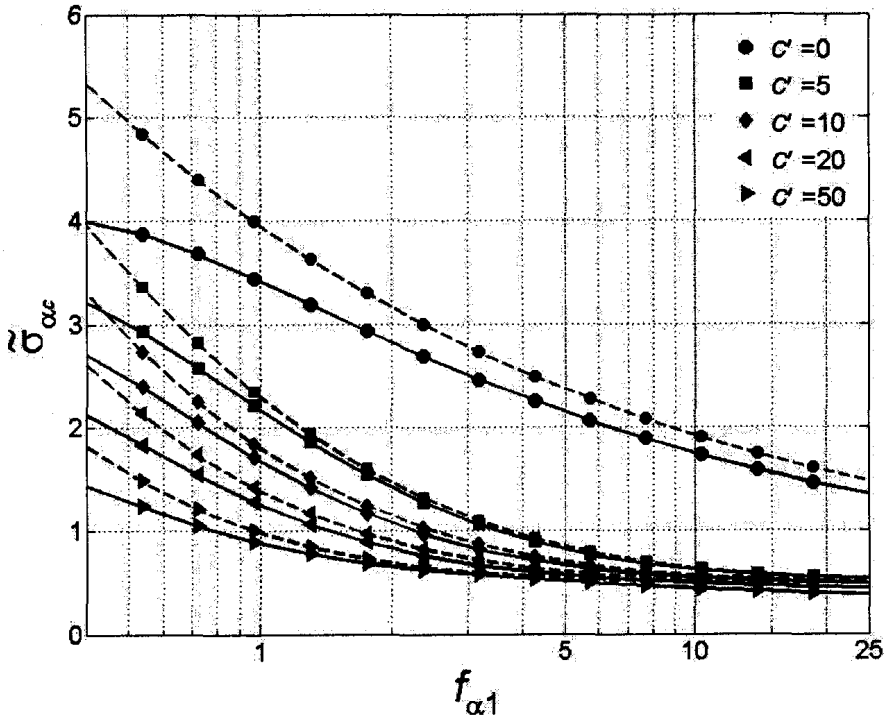

(b) Comparison of numerical and approximate solutions for $\tilde{\sigma}_{\alpha c}$

Figure 2.11 Normalized standard deviation of torsional displacement under cross wind fluctuation with and without spatial correlation (for $\xi = 0.5\%$ and $\xi_a = 0$).

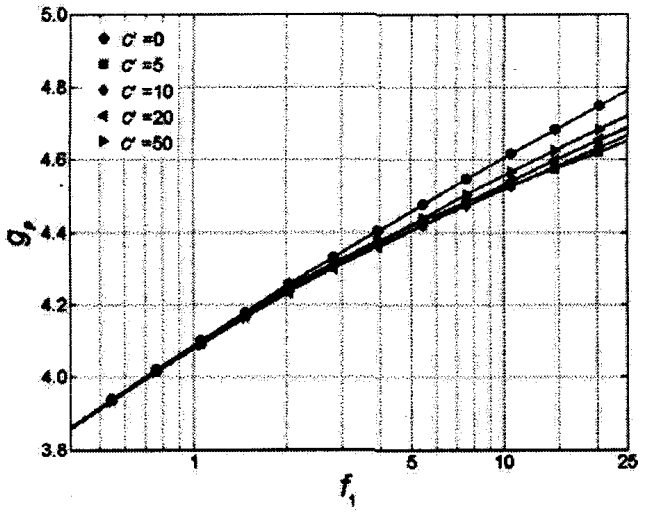

(a) Peak factor

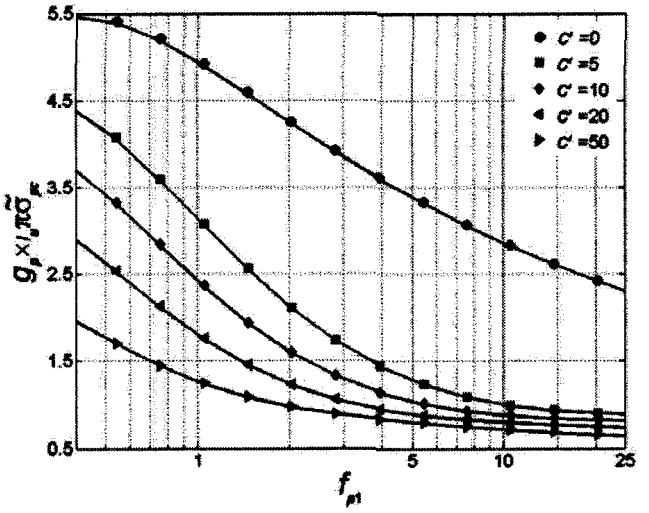

(b) $g_P \times I_u \pi \tilde{\sigma}_{pc}$ for $I_u = 0.11$

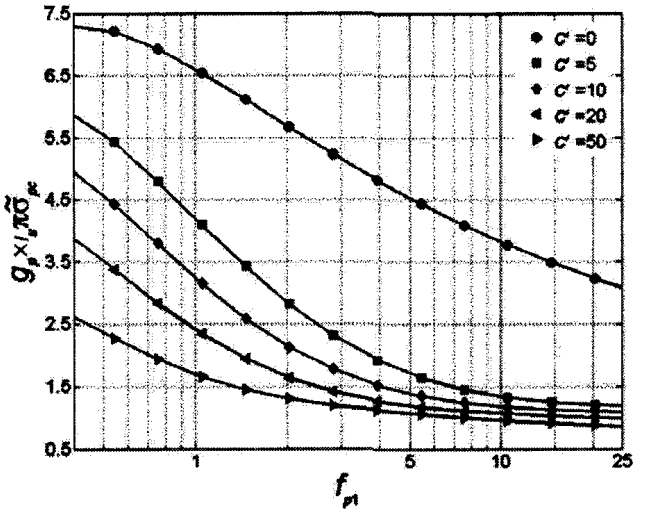

(b) $g_P \times I_u \pi \tilde{\sigma}_{pc}$ for $I_u = 0.15$

Figure 2.12 Peak factor and $g_P \times I_u \pi \tilde{\sigma}_{pc}$ for fluctuating cross wind excitations.

Chapter 3 Calibration of wind load factors for Canadian bridge design code

3.1 Introduction

Canadian Highway Bridge Design Code (CHBDC) (CAN/CSA S6-6 2006) recommends that a gust effect coefficient (or factor) of 2.0 and a wind load factor of 1.65 should be used for bridges of spans less than 125 m. The code further recommends that for wind sensitive structures the wind loads are to be determined on the basis of a detailed analysis of dynamic wind action, using an approved method and including buffeting effects. For wind loads determined from wind tunnel tests, the code recommends that the wind load factor is to be calculated from an equation, which depends on the coefficient of variation of the annual maximum hourly mean wind velocity. Use of these values is aimed at achieving reliability consistency in bridge designs.

The application of the gust factor approach simplifies the designers' task in evaluating wind load. However, since the gust factor varies and depends on the dynamic characteristics of structural characteristics and statistics of the fluctuating wind speed, use of the suggested value of the gust factor (i.e., 2.0) may not result in reliability-consistent bridge designs for a wide variety of design cases. The evaluation of the gust factor can be carried out in frequency-domain or time-domain. Methods and techniques for such evaluation are well established (Davenport 1962, 1981, 1983, Jain et al. 1996, Simiu and Scanlan 1996, Sun et al. 1999, Chen et al. 2000, Caracoglia and Jones 2003). Results from the numerical analyses can be used to verify the accuracy of a simple to use approximate analytical equation, that was elaborated in Davenport (1981, 1983) and, Davenport and King (1982), to predict the gust factor for bridge design. In some cases bridges could be sensitive to the aeroelastic self-excited forces that can lead to the bridge instability (Scanlan and Tomko 1971). A review of bridge flutter analysis was given by Ge and Tanaka (2000). Since this study is focused on the wind loading used in strength design, the aerodynamic instability problem which are extremely important for wind sensitive bridges are not considered.

Calibration of the wind load factors employed in the current CHBDC was reported by Bartlett and King (2002). The calibration uses some simplifying assumptions and approaches, including the use of lognormal models, and distribution tail fitting. It

provided a forward step towards rational consideration of wind load in the CHBDC for a reliability index of 3.5 considering a service period of 75 years. Since the gust factor is not only a function of the frequency of the first vibration mode but also a function of the time-averaged wind speed, use of simple curves for gust factor instead of a single gust factor value could be desirable for a wide range of bridge design cases. Furthermore, use of more efficient and/or accurate reliability analysis approaches such as the first-order reliability method (Madsen et al. 1986) and nested reliability method (Wen and Chen 1989) or simulation techniques in calibrating the wind load factor is needed to take into account that the probability distribution of the gust factor is conditioned on the time-averaged wind speed. The objective of this chapter is to present the basis, calibration procedure and results for recommending the wind load factors and gust factor curves for a future edition of the CHBDC.

3.2 Wind load and responses

3.2.1 Design wind load

Wind load in the CHBDC (2006) is defined based on the hourly mean reference (*T*-year return period value of) wind pressure, q_T,

$$q_T = \frac{1}{2}\rho v_T^2, \tag{3.1}$$

where ρ is the air mass density, v_T is reference (*T*-year return period value of) wind velocity. Values of q_T for return period of 10, 25, 50 and 100 years are tabulated in the CHBDC (2006) for many locations. For bridges with spans less than 125 m, 50-year return period value of q_T is to be used; for bridges with spans equal to or greater than 125 m, 100-year return period value of wind pressure is to be used (see Clause 3.10.1.2 of the CHBDC). q_T is calculated directly using v_T. The horizontal wind load pressure, p_T, is then evaluated using,

$$p_T = q_T C_e C_g C_h, \tag{3.2}$$

where C_e, C_g and C_h denote the exposure, gust effect and horizontal wind drag coefficients. The wind load effect W_n that is directly proportional to p_T is expressed as,

$$W_n = C \times C_e C_g C_h v_T^2, \tag{3.3}$$

where C denotes the analysis coefficient including the exposure area and air density.

This wind load effect needs to be considered in the load combinations for ultimate limit states (ULS). In particular, if the secondary prestress effects, loads due to earth pressure and hydrostatic pressure, and the load effect caused by restraint of deformations due to temperature change and temperature differential, concrete shrinkage, differential shrinkage, and creep, are not present, the design requirements given in the CHBDC (2006),

$$R_D \geq \alpha_D D_n + \alpha_W W_n \tag{3.4a}$$

for the dead load and wind load combination (ie., ULS combination 4) and,

$$R_D \geq \alpha_D D_n \tag{3.4b}$$

for the dead load acting alone (i.e., ULS combination 9) are to be satisfied, where R_D denotes the factored resistance, α_D and α_W are the dead load and wind load factors, and D_n is nominal dead load effect. α_D for cast-in-place concrete, wood, and all non-structural components equals 1.20 for Eq. (3.4a) and 1.35 for Eq. (3.4b), and α_D takes value less than 1.0 if the dead load effect counteracts the wind load effect; α_W equals 1.65 for the ULS combination 4, where the basis for the suggested wind load factor will be discussed shortly.

3.2.2 Response to buffeting and aeroelastic self-excited forces

The wind load shown in Eq. (3.2) depends on the exposure, horizontal wind drag and gust effect coefficients (C_e, C_h and C_g). According to the CHBDC (2006), the exposure coefficient is a function of the height and varies from 1.0 to 1.6; the drag coefficient is considered to be 2.0 for horizontal wind load. The commentary to the CHBDC code states that the drag coefficient of 2.0, based on the entire exposed frontal area, is conservative for common slab, plate girder, and box girder superstructures. Furthermore, the CHBDC (2006) recommends that a gust effect coefficient (or factor) of 2.0 should be used for bridges of spans less than 125 m. Use of a gust factor of 2.0 may not necessarily be economic and/or unconservative since the gust factor depends on the structural and wind characteristics. To show this, we note that the wind actions per unit span length of the bridge deck are grouped into drag force $D(t)$, lift force $L(t)$ and pitching moment $M(t)$; and they are expressed as the sum of the time-averaged static, buffeting and aeroelastic self-excited contributions (Simiu and Scanlan 1996),

$$D(t) = D_s + D_b(t) + D_{ae}(t), \tag{3.5a}$$

$$L(t) = L_s + L_b(t) + L_{ae}(t), \tag{3.5b}$$

and,

$$M(t) = M_s + M_b(t) + M_{ae}(t), \tag{3.5c}$$

where the subscripts *s*, *b* and *ae* represent the static, buffeting and aeroelastic self-excited forces. The static wind forces for the unit length of a bridge deck of width *B* are given by,

$$D_s = \frac{1}{2}\rho B C_h U^2, \tag{3.6a}$$

$$L_s = \frac{1}{2}\rho B C_L U^2, \tag{3.6b}$$

and,

$$M_s = \frac{1}{2}\rho B^2 C_M U^2, \tag{3.6c}$$

where U (or $U(z)$) denotes the mean wind velocity at the elevation of the bridge deck z (m); C_h, C_L and C_M are the drag, lift and moment coefficients, which are commonly determined based on tests at the boundary layer wind tunnel and are functions of angle of attack. Since the reference (T-year return period value of) wind velocity v_T is given at the height of 10 m, the wind speed at the elevation of the bridge deck z (m) can be calculated from the power law or logarithmic law. In particular, if the power low or logarithmic law is adopted (Simiu and Scanlan 1996), $U(z)$ is calculated from,

$$U(z) = v_T h(z), \tag{3.7}$$

where $h(z)$ represents the ratio of $U(z)$ to the wind speed at the height of 10 m.

The buffeting forces are due to stochastic fluctuating along and cross wind excitations, which are commonly characterized by their power spectral density (PSD) functions and coherence function (Davenport 1966, Simiu and Scanlan 1996). The aeroelastic self-excited forces are due to the interaction of the wind flow and oscillation of bridge (Scanlan 1978, Jain *et al.* 1996, Simiu and Scanlan 1996).

Based on the above wind load characterization, if the aeroelastic self-excited forces are ignored, the mean of the wind-induced peak response (such as displacement or rotation) η, denoted by m_η, can be expressed as (Davenport 1962),

$$m_\eta = \bar{r} + g_p \sigma_r, \tag{3.8a}$$

where $g_p = \sqrt{2\ln(v_0^+ T)} + 0.577/\sqrt{2\ln(v_0^+ T)}$ is the peak factor and depends on the zero-upcrossing rate v_0^+, and

$$g_T = 1 + v_r g_p, \tag{3.8b}$$

is the gust factor, in which v_r equals $\sigma_r / \bar{r}$, representing the coefficient of variation (cov) of the response, and $\bar{r}$ denotes response due to the mean wind speed. The notation g_T is used in here to distinguish it from C_g used in the CHBDC (2006).

Methods and techniques for evaluating the gust factor in the frequency-domain or time-domain are well established (Davenport 1981, Jain et al. 1996, Simiu and Scanlan 1996, Sun et al. 1999, Chen et al. 2000, Caracoglia and Jones 2003). If the Kaimal's PSD function (as shown in Simiu and Scanlan 1996) and Davenport's coherence function are adopted, it can be shown that the mean peak response for a simply supported bridge of span length L (m) (see Chapter 2) is a function of damping ratio, and other two parameters: the scaled exponential decay coefficient c' and the Monin coordinate f_1 evaluated at the frequency of the first vibration mode. They are defined as:

$$c' = C_{ED} L / z \text{ and } f_1 = z\omega_1 / (2\pi U), \tag{3.9}$$

where C_{ED} denotes the exponential decay coefficient for fluctuating wind, and ω_1 represents the frequency of the first vibration mode for horizontal, vertical or torsional displacement.

For a typical turbulence intensity I_u of 0.11, the calculated peak factor and gust factor for fluctuating along wind by using the finite element method and random vibration theory (See Chapter 2) are shown in Figures 3.1 and 3.2 for ranges of c' and f_1 values. The curves shown in the figures are for horizontal, vertical and torsional displacements. Figure 3.2 indicates that g_T can differ significantly from 2.0: g_T is smaller than 2.0 for a large c' value, stiff structures and/or low mean wind speed value; it is greater than 2.0 for a small c' value, flexible structures and/or high mean wind speed. Most importantly, since g_T is a function of f_1 which is inversely proportional to U, this dependency should be considered in evaluating bridge reliability and code calibration under the wind loading. Figure 3.1 indicates that the peak factor is an increasing function of logarithmic of f_1, and for a range of c' values that are not equal to zero, it can be approximated by,

$$g_p = a_0 + a_1 \ln(f_1) \tag{3.10}$$

where a_0 and a_1 are 4.0 and 0.16 for along-wind induced vibrations, respectively.

Rather than using the numerical procedure to assess the gust factor, we follow Davenport (1981) and Davenport and King (1982) but considering that Kaimal's PSD function is adequate, and obtained the equation below to estimate g_T for fluctuating along wind,

$$g_T = 1 + g_P I_u \pi \times \tilde{\sigma}(0.049, c', f_1), \tag{3.11a}$$

where,

$$\tilde{\sigma}(b, c', f_1) = \sqrt{\frac{1}{\pi^2/4 + L/\lambda} + \frac{1}{\pi^2/4 + c' f_1} \frac{\pi}{4(\xi + \xi_a)} b f_1^{-2/3}}, \tag{3.11b}$$

ξ represents the damping coefficient which is taken equal to 0.5% throughout this study, ξ_a represents the damping coefficient due to aerodynamic damping and λ is a constant known as integral spanwise turbulence scale which is equal to about 60 m (Davenport 1981). The approximation shown in Eq. (3.11b) is a function of L, c' and f_1 while the results obtained based on theoretical formulation depend on c' and f_1. The inclusion of L as an argument is not convenient since different sets of curves may be needed for different spans. To make this approximation more consistent with that shown in Figure 3.2, we replace Eq. (3.11b) by,

$$\tilde{\sigma}(b, c', f_1) = \sqrt{\frac{1}{\pi^2/4 + 0.025c'} + \frac{1}{\pi^2/4 + c' f_1} \frac{\pi}{4(\xi + \xi_a)} b f_1^{-2/3}}, \tag{3.11c}$$

which depends on c', and f_1. Substituting Eq. (3.11c) instead of Eq. (3.11b) into Eq. (3.11a) provides a better approximation to the results shown in Figure 3.2. Ratios of the gust factors shown in Figure 3.2 to those estimated by using Eqs. (3.10), (3.11a) and (3.11b) are shown in Figure 3.3 for ξ_a equal to zero. The figure indicates that the proposed approximation mimics well the numerical results with the ratio within 0.95 to 1.05. This provided the basis and justification for using the proposed approximation in code calibration and for possibly including them in design code in addition to the curves shown in Figure 3.2.

Now, if the aeroelastic self-excited forces are considered and quasi-steady theory is adopted, it can be shown that the aerodynamic damping coefficient can be expressed as

(Davenport and King 1982),

$$\xi_a = -\rho B^2 H_1^* \left(\frac{\omega_{h1} B}{U} \right) / (4m), \tag{3.12}$$

for vertical displacement and,

$$\xi_a = -\rho B^4 A_2^* \left(\frac{\omega_{\alpha 1} B}{U} \right) / (4I_m), \tag{3.13}$$

for torsional displacement, where $H_1^*(K)$ and $A_2^*(K)$ denote the aerodynamic derivatives evaluated at K, ω_{h1} represents the frequency of the first vertical vibration mode, and $\omega_{\alpha 1}$ represents the frequency of the first torsional vibration mode. The adequacy of using these equations was already assessed in Chapter 2 of this study for a thin-airfoil cross section.

3.3 Probabilistic models and wind load factor

3.3.1 Probabilistic models

The wind load effect, dead load effect and the structural member strength are uncertain. These uncertainties are considered in the limit state design approach by using load and resistance factors (or material resistance factors), such as that shown in Eq. (3.4). By considering the resistance R, the dead load effect D, and the wind load effect W, these factors are calibrated such that the probability that $g \leq 0$, $P(g \leq 0)$, where,

$$g = R - (D + W), \tag{3.14}$$

equals, on average, a selected tolerable value P_{fT}. The estimated $P(g \leq 0)$ could be sensitive to the selected probabilistic models of the random variables that need to be considered in the limit state function g (Madsen et al. 1986).

For simplicity, the calibration in this study will be based on structural steel, although probabilistic member resistance characterization for steel concrete structural members can be found in Hong and Zhou (2000). For structural steel, the resistance R is considered to be lognormally distributed with mean to nominal ratio of 1.13 and a cov of 0.10. These values are in agreement with those reported in the literature (Ellingwood et al. 1980; Nowak 1999), although the mean is less than that recommended by Bartlett et al. (2003) for buildings. For easy reference, this and subsequently adopted probabilistic models are summarized in Table 3.1.

Dead load represents the self-weight of the materials used in constructing the bridge. Nowak (1999) suggested that the mean to nominal ratio of dead load ranges from 1.03 to 1.05 depending on the considered component (e.g., weight of factory made material, cast-in-place concrete, wearing surface, etc.) and a cov value varies from 0.08 to 0.1 (except for asphalt a cov of 0.25 is appropriate). This leads us to consider the dead load as a normal variate with a mean of 1.05 and a cov of 0.10.

The wind load effect, as discussed in the previous section, is expressed as a multiplication of several variables that are uncertain. By considering the suggested statistics given in Ellingwood et al. (1980) and Bartlett and King (2002), it is assumed that C can be modeled as a normal variate with a mean to nominal ratio of 1.0 and a cov of 0.056.

The exposure coefficient C_e depends on the structural surrounding and is considered to have a cov value ranging from 0.13 to 0.20 for building (Ellingwood et al. 1980, Davenport 1981, Ellingwood and Tekie 1999, Davenport 2000). Davenport et al. (1993) recommended a cov of 0.075 for calibrating the wind load factors for the Confederation Bridge (MacGregor et al. 1997). In all cases, the mean to nominal value is assumed to be equal to 1.0. Since the calibration of the wind load factor used for designing bridges with spans less than 125 m (i.e., simple procedure) requires the consideration for designing a wide range of bridges and their locations, for the present study, C_e is assumed to be normally distributed with a mean to nominal ratio of 1.0 and a cov of 0.15. However, for bridges that require detailed analysis and wind tunnel testing (i.e., detailed procedure), the cov of C_e is assumed to be equal to 0.075 since the magnitude of uncertainty in C_e (i.e., cov) for such design cases is likely to be reduced.

For typical highway bridges, and considering the width-to-depth ratio ranging from 1 to 16 and the fact that a value of 2.0 is recommended by CHBCD (2006), Bartlett and King (2002) concluded that for the simple procedure the mean to nominal ratio for C_h equal to 0.71 and cov equal to 0.14 are adequate. Therefore, C_h is assumed to be normally distributed with these statistics. For bridges or bridge sections that require wind tunnel testing, it is assumed that the mean and cov of C_h are equal to 1.0 and 0.075, respectively. Such an assumption was adopted by Bartlett and King (2002).

As shown in the previous section, the gust factor depends not only on the dynamic

characteristics of the bridge but also is a function of f_1, which is inversely proportional to the mean wind velocity (See Eq. (3.9)). Therefore, the gust factor is conditioned on the time-averaged wind velocity. By considering that g_T can be estimated from Figure 3.2 or using Eqs. (3.10), (3.11a) and (3.11c) as well as the bias shown in Figure 3.3 and that the code recommended a gust factor of 2.0, the mean to nominal ratio for C_g can be evaluated for the current CHBDC. The suggested cov values of C_g vary significantly, and range from 0.05 to 0.20 for buildings (Ellingwood et al. 1980, Davenport 1981, Davenport 2000). Also, a cov value of 0.075 was suggested by Davenport et al. (1993) for calibrating the wind load factor for the Confederation Bridge (MacGregor et al. 1997). Therefore, it seems reasonable to consider a cov of 0.10 for the present study.

Finally, the annual maximum wind speed V is commonly modeled as a Gumbel variate. The mean and cov of the annual wind speed for more than 230 locations, each having more than at least 10 years of record, that were provided by the Engineering Climatology Section of the Canadian Meteorological Centre in Downsview for the calibration of 2005 edition of NBCC were considered (Bartlett et al. 2003). For majority of the locations, the statistics indicate that the cov of the annual maximum wind speed, v_v, ranges from about 0.08 to about 0.18 and an overall cov value of about 0.13, and that the mean of V, m_v, varies from about 10 to 30 (m/s), and an overall mean of about 18 (m/s). An inspection of the data also suggests that there is no clear trend between cov and the mean of V, and that the overall mean of 50- and 100-year return period values of V are about 24.4 and 25.7 (m/s), respectively. Therefore, v_v equal to 0.11, 0.13 and 0.15, and m_v equal to 15.0, 18.0 and 21.0 (m/s) were considered for the wind load factor calibration and verification analysis for bridges of spans less than 125 m. Wider ranges of the mean and cov values of V were considered to calibrate information-sensitive wind load factors for bridges that require detailed analysis and wind tunnel testing.

The T-year return period value for the Gumbel distributed annual maximum wind velocity v_T is given by,

$$v_T = m_v\left(1-\frac{\sqrt{6}v_v}{\pi}\left(0.577+\ln\left(-\ln\left(\frac{T-1}{T}\right)\right)\right)\right). \tag{3.15}$$

3.3.2 Analysis procedure and results

For the calibration, it is considered that the structural member of the bridge is

designed to satisfy the minimum strength requirement. This and Eq. (3.4) lead to,

$$R_D = \max(1.35, \alpha_D + \alpha_W \gamma) D_n \tag{3.16}$$

where γ denotes the ratio of nominal wind load to nominal dead load. Therefore, except a positive scaling constant the limit state function g shown in Eq. (3.14) can be re-written as,

$$g = \frac{1}{\phi_s} \frac{R}{R_n} - \frac{1}{\max(1.35, \alpha_D + \alpha_W \gamma)} \left(\frac{D}{D_n} + \gamma X_c X_{ce} X_{cg} X_{ch} \left(\frac{V}{v_T} \right)^2 \right) \tag{3.17}$$

where ϕ_s that equals 0.95 denotes the resistance factor for the structural steel considering flexure, tension or shear failure (Clause 10.5.7, CAN/CSA S6-06 2006); X_c, X_{ce} X_{cg} and X_{ch} denote the ratios of C, C_e, C_g and C_h to their corresponding nominal values, respectively; and V denotes the annual maximum wind speed model as a Gumbel variate.

If the simple procedure is employed for bridge design, two more issues need to be considered in establishing the limit state function. They are related to the directionality effect and static failure mode effect. The directionality effect considers that the direction of the largest extreme wind speed may not be along the (critical) direction, where largest wind load effect can be produced. The static failure mode effect considers that the dynamic load effect can be increased before significant yield occurs in a well designed structure. According to Bartlett and King (2002) reductions for the former and the latter are equal to 1.25. By considering these reductions, Eq. (3.17) can be expressed as,

$$g = \frac{1}{\phi_s} \frac{R}{R_n} - \frac{1}{\max(1.35, \alpha_D + \alpha_W \gamma)} \left(\frac{D}{D_n} + \frac{\gamma X_c X_{ce} X_{cg} X_{ch}}{1.25 \times 1.25} \left(\frac{V}{v_T} \right)^2 \right) \tag{3.18a}$$

However, if the detailed procedure is followed, the directionality effect needs not to be considered because it has already been taken into account in the detailed (climatology) analysis and wind tunnel testing. In such a case, Eq. (3.17) is expressed as,

$$g = \frac{1}{\phi_s} \frac{R}{R_n} - \frac{1}{\max(1.35, \alpha_D + \alpha_W \gamma)} \left(\frac{D}{D_n} + \frac{\gamma X_c X_{ce} X_{cg} X_{ch}}{1.25} \left(\frac{V}{v_T} \right)^2 \right) \tag{3.18b}$$

Since the mean of X_{cg} is conditioned on the (time-averaged) wind velocity at the bridge deck height which is a function of v, the calculation of $P(g \le 0)$ for given α_D, α_W and γ values can be carried out using the nested reliability method (Wen and Chen 1989)

or combination of the first order reliability method and point estimate method for numerical efficiency (Hong 1996). Alternatively, $P(g \leq 0)$ for a service period of 75 years can be estimated using simple simulation technique according to the steps below:

1) Sample values of the random variables R/R_n, D/D_n, X_c, X_{ce}, and X_{ch};
2) Sample value of V, v, and the mean of X_{cg} to define its probabilistic model; and sample X_{cg} and evaluate the limit state function g;
3) Repeat Step 2) up to 75 times (years) if g is greater than zero before the end of 75 years;
4) Repeat Steps 1) to 3) n times and count number of times, n_f, that g is less than zero; and the estimated $P(g \leq 0)$ equals n_f/n.

Using the estimated failure probability, $P(g \leq 0)$, the corresponding reliability index β defined as,

$$\beta = \Phi^{-1}(1 - P(g \leq 0)) \tag{3.19}$$

can be evaluated for combinations of α_D, α_W, and γ values, and wind characteristics, where $\Phi^{-1}(\ )$ denotes the inverse of the standard normal distribution function. In the present study, the simulation cycle n is selected such that there is at least 50 failure samples (i.e., n is selected to be greater than $50/P(g \leq 0)$).

3.3.2.1 Results for simple procedure

First, reliability estimates are carried out by using the above outlined procedure and considering the simple procedure. For the analysis, α_D = 1.2 and α_W = 1.65, that are recommended in the CHBDC (2006), are employed for Eq. (3.4a); α_D = 1.35 is used for Eq. (3.4b). f_1 equal to 5 and 10 (calculated based on the design wind speed) and, c' equal to 10 and 40 are selected. The selected values are based on the consideration that ω_1 ranges from 6 to 60 (rad/s) for typical bridges with spans less than 125 m (Billing and Green 1984, Barth and Wu 2007), C_{ED} takes a value of 8 or 16 (Simiu and Scanlan 1996), z is between 10 to 20 (m), and L varies from 10 to 125 (m). Typical obtained results of the reliability index for a 75-year design life, β_{75}, are shown in Figure 3.4 for γ varying from 0 to 1.0, and combinations of wind characteristics. The figure shows that β_{75} for I_u = 0.11 is greater than that for I_u = 0.15. This is expected since as the turbulence intensity increases the gust factor g_T and the mean to nominal ratio of the wind load effect

increases. Furthermore, the estimated β_{75} is insensitive to the cov of wind velocity, v_v, for γ less than about 0.3. For γ equal to 1/11 representing the condition where the factored design load effect by Eq. (3.4a) equals to that by Eq. (3.4b), β_{75} takes, on average, a value of about 2.8. In all cases, the results show that if the design condition is for γ near 1/11, β_{75} is significantly lower than the target reliability index of 3.5, while if the wind load becomes significant part of the total design load, β_{75} is significantly higher than the target reliability index of 3.5. The latter implies that there is potential for the wind load factor to be reduced without compromise the desired safety level. The former, although, is expected since the target reliability level for permanent load alone is often considered to be less than that for variable loads, an increase in the dead load factor is desirable. For example, if α_D equal to 1.25 is used to replace 1.20, β_{75} takes, on average, a value of about 2.87 for γ equal to 1/14. Therefore, to achieve an improved reliability consistency, α_D equal to 1.25 seems to be desirable.

To suggest new wind load factor and to adequately take into account the dead load effect, the above reliability analyses were repeated by varying α_W from 1.3 to 1.65 with an increment of 0.05 but considering $\alpha_D = 1.25$. It was found that if the wind load factor α_W equal to 1.40 is employed, the estimated β_{75} values for γ ranging from 0.2 to 0.3, as illustrated in Figure 3.5, are close to the target reliability index of 3.5 for combinations of wind characteristics shown in Table 3.1. The consideration of γ ranging from 0.2 to 0.3 is justified since the contribution of the wind load effect to the total load effects is usually small for bridges of spans less than 125 m. Therefore, it is recommended that $\alpha_D = 1.25$ and $\alpha_W = 1.40$ are to be implemented in a future CHBDC for the simple procedure.

3.3.2.2 Results for detailed procedure

By considering the detailed procedure with the corresponding limit state function shown in Eq. (3.8b), the reliability analysis similar to the simple procedure is carried out. The estimated β_{75} values by adopting the probabilistic models shown in Table 3.1 are illustrated in Figure 3.6 for $f_1 = 0.5$ or 1, $c' = 40$ and $m_v = 18$ (m/s). The trends of the estimated β_{75} shown in the figure are similar to those presented in Figure 3.4. The results are calculated using the CHBDC recommended dead and wind load factors: $\alpha_D = 1.20$ and α_W equal to the value estimated using (see Clause 3.10.5.2 of the CHBDC),

$$\alpha_W = 0.80\delta_W \exp\left(3.5 v_W \sqrt{\frac{v_W^2}{0.15^2 + v_W^2}}\right) \tag{3.20}$$

that equals 1.53, 2.07 and 2.88 for the bias factor δ_W = 1.0, and the cov of wind load effect, v_W, equal to 0.22, 0.30 and 0.39 (i.e., for v_v = 0.08, 0.13 and 0.18).

The results shown in Figure 3.6 indicate that the estimated β_{75} values can be significantly higher than the target reliability index of 3.5 if γ is greater than 0.3 and v_v equals 0.13 and 0.18, and that the estimated β_{75} is much lower than the target reliability index of 3.5 if γ is less than 0.2 and v_v equals 0.13. Also, if v_v equals 0.08, the estimated β_{75} is less than 3.5; this and the above indicate that Eq. (3.20) does not lead to consistent reliability levels. Therefore, to improve reliability consistency in bridge design and considering the possible differences caused by permanent load and variable loads in cost effectiveness bridge design, again, α_D = 1.25 for ULS combination 4 could be recommended for a future CHBDC. It must be noted that according to the current CHBDC v_T represents 100-year return period, although the wind load factor for the detailed procedure was calibrated based on 50-year return period value (Bartlett and King 2002).

Additional analyses by considering c' within 20 to 80 are carried out and the differences between the obtained results to those shown in Figure 3.6 are less than 5%. This simply implies that the estimated β_{75} is insensitive to c' if it is greater than 20.

Based on these considerations, the following calibration analyses for the wind load factor are carried out using c' = 40, α_D = 1.25 and the probabilistic models shown in Table 3.1. For the analyses, a range of values of α_W is considered. For a given v_v value within 0.08 and 0.18 and m_v = 18 (m/s), the value of α_W that leads to β_{75} equal to 3.5 for γ equal to 1.0 are presented in Figure 3.7a, and the estimated β_{75} values by using these α_W values are illustrated in Figure 3.7b for γ within 0 to 1.0 and v_v = 0.08, 0.13 and 0.18. Figure 3.7b shows that in all cases, the calculated β_{75} values are greater than 3.5 for γ greater than about 0.4, and as expected for γ = 1.0 the calculated β_{75} values are, on average, equal to 3.5.

The analyses leading to the curve shown in Figure 3.7a is repeated for m_v equal to 10 and 28 (m/s) and the obtained relations between α_W and v_v are almost identical to that

shown in Figure 3.7a, indicating that the relation between α_W and v_v is insensitive to m_v. Therefore, it is not shown. The difference between the calibrated α_W values to those estimated by using Eq. (3.20) increases as v_v increases. A simple fitting exercise to the estimated α_W versus v_v shown in Figure 3.7a indicates that the following empirical equation could be adequate,

$$\alpha_W = 0.92 + 8 \times v_v \tag{3.21}$$

for v_v within 0.08 to 0.18.

By repeating the analyses but considering a target reliability index, β_T, of 3, 4, or 4.5, it was concluded that the following equation for estimating α_W for β_T within 3 to 4.5 could be recommended,

$$\alpha_W = 0.89 + (5 - 5 \times \beta_T + 1.68 \times \beta_T^2) \times v_v \tag{3.22}$$

3.4 Conclusions

It is shown that use of gust effect coefficient (or factor) of 2.0 and a corresponding wind load factor of 1.65 for bridges of spans less than 125 m in the current CHBDC for the simple procedure is too conservative considering a target reliability index of 3.5 for a service life of 75 years. The suggested equation for estimating the wind load factor recommended in the code does not ensure the reliability consistency for the detailed procedure unless different bias factor for wind loading is considered. Furthermore, the results indicate that use of a dead load factor of 1.20 could lead to a reliability index significantly lower than 3.5 for wind to dead load ratio about 0.09. Based on these observations and calibration results, it is recommended that:

(1) A dead load factor α_D for cast-in-place concrete, wood, and all non-structural components equal to 1.25 is to be used to replace the current value of 1.20 for the ULS combination 4;

(2) A wind load factor α_W equal to 1.40 is to be used to replace current 1.65 for the simple procedure since the latter leads to significantly conservative design for a target reliability index of 3.5; and

(3) For the detailed procedure (i.e., for wind loads determined from wind tunnel tests), a new equation for evaluating α_W (i.e., Eq. (3.22)) is proposed. Also, simple to use

charts and corresponding equations are recommended for estimating the gust factor.

References

Barth, K.E. and Wu, H. (2007), "Development of improved natural frequency equations for continuous span steel I-girder bridges", Engineering Structures, Vol. 29(12), 3432–3442.

Bartlett, F.M. and King, J.P.C. (2002), "Wind load factors for the Canadian Highway bridges design code", Developments in Short and Medium Span Bridge Engineering – 2002, I, 683-690

Bartlett, F.M., Hong, H.P. and Zhou, W. (2003), "Load factor calibration for the proposed 2005 edition of the National Building Code of Canada: Statistics of loads and load effects", Canadian Journal of Civil Engineering, Vol. 30(2), 429-439.

Billing, J.R. and Green, R. (1984)., "Design provisions for dynamic loading of highway bridges". Transportation research record 950, Washington DC, 94–103.

Caracoglia, L. and Jones, N.P. (2003), "Time domain vs. frequency domain characterization of aeroelastic forces for bridge deck sections", Journal of Wind Engineering & Industrial Aerodynamics, Vol.91(3), 371 -402.

CHBDC (2006), Canadian Standards Association, Canadian Highway Bridge Design Code (CAN/CSA S6-6), Toronto.

Chen, X, Matsumoto, M. and Kareem, A. (2000), "Time Domain Flutter and Buffeting Response Analysis of Bridges", Journal of Engineering Mechanics, Vol. 126(1, 7-16.

Davenport, A.G. (1962), "Buffeting of a suspension bridge by storm winds", Journal of Structural Engineering, ASCE 1962; 88(ST3), 233-68.

Davenport, A.G. (1981), "Reliability of long span bridges under wind loading", Proceedings of ICOSSAR '81, Trondheim, Norway, 679-694.

Davenport, A.G. (1983), "The Relationship of Reliability to Wind Loading", Journal of Wind Engineering & Industrial Aerodynamics, Vol. 13, 3–27.

Davenport, A.G. (2000), "A comparison of seismic and windstorm hazards". In Proceedings of the 6th Environmental Specialty Conference of the Canadian Society for Civil Engineering, 7–10 June 2000, London, Ont. Canadian Society for Civil Engineering, Montréal, Que. , 504–509.

Davenport, A.G. and King, J.P.C. (1982), "The incorporation of dynamic wind loads into

the design specification for long span bridges", ACE Fall Convention and Structures Congress, New Orleans, Louisiana.

Davenport, A.G., King, J.P.C. and Mikitiuk, M.J. (1993), "The Northumberland Strait Crossing — reliability of wind loading", Boundary Layer Wind Tunnel, London, Ont.

Ellingwood, B.R, and Tekie, P.B. (1999), "Wind load statistics for probability-based structural design", Journal of Structural Engineering, ASCE, Vol. 125(4), 453-463.

Ellingwood, B.R. and Reinhold, T.A, (1980), "Reliability analysis of steel beam-columns", Journal of the Structural Division, ASCE, Vol. 106(12), 2560-2564.

Ge, Y.J. and Tanaka, H. (2000), "Aerodynamic flutter analysis of cable-supported bridges by multi-mode and full-mode approaches", Journal of Wind Engineering & Industrial Aerodynamics,Vol. 86(2-3), 123-153.

Hong, H.P. (1996), "Evaluation of the Probability of Failure with Uncertain Distribution Parameters", Civil Engineering Systems, Vol. 13, 157-168.

Hua, X.G., Chen, Z.Q., Ni, Y.Q. and Ko, J.M. (2007), "Flutter analysis of long-span bridges using ANSYS", Wind and structures, Vol.10(1), 61-82.

Jain, A., Jones, N.P. and Scanlan, R.H. (1996), "Coupled flutter and buffeting analysis of long-span bridges", Journal of Structural Engineering, ASCE, Vol. 122(7), 716-725.

MacGregor, J.G., Kennedy, D.J.L, Bartlett, F.M., Chernenko, D., Maes, M.A., and Dunaszegi, L (1997), "Design criteria and load and resistance factors for the Confederation Bridge", Canadian Journal of Civil Engineering, Vol. 24(6), 882-897.

Madsen, H.O., Krenk, S. and Lind, N.C. (1986), Methods of structural safety, Prentice-Hall, Englewood Cliffs, N. J.

Miyata, T., Yamada, H., Boonyapinyo, V. and Santos, J.C. (1995), "Analytical investigation on the response of a very long suspension bridge under gusty wind", Proceedings of Ninth ICWE, New Delhi, Vol. 2, 1006-1017.

Nowak, A.S. (1999), Calibration of LRFD bridge design code, NCHRP report 368, Transportation Research Board, Washington, D.C.

Scanlan, R.H. and Tonko, J.J. (1971), "Airfoil and bridge deck flutter derivatives", Journal of Engineering Mechanics, ASCE, Vol. 97, 1717 – 1737.

Scanlan, R.H. (1978), "Action of flexible bridges under wind, I. Flutter theory", Journal of Sound and Vibration, Vol. 60(2), 187-199.

Simiu, E. and Scanlan, R.H. (1996), Wind effects on structures, fundamentals and application to design, New York, John Wiley

Sun, D.K., Xu,Y.L., Ko, J.M, and Lin, J.H. (1999), "Fully coupled buffeting analysis of long-span cable-supported bridges: formulation", Journal of Sound and Vibration, Vol. 228(3), 569-588.

Zhou, W. and Hong, H.P. (2000), "Modeling error of strength of short RC columns", ACI Structural Journal, Vol. 97(3), 427-435.

Wen, Y.K. and Chen, H.C. (1987), "On fast integration for time variant structural reliability". Probabilistic Engineering Mechanics; Vol. 2(3), 156–62.

Table 3.1 Probabilistic models adopted for design code calibration[1].

Parameter	Mean	Coefficient of variation	Distribution type
Mean to nominal ratio for R, R/R_n	1.13	0.10	Lognormal
Mean to nominal ratio for D, D/D_n	1.05	0.10	Normal
Mean to nominal ratio for C, X_c	1.0	0.056	Normal
Mean to nominal ratio for C_e, X_{ce}	1.0	0.15 (0.075)	Normal
Mean to nominal ratio for C_h, X_{ch}	0.71 (1.0)	0.14 (0.075)	Normal
Mean to nominal ratio for C_g, X_{cg}	See Note 2	0.10	Normal
Annual maximum wind speed V (m/s)	15, 18, 21 (10 to 30)	0.11, 0.13,0.15 (0.08 to 0.18)	Gumbel

Note:

1) In cases where values considered for the simple procedure are different from those for the detailed procedure, the values associated with detailed procedure are given within the parenthesis.
2) For the simple procedure, the mean of X_{cg}, m_{xcg}, is given by the ratio of g_T (shown in Figure 3.2) evaluated at the sampled wind speed at deck height to the code value of 2.0, and for the detailed procedure, m_{xcg}, is given by ratio of g_T evaluated at the sampled wind speed at deck height to that evaluated at the design wind speed at deck height.

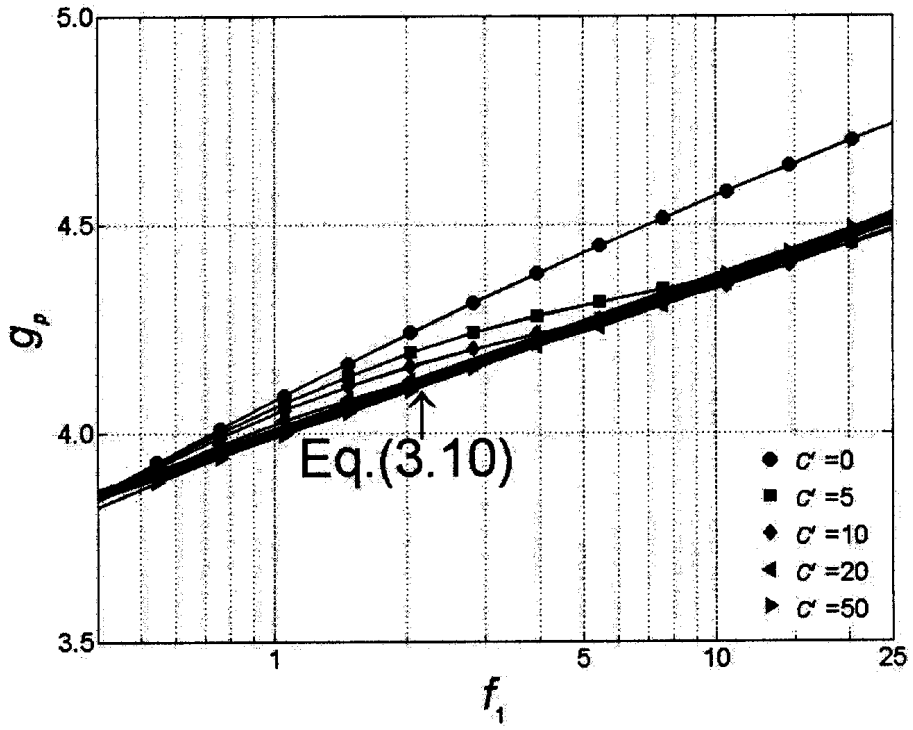

(a) For horizontal/vertical vibration ($f_1 = f_{p1}$ or f_{h1})

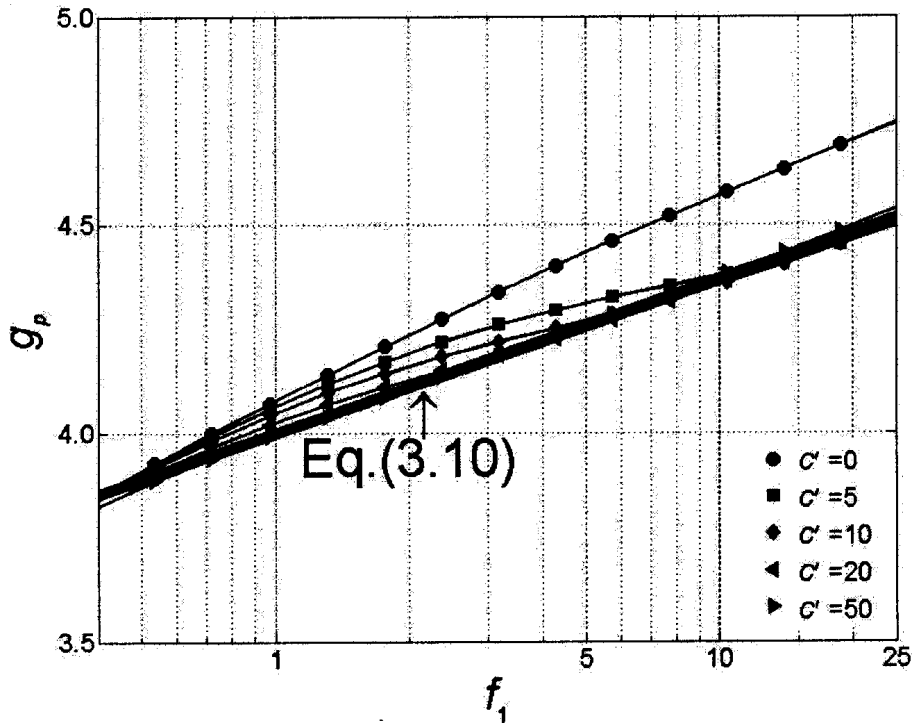

(b) For torsional vibration ($f_1 = f_{\alpha 1}$)

Figure 3.1 Peak factor from numerical results and proposed approximation (see Eq. (3.10)).

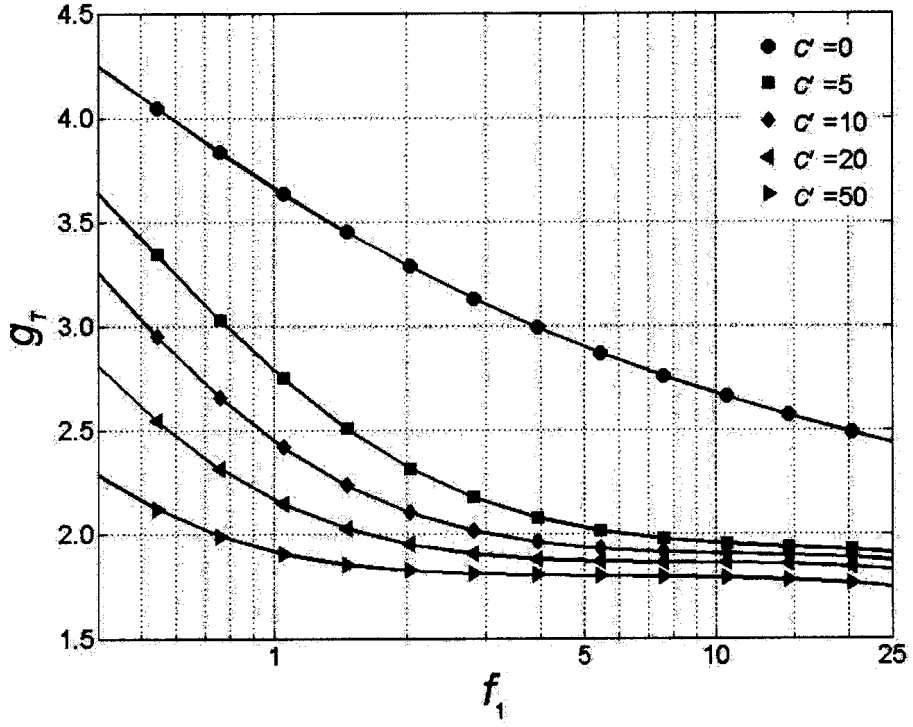

(a) For horizontal and vertical vibration (f_1=f_{p1} or f_{h1})

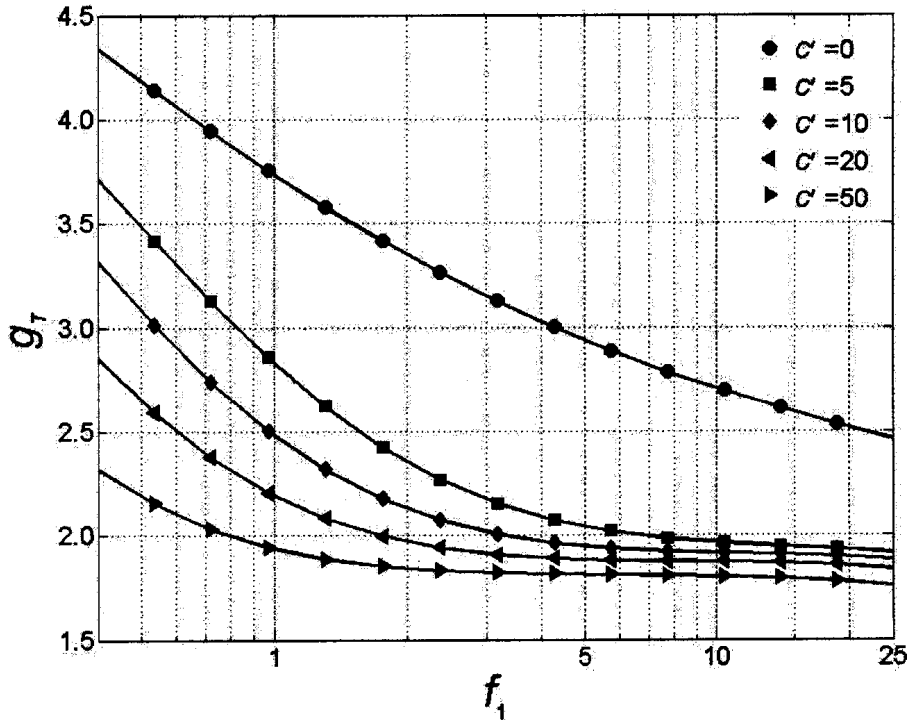

(c) For torsional vibration (f_1=$f_{\alpha 1}$)

Figure 3.2 Estimated gust factor using numerical procedure for I_u=0.11 (see Chapter 2).

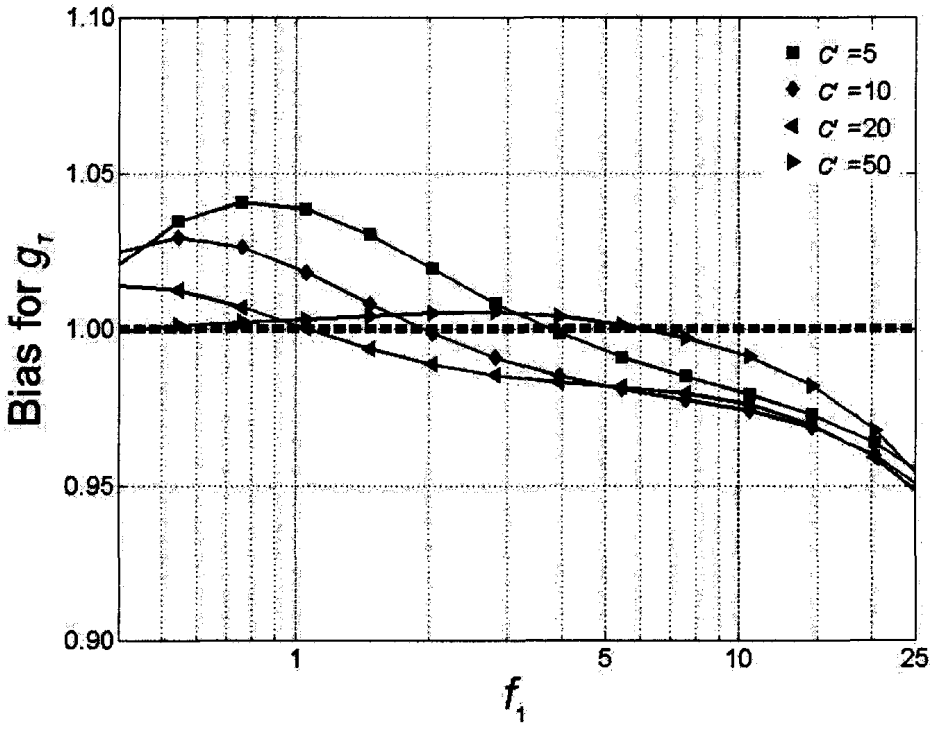

(a) For horizontal or vertical vibration ($f_1=f_{p1}$ or f_{h1})

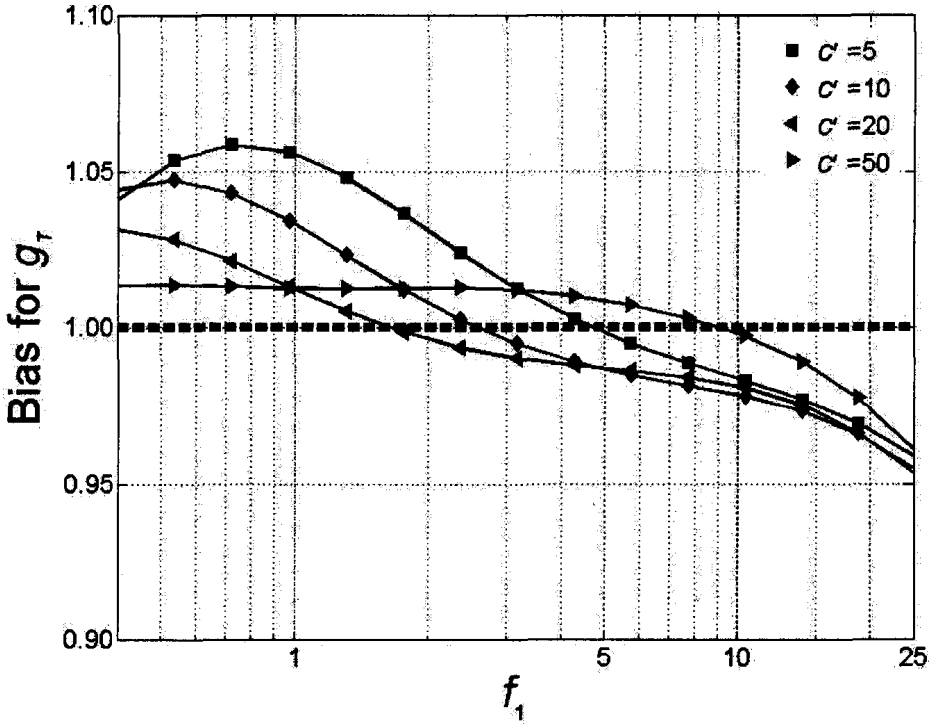

(b) For torsional vibration ($f_1=f_{\alpha 1}$)

Figure 3.3 Ratio of the calculated gust factor to that estimated based on Eqs. (3.10), (3.11a) and (3.11b) for I_u=0.11.

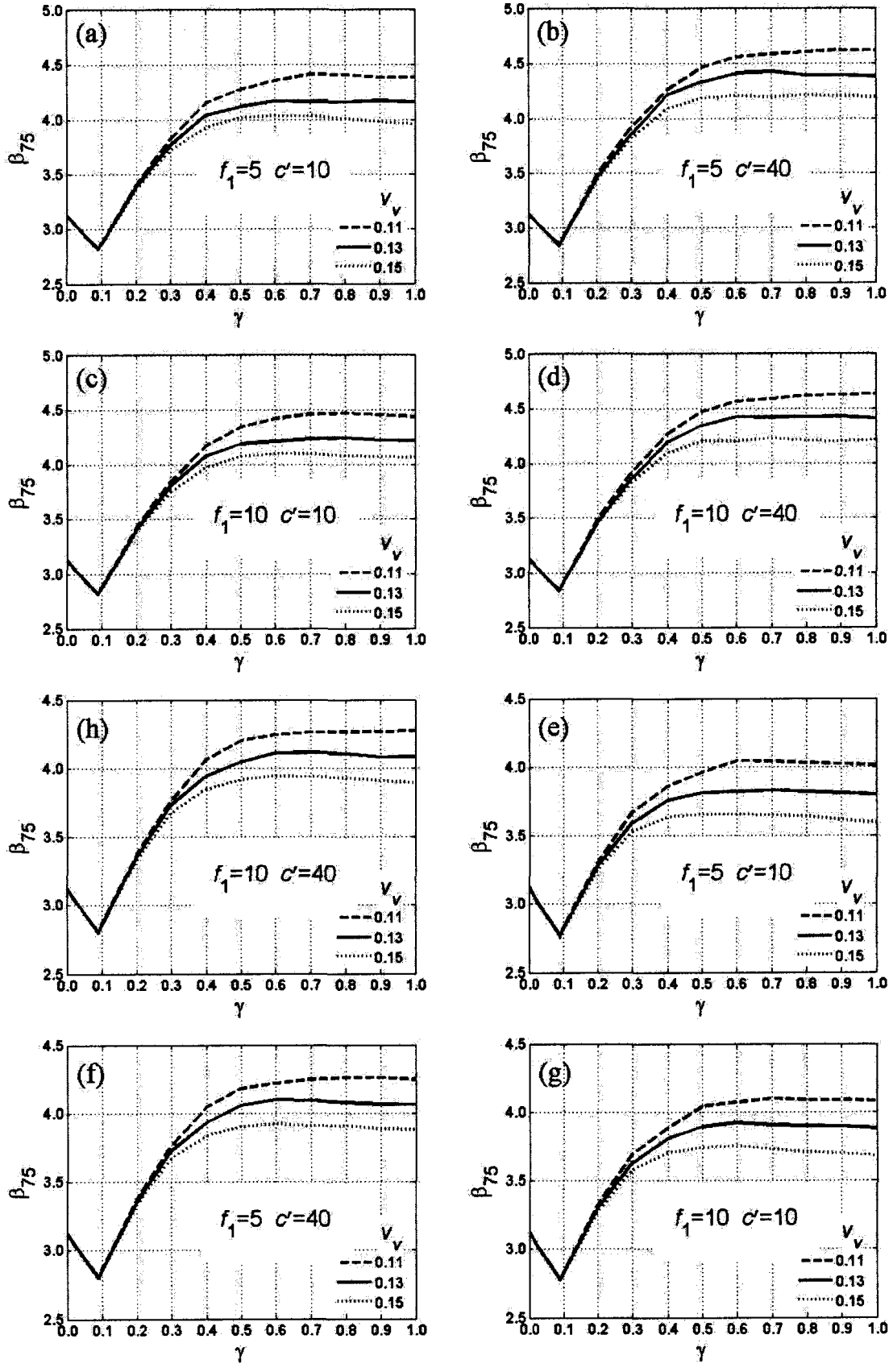

Figure 3.4 Estimated reliability for α_D=1.20 and α_W=1.65 (results shown in a) to d) are for I_u=0.11 and in e) to h) are for I_u=0.15).

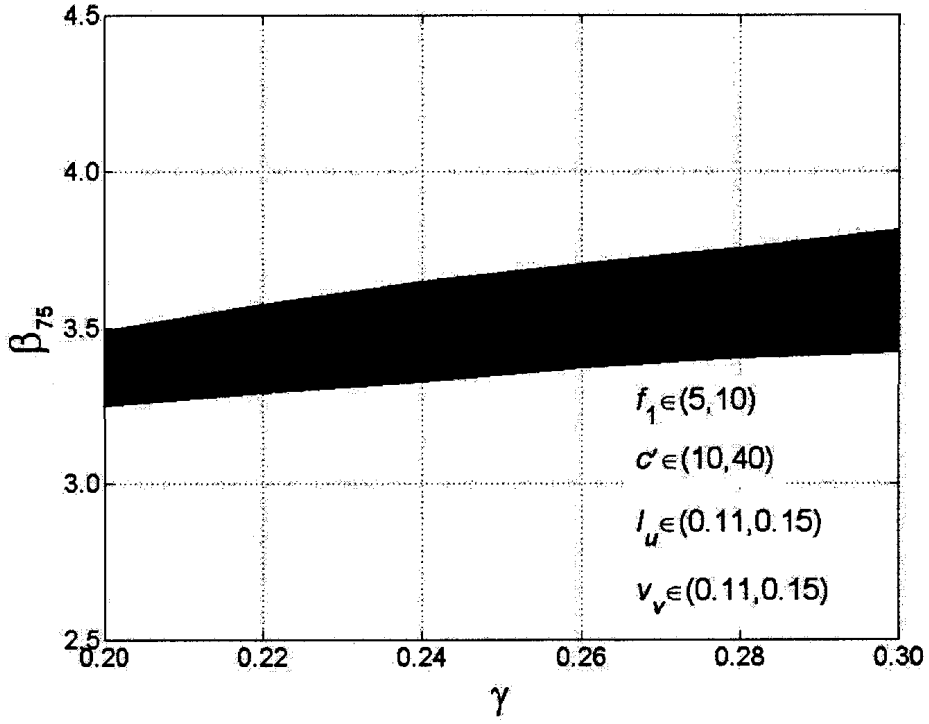

Figure 3.5. Estimated reliability considering α_D=1.25 and α_W=1.40.

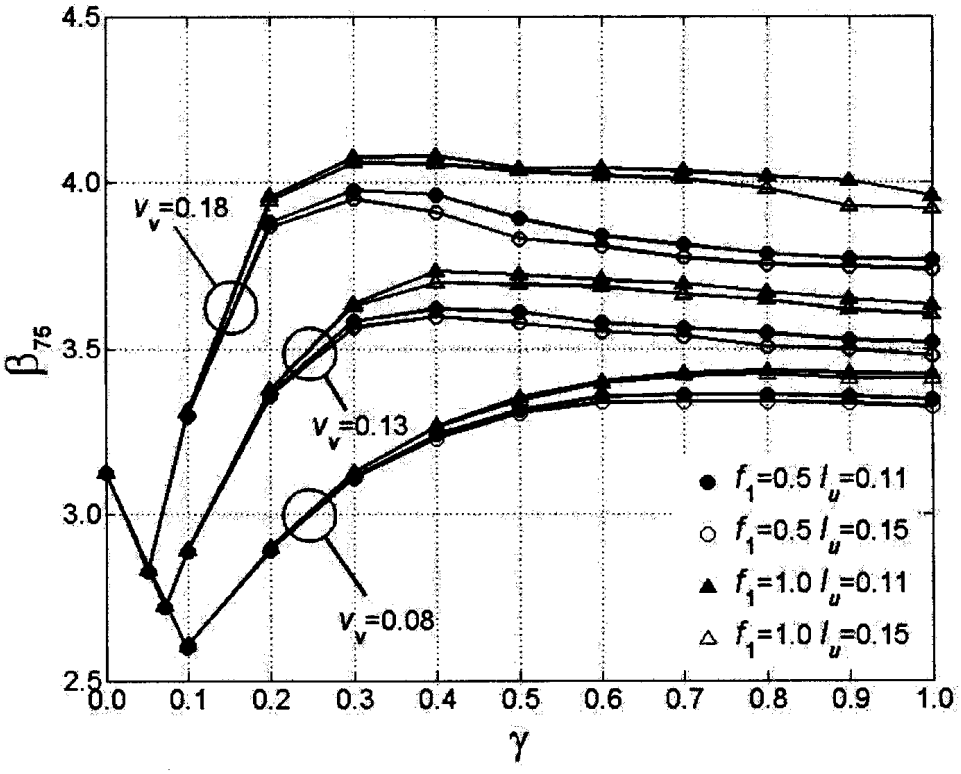

Figure 3.6 Calculated reliability considering the detailed procedure using α_D=1.20 and α_W estimated using code recommended equation (see Eq. (3.20)).

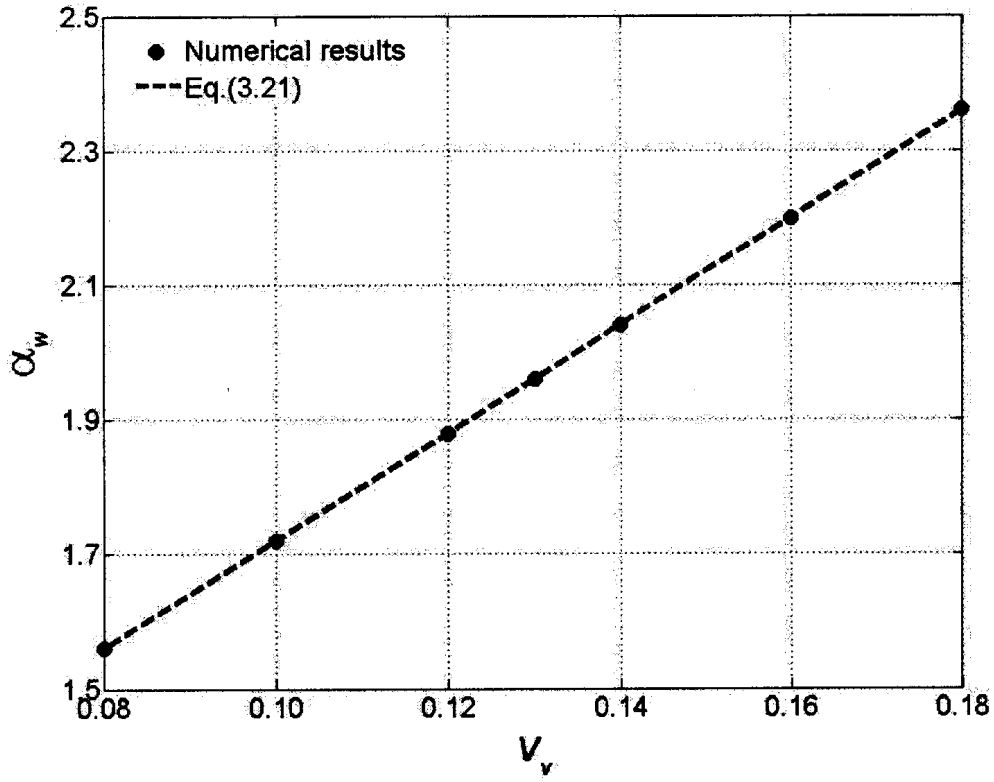

(a) Relation between α_W and v_v.

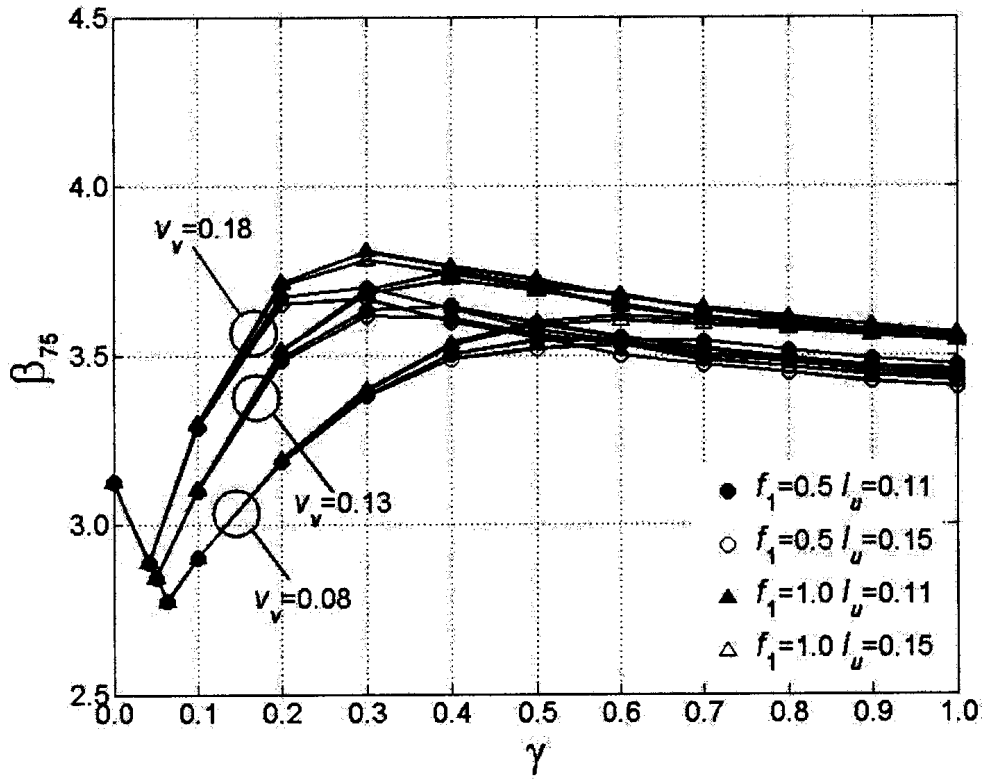

(b) Estimated β_{75} using $\alpha_D = 1.25$ and α_W shown in (a).

Figure 3.7 Derived new α_W and calculated β_{75} for the detailed procedure.

Chapter 4 Summary, conclusions and future works

4.1 Summary and conclusions

This study focused on the assessment of the gust factor considering the spatio-temporal along and cross fluctuating winds and aeroelastic forces, and the verification of the accuracy of simple approximate analytical expression for estimating the gust factor. It also provided the probability basis, calibration procedure and results for recommending the wind load factors and gust factor curves for a future edition of the CHBDC.

The conclusions that can be drawn from the study include:

1) The standard deviation of a response of interest, such as the bridge midspan horizontal, vertical or torsional displacement, is directly proportional to a normalized standard deviation that depends on: a scaled exponential decay coefficient for the spanwise coherence of the fluctuating wind, Monin coordinate evaluated at the frequency of the first vibration mode, and structural damping ratio. This simplifies the parametric investigation.
2) A set of curves for gust factor, which could be implemented in bridge design codes, was obtained based on the finite element analysis. Comparison of the curves to an often used practical approximation indicates that although the approximation is sufficiently accurate, it slightly underestimates the gust factor. The underestimation depends on the spanwise coherence of the fluctuating wind, and is more significant for an increased bridge span length. Furthermore, the approximation can be slightly biased if the effect of aeroelastic self-excited contributions is considered.
3) It is shown that use of gust effect coefficient (or factor) of 2.0 and a corresponding wind load factor of 1.65 for bridges of spans less than 125 m in the current CHBDC for the simple procedure is too conservative considering a target reliability index of 3.5 for a service life of 75 years, and that the use of the current dead load factor of 1.20 leads to unconservative designs.
4) Calibration results indicate that for simple procedure, a dead load factor of 1.25 and a wind load factor of 1.4 can be recommended for a future edition of the CHBDC considering a target reliability index of 3.5 for a service life of 75 years.
5) For the detailed procedure (i.e., for wind loads determined from wind tunnel tests), a

new equation for evaluating α_W (i.e., Eq. (3.22)) is proposed. Also, simple to use charts and corresponding approximate equations are recommended for estimating the gust factor.

4.2 Suggested future works

Several topics which are not covered by the present study can be of interest and valuable for assessing the safety of bridges. Only two are listed below:

1) The effect of uncertainty in aerodynamic derivatives in the estimated aerodynamic damping, and critical wind speed. Such a study requires the information of the aerodynamic derivatives of bridge sections obtained from wind tunnel as well as the bridge dynamic characteristics.
2) An investigation of the cost-benefit effect and the consideration of structural deterioration such as corrosion on the selection of target reliability levels is needed. The investigation will indicate how close the currently adopted target reliability index is to that implied by the optimal design.

Appendix A Using ANSYS to evaluate the critical wind velocity

The following ANSYS Parametric Design Language (APDL) code is taken from Hua et al. (2007) with slight modifications and extra comments. The output from ANSYS is employed to find the critical wind velocity U_{cr} that is associated with instability (i.e., wind velocity corresponding to the incipient of positive real part of an eigenvalue).

```
FINISH
/CLEAR,START
/TITLE, Flutter Analysis for a simply supported-beam like bridge
! define the structure parameters
LL=300          !the length of the bridge (m)
TNE=30          !the total number of beam4 element
NN=TNE+1        !the total nodes
AA=10           !the area of cross-section (m^2)
IYY=10          !Iyy (m^4)
IZZ=85.714      !Izz (m^4)
IXX=5.076       !Ixx (m^4)
TKY=40          !the width of the bridge deck (m)
TKZ=0.25        !the height of the bridge deck (m)
IMM=4.5e2       !the mass moment of inertia per length (10^4 kg•m^4/m)
EXX=2.1e7       !the Young's modulus (10^4 Pa)
DE=0.2          !the mass of the bridge per length (10^4 kg/m^3)
SH=8.077e6      !the Shear modulus (10^4 Pa)

! Build the model of the bridge deck with beam4 and mass21 element
/PREP7
ET,1,BEAM4
ET,2,MASS21
N,1,0,0
N,NN,LL,0,0
FILL,1,NN
R,1,AA,IZZ,IYY,TKZ,TKY,,,
RMORE,0,IXX,,,,,,
R,2,,,,IMM*LL/TNE,,,
MP,EX,1,EXX
MP,DENS,1,DE
MP,GXY,1,SH
TYPE,1
REAL,1
*DO,i,1,TNE,1
E,i,i+1
*ENDDO
TYPE,2
REAL,2
*DO,i,2,TNE,1
E,i
*ENDDO
D,1,UX,0,0,,,UY,UZ,ROTX
D,NN,UY,0,0,,,,UZ,ROTX
FINISH
```

```
! Model analysis without Matrix 27
/SOLU
ANTYPE,MODAL
MODOPT,LANB,10
MXPAND,10
LUMPM,ON
ALLSEL,ALL,ALL
SOLVE           ! undamped eigenvalue analysis
FINISH

*DIM,freq0,ARRAY,10
*CFOPEN,naturalfrequency,TXT
/POST1
*DO,i,1,10,1
*GET,freq0(i),MODE,i,FREQ,,,
temp=freq0(i)
*VWRITE,i,temp
(5X,F10.2,5X,F20.10)
*ENDDO
FINISH
*CFCLOS

! Add Matrix 27 into the bridge model
/PREP7
ET,3,MATRIX27,,1,4,,,,,        ! Type 3 aeroelastic stiffness matrix
ET,4,MATRIX27,,1,5,,,,,        ! Type 4 aeroelastic damping matrix
R,3,,,,,,     ! Real constant 3 for aeroelastic stiffness matrix
R,4,,,,,,     ! Real constant 4 for aeroelastic damping matrix

NGEN,2,TNE,2,TNE,1,0,0,-10    ! create the fictitious nodes
TYPE,3
REAL,3
*DO,i,2,TNE,1
E,i,i+TNE
*ENDDO
TYPE,4
REAL,4
*DO,i,2,TNE,1
E,i,i+TNE
*ENDDO

NSEL,S,,,2+TNE,2*TNE
D,ALL,ALL
FINISH

*DIM,STIF,ARRAY,4,
*DIM,DMP,ARRAY,4,
*DIM,drv,TABLE,26,8,,,,,,
! input flutter derivatives from Flutterdrv.txt
*TREAD,drv,Flutterdrv,TXT,,,
*DIM,freqlr,ARRAY,10,
*DIM,freqli,ARRAY,10,

! Write the results into [result].txt
*CFOPEN,RESULT,TXT
```

```
B=40                    ! the width of the bridge deck (m)
p=1.248e-4              ! the air mass density (10^4 kg/m^3)
lle=LL/TNE              ! the length of one beam4 element

*DO,ii,0,160,1          ! define the wind velocity range 0-160 m/s
u=ii
*DO,jj,1,10,1           ! number of complex modes considered
flag=1
count=1
ntol=20                 ! Maximum iterations
omiga=freq0(jj)*2*3.1415926
f0=omiga/(2*3.1415926) ! set the initial oscillation frequency
*DOWHILE,flag
rv=u/(f0*B)             ! reduced wind velocity rv
uk=2*3.1415926*f0*B     ! uk=u*k=w*B
/PREP7
KKK=0.5*lle*p*uk*uk              ! stiffness coefficient
CCC=0.5*lle*p*B*uk               ! damping coefficient
STIF(1)=-KKK*drv(rv,8)        ! H4
STIF(2)=-KKK*B*drv(rv,7)      ! H3
STIF(3)=-KKK*B*drv(rv,4)      ! A4
STIF(4)=-KKK*B*B*drv(rv,3)    ! A3
DMP(1)=-CCC*drv(rv,5)         ! H1
DMP(2)=-CCC*B*drv(rv,6)       ! H2
DMP(3)=-CCC*B*drv(rv,1)       ! A1
DMP(4)=-CCC*B*B*drv(rv,2)     ! A2
RMODIF,3,24,STIF(1),STIF(2),
RMODIF,3,34,STIF(4)
RMODIF,3,69,STIF(1),STIF(2),
RMODIF,3,73,STIF(4)
RMODIF,3,84,STIF(3)
RMODIF,3,123,STIF(3)
RMODIF,4,24,DMP(1),DMP(2)
RMODIF,4,34,DMP(4)
RMODIF,4,69,DMP(1),DMP(2)
RMODIF,4,73,DMP(4)
RMODIF,4,84,DMP(3)
RMODIF,4,123,DMP(3)
FINISH

! Model analysis with Matrix 27
/SOLU
ANTYPE,MODAL
MODOPT,DAMP,20
MXPAND,20
LUMPM,ON
ALLSEL,ALL,ALL
SOLVE
FINISH

ik=2*(jj-1)+1
! extract the real part of complex mode
*GET,freqlr(jj),MODE,ik,FREQ,,,,
! extract the imaginary part of complex mode
*GET,freqli(jj),MODE,ik,FREQ,IMAG,,,
norm=abs((freqli(jj)-f0)/freqli(jj))  ! Define error norm
! Control if error norm is within tolerance
```

```
*IF,norm,LE,1e-3,THEN
flag=-1                          ! Exit loop if satisfied
*ELSE
f0=freqli(jj)                    ! Otherwise define a new frequency
count=count+1
*ENDIF

*IF,count,EQ,ntol,THEN
flag=-1                          ! Exit loop after ntol iterations
*ENDIF

*IF,abs(freqlr(jj)),LE,1e-5,THEN
freqlr(jj)=0
*ENDIF

*ENDDO

/POST1
temp1=freqlr(jj)
temp2=freqli(jj)
*VWRITE,u,temp1,temp2,count
(5X,F6.2,5X,F10.5,5X,F10.5,5X,F4.1)
FINISH
*ENDDO                            ! enddo jj
*ENDDO                            ! enddo u
*CFCLOS
```

Note the aerodynamic derivatives that are needed for the example analysis presented in Figure 2.4 are given in Table A.1.

Table A.1. Aerodynamic derivatives calculated based on Theodorsen's solution.

V	A_1	A_2	A_3	A_4	H_1	H_2	H_3	H_4
0	0.0000	0.0000	0.0000	0.0000	0.0000	0.0000	0.0000	1.5708
1	0.1264	-0.0324	0.0716	0.0096	-0.5058	-0.3703	-0.0901	1.5325
2	0.2597	-0.0713	0.1406	0.0354	-1.0390	-0.7146	-0.3661	1.4291
3	0.4026	-0.1216	0.2595	0.0728	-1.6105	-1.0137	-0.8417	1.2797
4	0.5555	-0.1862	0.4322	0.1179	-2.2221	-1.2554	-1.5325	1.0993
5	0.7180	-0.2667	0.6625	0.1680	-2.8720	-1.4332	-2.4535	0.8987
6	0.8893	-0.3640	0.9536	0.2213	-3.5570	-1.5440	-3.6180	0.6857
7	1.0685	-0.4782	1.3085	0.2763	-4.2738	-1.5871	-5.0377	0.4656
8	1.2548	-0.6092	1.7297	0.3321	-5.0190	-1.5633	-6.7225	0.2423
9	1.4474	-0.7564	2.2193	0.3880	-5.7894	-1.4742	-8.6808	0.0188
10	1.6456	-0.9195	2.7790	0.4435	-6.5823	-1.3221	-10.9196	-0.2032
11	1.8488	-1.0976	3.4103	0.4983	-7.3951	-1.1096	-13.4448	-0.4222
12	2.0564	-1.2902	4.1145	0.5520	-8.2255	-0.8392	-16.2615	-0.6373
13	2.2679	-1.4965	4.8926	0.6046	-9.0716	-0.5138	-19.3739	-0.8478
14	2.4829	-1.7160	5.7455	0.6560	-9.9317	-0.1360	-22.7855	-1.0533
15	2.7011	-1.9479	6.6739	0.7061	-10.8042	0.2916	-26.4993	-1.2536
16	2.9220	-2.1916	7.6786	0.7548	-11.6880	0.7665	-30.5179	-1.4485
17	3.1454	-2.4466	8.7600	0.8022	-12.5816	1.2865	-34.8435	-1.6380
18	3.3711	-2.7123	9.9185	0.8482	-13.4843	1.8492	-39.4778	-1.8222
19	3.5987	-2.9881	11.1547	0.8930	-14.3949	2.4526	-44.4225	-2.0011
20	3.8282	-3.2737	12.4688	0.9364	-15.3129	3.0947	-49.6788	-2.1749
21	4.0593	-3.5684	13.8611	0.9786	-16.2374	3.7737	-55.2480	-2.3436
22	4.2919	-3.8720	15.3318	1.0196	-17.1678	4.4880	-61.1309	-2.5075
23	4.5259	-4.1839	16.8812	1.0594	-18.1035	5.2358	-67.3285	-2.6667
24	4.7610	-4.5039	18.5095	1.0980	-19.0442	6.0157	-73.8415	-2.8213
25	4.9973	-4.8316	20.2167	1.1356	-19.9893	6.8263	-80.6704	-2.9716

Appendix B Evaluation of buffeting force

The derivation of the matrices shown in this appendix is provided in detail in Sun et al. (1999). For completeness and easy reference, they are listed below.

B.1) Derivation of *E* matrix for beam element

According to potential energy method, the buffeting force vector acting on the element of the bridge deck, $\mathbf{F}_b^e$, can be obtained by,

$$\mathbf{F}_b^e = \int_l \mathbf{B}^{e\mathrm{T}} \mathbf{A}_b^e \mathbf{q}^e dx \tag{B1}$$

where l is the length of the element; $\mathbf{q}^e = \left[u^e(t), w^e(t)\right]^{\mathrm{T}}$ denotes the fluctuating along and vertical cross wind velocities at midpoint of the element,

$\mathbf{A}_b^e = \begin{bmatrix} C_1 \dfrac{2C_D}{U} & C_1 \dfrac{2C_L}{U} & C_2 \dfrac{2C_M}{U} \\ C_1 \dfrac{C'_D}{U} & C_1 \dfrac{(C_D + C'_L)}{U} & C_2 \dfrac{C'_M}{U} \end{bmatrix}^{\mathrm{T}}$ does not change within the element length;

$\mathbf{B}^e$ is the 3×12 shape function matrix of the beam element, and is given as,

$$\mathbf{B}^e = \begin{bmatrix} 0 & \psi_1 & 0 & 0 & 0 & \psi_3 & 0 & \psi_2 & 0 & 0 & 0 & \psi_4 \\ 0 & 0 & \psi_1 & 0 & -\psi_3 & 0 & 0 & 0 & \psi_2 & 0 & -\psi_4 & 0 \\ 0 & 0 & 0 & 1-x/l & 0 & 0 & 0 & 0 & 0 & x/l & 0 & 0 \end{bmatrix} \tag{B2}$$

in which $\psi_1 = 1 - 3\left(\frac{x}{l}\right)^2 + 2\left(\frac{x}{l}\right)^3$, $\psi_2 = 3\left(\frac{x}{l}\right)^2 - 2\left(\frac{x}{l}\right)^3$ and

$\psi_3 = x\left(1 - \frac{x}{l}\right)^2$, $\psi_4 = \frac{x^2}{l}\left(\frac{x}{l} - 1\right)$.

So $\mathbf{E}_b^e$ for the bridge deck can be derived as follows:

$$\mathbf{E}_b^e = \int_l \mathbf{B}^{e\mathrm{T}} \mathbf{A}_b^e dx =$$

$$\begin{bmatrix} 0 & C_1 C_D \frac{l}{U} & C_1 C_L \frac{l}{U} & C_2 C_M \frac{l}{U} & -\frac{C_1 C_L}{6}\frac{l^2}{U} & \frac{C_1 C_D}{6}\frac{l}{U} \\ 0 & \frac{C_1 C_D'}{2}\frac{l}{U} & \frac{C_1(C_L'+C_D)}{2}\frac{l}{U} & \frac{C_2 C_M'}{2}\frac{l}{U} & -\frac{C_1(C_L'+C_D)}{12}\frac{l^2}{U} & \frac{C_1 C_D'}{12}\frac{l^2}{U} \end{bmatrix} \quad \text{(B3)}$$

$$\begin{bmatrix} 0 & C_1 C_D \frac{l}{U} & C_1 C_L \frac{l}{U} & C_2 C_M \frac{l}{U} & \frac{C_1 C_L}{6}\frac{l^2}{U} & -\frac{C_1 C_D}{6}\frac{l}{U} \\ 0 & \frac{C_1 C_D'}{2}\frac{l}{U} & \frac{C_1(C_L'+C_D)}{2}\frac{l}{U} & \frac{C_2 C_M'}{2}\frac{l}{U} & \frac{C_1(C_L'+C_D)}{12}\frac{l^2}{U} & -\frac{C_1 C_D'}{12}\frac{l^2}{U} \end{bmatrix}^{\mathrm{T}}$$

The bridge tower can also be modeled as a beam element, similarly the buffeting force vector acting on the element of the bridge tower, $\mathbf{F}_{b,t}^e$, can be derived by,

$$\mathbf{F}_{b,t}^e = \int_l \mathbf{B}^{e\mathrm{T}} \mathbf{A}_{b,t}^e \mathbf{r}^e dx \quad \text{(B4)}$$

where, $\mathbf{r}^e = \begin{bmatrix} u^e(t) & v^e(t) \end{bmatrix}^{\mathrm{T}}$ denotes the fluctuating along and lateral cross wind velocities at midpoint of the element ; $\mathbf{A}_{b,t}^e = \begin{bmatrix} C_{1,t}\frac{2C_{D,t}}{U} & C_{1,t}\frac{2C_{L,t}}{U} & C_{2,t}\frac{2C_{M,t}}{U} \\ C_{1,t}\frac{C_{D,t}'}{U} & C_{1,t}\frac{(C_{D,t}+C_{L,t}')}{U} & C_{2,t}\frac{C_{M,t}'}{U} \end{bmatrix}^{\mathrm{T}}$ does not change within the element length, where the second subscript t denotes the corresponding symbols for the bridge tower. It should notice that the wind angle of attack here is the angle of normal incident wind referring to the vertical plane of the tower segment.

$\mathbf{E}_b^e$ for the bridge tower, termed as $\mathbf{E}_{b,t}^e$, can be derived as,

$$\mathbf{E}_{b,t}^e =$$

$$\begin{bmatrix} 0 & C_{1,t}C_{D,t}\frac{l}{U} & C_{1,t}C_{L,t}\frac{l}{U} & C_{2,t}C_{M,t}\frac{l}{U} & -\frac{C_{1,t}C_{L,t}}{6}\frac{l^2}{U} & \frac{C_{1,t}C_{D,t}}{6}\frac{l}{U} \\ 0 & \frac{C_{1,t}C_{D,t}'}{2}\frac{l}{U} & \frac{C_{1,t}(C_{L,t}'+C_{D,t})}{2}\frac{l}{U} & \frac{C_{2,t}C_{M,t}'}{2}\frac{l}{U} & -\frac{C_{1,t}(C_{L,t}'+C_{D,t})}{12}\frac{l^2}{U} & \frac{C_{1,t}C_{D,t}'}{12}\frac{l^2}{U} \end{bmatrix}$$

$$\begin{bmatrix} 0 & C_{1,t}C_{D,t}\frac{l}{U} & C_{1,t}C_{L,t}\frac{l}{U} & C_{2,t}C_{M,t}\frac{l}{U} & \frac{C_{1,t}C_{L,t}}{6}\frac{l^2}{U} & -\frac{C_{1,t}C_{D,t}}{6}\frac{l}{U} \\ 0 & \frac{C_{1,t}C_{D,t}'}{2}\frac{l}{U} & \frac{C_{1,t}(C_{L,t}'+C_{D,t})}{2}\frac{l}{U} & \frac{C_{2,t}C_{M,t}'}{2}\frac{l}{U} & \frac{C_{1,t}(C_{L,t}'+C_{D,t})}{12}\frac{l^2}{U} & -\frac{C_{1,t}C_{D,t}'}{12}\frac{l^2}{U} \end{bmatrix}^{\mathrm{T}} \quad \text{(B5)}$$

B.2) Derivation of *E* matrix for cable element

The buffeting force vector acting on the element of the bridge cable, $\mathbf{F}_{b,c}^{e}$, can be expressed as,

$$\mathbf{F}_{b,c}^{e} = \int_{l} \mathbf{B}_{c}^{e\mathrm{T}} \mathbf{A}_{b,c}^{e} \mathbf{u}^{e} dx \tag{B6}$$

where $\mathbf{u}^{e} = [u^{e}(t)]$ denotes the fluctuating along wind velocity at midpoint of the element; $\mathbf{A}_{b,c} = \left[C_{1,c} \dfrac{2C_{D,c}}{U} \quad C_{1,c} \dfrac{2C_{L,c}}{U} \right]^{\mathrm{T}}$ does not change within the element length, where the second subscript c denotes the corresponding symbols for the bridge cable. $\mathbf{B}_{c}^{e}$ is the 2×6 shape function matrix of the cable element which is given as,

$$\mathbf{B}_{c}^{e} = \begin{bmatrix} 0 & 1-x/l & 0 & 0 & x/l & 0 \\ 0 & 0 & 1-x/l & 0 & 0 & x/l \end{bmatrix}. \tag{B7}$$

$\mathbf{E}_{b}^{e}$ for the bridge cable , termed as $\mathbf{E}_{b,c}^{e}$, can be derived as,

$$\mathbf{E}_{b,c}^{e} = \left[0 \quad C_{1,c}C_{D,c}\frac{l}{U} \quad C_{1,c}C_{L,c}\frac{l}{U} \quad 0 \quad C_{1,c}C_{D,c}\frac{l}{U} \quad C_{1,c}C_{L,c}\frac{l}{U} \right]^{\mathrm{T}} \tag{B8}$$

B.3) Derivation of $\mathbf{T}^{e}$ matrix for simply supported beam

For the simply supported beam, the element number is assigned in sequence from left to right, so the right node of (k-1)-th element and left node of k-th element are the same. Then, the transformation matrix $\mathbf{T}^{e}$ is derived as,

$$\mathbf{T}^{e} = \left[\underbrace{\mathbf{0} \quad \cdots \quad \mathbf{0}}_{6(k-1)} \quad \mathbf{I} \quad \underbrace{\mathbf{0} \quad \cdots \quad \mathbf{0}}_{6(n-k)} \right]^{\mathrm{T}} \tag{B9}$$

where $\mathbf{I}$ is the 12×12 identity matrix, $\mathbf{0}$ is the 12×1 zero array.

Appendix C Simplified approach for evaluating buffeting effect on short and medium span bridges

Consider a simply supported bridge at the height z above the ground shown in Figure C.1. The governing equation of motion for lateral deflection of the beam p, $p = p(x, t)$, is well known and can be expressed as (Clough and Penzien 1993),

$$EI_z \frac{\partial^4 p(x,t)}{\partial x^4} + m\frac{\partial^2 p(x,t)}{\partial t^2} = D(x,t), \tag{C1}$$

where EI_z is the flexural rigidity of the beam, E is the Young's modulus, of elasticity of the beam, I_z is the moment of inertia, m is mass of the beam per unit length, x denotes the coordinate along the bridge axis, $D(x,t)$ represents the time-dependent wind-induced pressure at x.

Before solving the governing equation, we note that the wind pressure $D(x, t)$ varies in time and space and is a stochastic process. It can be related to the wind velocity at the height z,

$$D(x,t) = \frac{1}{2}\rho B C_D (U + u(x,t))^2, \tag{C2}$$

where, U and $u(x,t)$ are the mean component and the longitudinal fluctuating of the wind velocity at the height z, respectively; C_D is the pressure coefficient; B is the width of the bridge deck; and ρ is the air density. Since the fluctuating wind velocity is considered to be much smaller than its corresponding mean component in magnitude, Eq. (C2) is approximated by,

$$D(x,t) \approx D_s + d(x,t) \tag{C3}$$

where $D_s = \rho B C_D U^2/2$, and $d(x,t) = 2D_s u(x,t)/U$. $u(x,t)$ at the height z (m) above the ground surface is usually treated as a stationary process and is characterized by its power spectral density (PSD) function $S_u(z,\omega)$, where ω is the frequency. The PSD function $S_u(z,\omega)$ could be modeled using the Davenport spectrum, Kaimal spectrum, or von Karman spectrum (see Simiu and Scanlan 1996). The Kaimal spectrum as given in Simiu and Scanlan (1996), which is adopted in the present study, is shown in Eq. (2.4a) for the longitudinal fluctuating wind speed. By using this PSD function, the PSD function of the

fluctuating wind pressure $d(x,t)$, $S_{dd}(z, \omega)$ can be expressed as,

$$S_{dd}(z,\omega) = 4D_s^2 I_u^2 S_u(z,\omega)/\sigma_u^2 \tag{C4}$$

where I_u denotes the longitudinal turbulence intensity which equals σ_u / U, and σ_u is the standard deviation of $u(x,t)$.

To take into account the spatial variability of fluctuating wind, it is considered that the co-spectrum of the wind fluctuation for two points on the bridge deck with coordinates x and x', $S_u^C(x,x',\omega)$ can be expressed as,

$$S_u^C(x,x',\omega) = S_u(z,\omega)R(x,x',\omega) \tag{C5}$$

where $R(x,x',\omega)$ is the normalized co-spectrum of wind fluctuation, and can expressed as,

$$R(x,x',\omega) = \exp\left(-\frac{C_x \omega}{2\pi U}|x-x'|\right) \tag{C6}$$

and C_x is known as the exponential decay coefficient for the spanwise coherence of along wind fluctuation.

Based on Eqs. (C4) and (C6), Eq. (C5) can be written as,

$$S_{dd}^C(x,x',\omega) = (2D_s I_u)^2 \frac{S_u(z,\omega)}{\sigma_u^2} \exp\left(-\frac{C_x \omega L}{2\pi U}|\eta-\eta'|\right) \tag{C7}$$

where $\eta = x/L$ and $\eta' = x'/L$ represent the normalized coordinates, and L is the bridge span length.

To solve the governing equation given in Eq. (C1) under the above described wind loading, we note that for the simply supported beam, the frequency of j-th vibration mode ω_j is given by,

$$\omega_j = (j\pi/L)^2 \sqrt{EI_z/m} \text{ (rad/sec)}, \tag{C8}$$

and the shape function $\phi_j(x)$ is given by,

$$\phi_j(x) = \sin(j\pi x/L), \tag{C9}$$

By introducing viscous damping to the system, the solution of the equation can be expressed as,

$$p(x,t) = \sum_j \phi_j(x) y_j(t), \tag{C10}$$

where $y_j(t)$ is governed by

$$\tilde{M}_j\ddot{y}_j(t)+2\xi_j\sqrt{\tilde{K}_j\tilde{M}_j}\dot{y}_j(t)+\tilde{K}_j y_j(t)=\tilde{D}_j(t), \tag{C11}$$

in which ξ_j represents the damping ratio for the *j*-th modal, and the generalized mass $\tilde{M}_j$, stiffness $\tilde{K}_j$ and force $\tilde{D}_j(t)$ are given by,

$$\tilde{M}_j=\int_0^L m\left(\phi_j(x)\right)^2dx=mL/2 \tag{C12a}$$

$$\tilde{K}_j=\int_0^L EI_z\left(\phi''_j(x)\right)^2dx=j^4\frac{\pi^4EI_z}{2L^3} \tag{C12b}$$

and,

$$\tilde{D}_j=D_s\int_0^L\phi_j(x)dx+\int_0^L d(x,t)\phi_j(x)dx \tag{C12c}$$

The response due to mean wind pressure by considering the *j*-th mode, $\bar{y}_j$, is simply given by,

$$\bar{y}_j=D_s\int_0^L\phi_j(x)dx/\tilde{K}_j\ , \tag{C13}$$

The response due to fluctuating wind pressure can be evaluated based on the random vibration theory (Simiu and Scanlan 1996). In such a case, the PSD function of $p(x,t)$, $S_{pp}(x,\omega)$, is given by,

$$S_{pp}(x,\omega)=\sum_j\sum_k\phi_j(x)\phi_k(x)H_j(\omega)H_k^*(\omega)S_{Q_jQ_k}(\omega)/\tilde{K}_j\tilde{K}_k \tag{C14}$$

where the superscript $*$ denotes the complex conjugate;

$$S_{Q_jQ_k}(\omega)=\int_0^L\int_0^L S_{dd}^C(x,x',\omega)\phi_j(x)\phi_k(x')dxdx' \tag{C15}$$

and,

$$H_j(\omega)=\frac{1}{1-\left(\omega/\omega_j\right)^2+2i\xi\left(\omega/\omega_j\right)}. \tag{D16}$$

The variance of $p(x,t)$, $\sigma_p^2(x)$, due to fluctuating wind velocity is calculated from,

$$\sigma_p^2(x)=\sum_j\sum_k\frac{\phi_j(x)\phi_k(x)}{\tilde{K}_j\tilde{K}_k}\int_0^\infty H_j(\omega)H_k^*(\omega)S_{Q_jQ_k}(\omega)d\omega, \tag{C17}$$

Based on Eqs. (C4), (C7), (C14), (C15), (C16), and (C17), we have

$$\left(\sigma_p(x)/\left(\bar{p}I_u\pi\right)\right)^2 = \sum_j\sum_k \sin(j\pi x/L)\sin(k\pi x/L)\times$$

$$\int_{\mathcal{D}f}\int_0^1\int_0^1 \frac{200}{6(1+50f)^{5/3}}\exp\left(-c'f|\eta-\eta'|\right)\sin(j\pi\eta)\sin(k\pi\eta')H_j(f,f_{p1})H_k^*(f,f_{p1})d\eta d\eta' df \tag{C18a}$$

where,

$$\bar{p} = D_s\int_0^L \sin(\pi x/L)dx/\tilde{K}_1 = \frac{4D_sL^4}{\pi^5 EI_z}\ , \tag{C18b}$$

represents the horizontal response at bridge midspan to the mean wind pressure by considering only the first vibration mode; $c'=C_xL/z$, $f_{p1}=z\omega_1/(2\pi U)$; $f=z\omega/(2\pi U)$; and $H_j(f,f_{p1})=\dfrac{1}{j^4-\left(f/f_{p1}\right)^2+2i\xi_j\left(f/f_{p1}\right)j^2}$. The variable f is known as the Monin (or similarity) coordinate. In particular, based on Eq. (C18a) the standard deviation of the displacement at bridge midspan, σ_p, can be written as,

$$\left(\sigma_p/\left(\bar{p}I_u\pi\right)\right)^2 = \sum_j\sum_k \sin(j\pi/2)\sin(k\pi/2)\times$$

$$\int_{\mathcal{D}f}\int_0^1\int_0^1 \frac{200}{6(1+50f)^{5/3}}\exp\left(-c'f|\eta-\eta'|\right)\sin(j\pi\eta)\sin(k\pi\eta')H_j(f,f_{p1})H_k^*(f,f_{p1})d\eta d\eta' df \tag{C19}$$

Let $\tilde{\sigma}_p$ denotes the normalized standard deviation of the displacement defined as,

$$\tilde{\sigma}_p = \sigma_p/\left(\bar{p}I_u\pi\right) \tag{C20}$$

Use of this definition is convenient since given value of $\tilde{\sigma}_p$ the coefficient of variation of the response at the mid-span v_p can be simply calculated from,

$$v_p = \pi I_u\tilde{\sigma}_p \tag{C21}$$

Note that $\bar{p}$ shown in Eq. (C18b) differs about 0.3% from $\bar{p}=5D_sL^4/\left(384EI_z\right)$ which is obtained based on static analysis, and that for practical applications, σ_p, is commonly approximated by the following equation (Davenport 1981),

$$\sigma_p^2 = \frac{1}{\tilde{K}_1^2}\sigma_{Q_1}^2 + \frac{1}{\tilde{K}_1^2}S_{Q_1Q_1}(\omega_1)\frac{\pi\omega_1}{4\xi} \tag{C22}$$

in which $\sigma_{Q_1}^2 = \int_0^\infty S_{Q_1Q_1}(\omega)d\omega$,

In Eq. (C22), the first term on the right hand side represents the background component of the response and is termed as σ_B^2; the second term represents the resonant component of the response and is denoted as σ_R^2. Based on Eqs. (C15) and (C22), considering $S_u(z,\omega) = 0.045 f^{-2/3}\sigma_u^2/\omega$ (Davenport 1981), it can be shown that at the midspan, σ_B^2 is approximated by (Davenport 1981)

$$\sigma_B^2 = (\bar{p} I_u \pi)^2 |J(L/\lambda)|^2 \tag{C23a}$$

while by including the aerodynamic damping ξ_a, σ_R^2 is given by,

$$\sigma_R^2 = (\bar{p} I_u \pi)^2 \frac{\pi}{4(\xi+\xi_a)} \frac{\omega_1 S_u(\omega_1)}{\sigma_u^2} \left| J\left(\frac{C_x \omega_1 L}{2\pi U}\right)\right|^2, \tag{C23b}$$

where λ is a constant known as integral spanwise turbulence scale which is equal to about 60 m, and $|J(A)|^2$ is known as the joint acceptance function evaluated from,

$$|J(A)|^2 = \int_0^1 \int_0^1 \exp(-|\eta-\eta'|A)\sin(\pi\eta)\sin(\pi\eta')d\eta d\eta'. \tag{C24}$$

In particular, for single span simply supported bridge, the joint acceptance function can be approximated by (Davenport 1977),

$$|J(A)|^2 \approx \frac{1}{A+\pi^2/4}. \tag{C25}$$

Based on the above equations (i.e., Eqs. (C20), (C22) to (C25)), $\tilde{\sigma}_p$ is approximated by,

$$\tilde{\sigma}_p = \sqrt{\frac{1}{\pi^2/4 + L/\lambda} + \frac{1}{\pi^2/4 + c' f_{p1}} \frac{\pi}{4(\xi+\xi_a)} 0.045 (f_{p1})^{-2/3}}, \tag{C26}$$

which depends only on $c' = C_x L/z$, L, and $f_{p1} = z\omega_1/(2\pi U)$. Values of $\tilde{\sigma}_p$ for a few sets of L and c' values by using Eq. (C26) are calculated and illustrated in Figure C.2 for a range of f_{p1} values.

References

Clough, R.W. and Penzien, J. (1993) "Dynamics of structures", 2nd edition, McGraw-Hill, New York.

Simiu, E., Scanlan, R. H. (1996), "Wind effects on structures, fundamentals and application to design", New York: John Wiley

Davenport, A. G. (1981), "Reliability of long span bridges under wind loading", Proceedings of ICOSSAR '81, Trondheim, Norway, pp. 679-694.

Davenport, A. G. (1977), "The Prediction of the Response of Structures to Gusty Wind", Intnl. Res. Sem. Safety of Struct. under Dynamic Loading, Trondheim, Norway

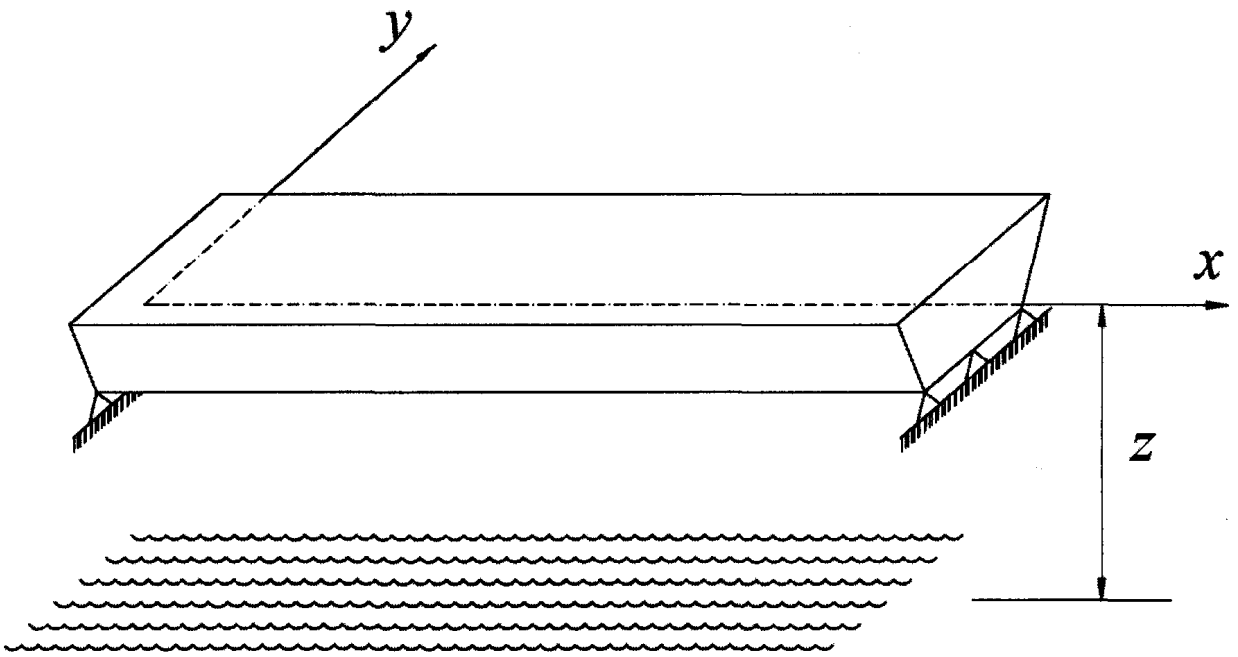

Figure C.1 An illustration of a simply supported bridge at the elevation *z*.

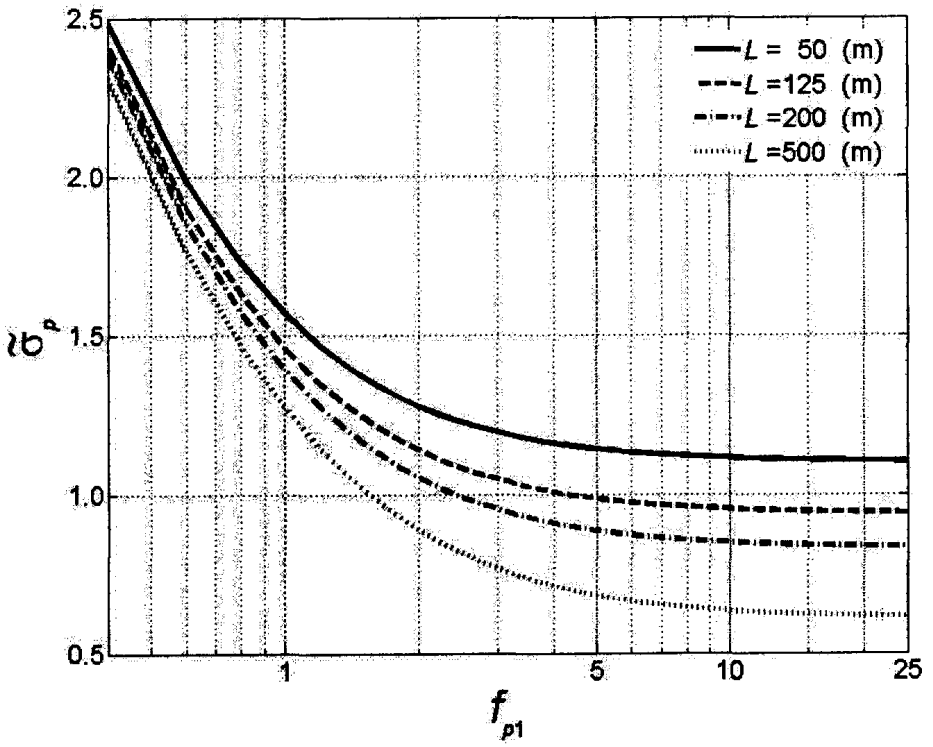

(a) for $c'=20, \xi=0.5\%, \xi_a=0$

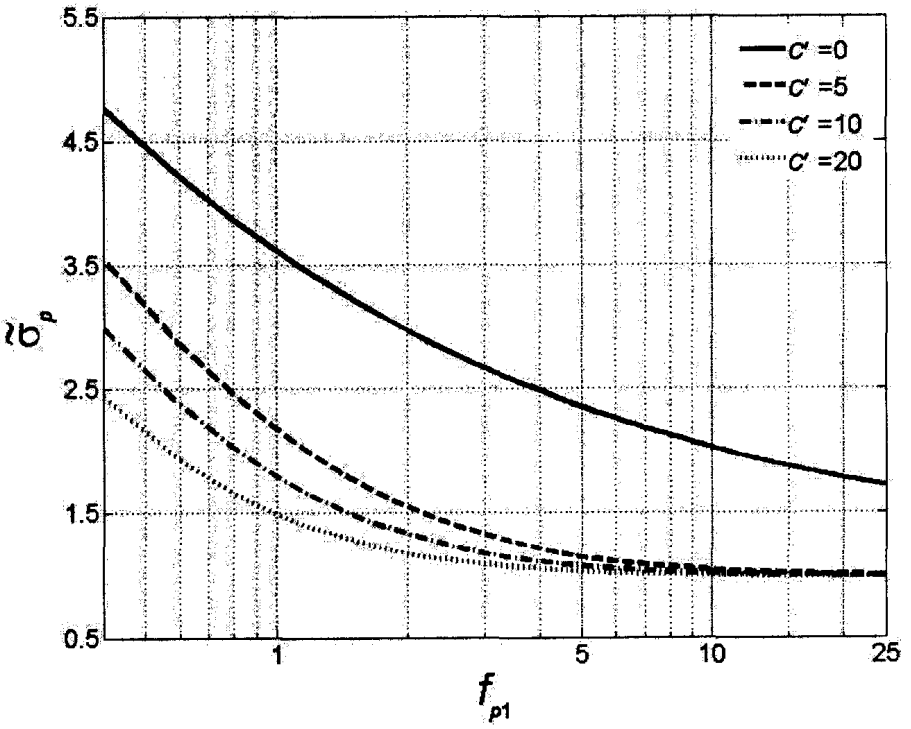

(b) for $L=100(m), \xi=0.5\%, \xi_a=0$

Figure C.2 An illustration of the standardized standard deviation $\tilde{\sigma}_p$.